E- ISSN: 2148-9505

TURKISH JOURNAL OF ORTHODONTICS

TJO

The Official Journal of Turkish Orthodontic Society

galenos Publishing House

Volume 38
Issue 04
December 2025

The Official Journal of Turkish Orthodontic Society

TURKISH JOURNAL OF ORTHODONTICS

TJO

galenos Publishing House

Publisher Contact
Address: Molla Gürani Mah. Kaçamak Sk. No: 21/1
34093 İstanbul, Türkiye
Phone: +90 (530) 177 30 97
E-mail: info@galenos.com.tr/yayin@galenos.com.tr
Web: www.galenos.com.tr
Publisher Certificate Number: 14521

Printing Date: December 2025
E-ISSN: 2148-9505
International scientific journal published quarterly.

The Official Journal of Turkish Orthodontic Society

TURKISH JOURNAL OF ORTHODONTICS

TJO

Editorial Board

Please refer to the journal's webpage **(https://turkjorthod.org/)** for "Ethical Policy", "Instructions to Authors" and "About Us".

The editorial and publication processes of the journal are shaped in accordance with the guidelines of the ICMJE, WAME, CSE,COPE, EASE, and NISO. Turkish Journal of Orthodontics is indexed in PubMed Central, Web of Science-Emerging Sources Citation Index, DOAJ, Scopus, CNKI, Gale, EBSCO and TUBITAK ULAKBİM TR Index.

The journal is published online.

Owner: Gökmen Kurt on behalf of the Turkish Orthodontic Society

Responsible Manager: Çağla Şar

Editor in Chief: Çağla Şar

Address: Sütlüce Mah. İmrahor Cad. No: 82 Beyoğlu, İstanbul/Türkiye

Phone: +90 (212) 416 61 13

E-mail: info@turkjorthod.org

The Official Journal of Turkish Orthodontic Society

TURKISH JOURNAL OF ORTHODONTICS

TJO

Contents

Original Articles

Index

TURKISH JOURNAL OF
ORTHODONTICS

DOI: 10.4274/TurkJOrthod.2025.2025.21

Original Article

Three-Dimensional Evaluation of Midfacial Changes After Maxillary Skeletal Expander Application: A Retrospective Study

Fırat Vural, Yeşim Kaya, Özer Alkan

Ankara Yıldırım Beyazıt University Faculty of Dentistry, Department of Orthodontics, Ankara, Türkiye

Cite this article as: Vural F, Kaya Y, Alkan Ö. Three-dimensional evaluation of midfacial changes after maxillary skeletal expander application: a retrospective study. *Turk J Orthod.* 2025; 38(4): 190-198

Main Points

- The maxillary skeletal expander 2 application resulted in greater skeletal expansion and less dental tipping.
- The coronal zygomatic section exhibited a pyramidal skeletal expansion pattern.
- An axial palatal section showed a parallel split of the midpalatal suture.

ABSTRACT

Objective: This study aimed to investigate the skeletal and dental effects of the maxillary skeletal expander (MSE) using cone beam computed tomography (CBCT) images analyzed in the coronal zygomatic and axial palatal sections (APS).

Methods: Pre- and post-expansion CBCT images of 18 subjects (10 females and 8 males) aged 12-16 years with maxillary transverse deficiency who were treated with MSE 2 were included in this retrospective study. In the coronal zygomatic section (CZS), upper interzygomatic distance and lower interzygomatic distances (LID), orbital distance (OD), alveolar distances (AD), and dental distances (DD), as well as nasal cavity width (NCW) and molar basal bone angle, were assessed. In the APS, the separation between the anterior nasal spine (ANS) and posterior nasal spine (PNS) was assessed. All measurements were performed using OnDemand3D software. Pre- and post-expansion treatment changes were compared using paired t-tests, with statistical significance set at $p<0.05$.

Results: In the CZS, a pyramidal skeletal expansion pattern was observed, with the greatest increase in DD (R: 2.83 mm, L: 3.18 mm), followed by AD (R: 1.63 mm, L: 1.97 mm), NCW (R: 1.66 mm, L: 2.28 mm), LID (R: 1.48 mm, L: 1.92 mm), and OD (R: 0.42 mm, L: 0.56 mm). Along with greater skeletal expansion, slightly reduced dental tipping and minimal alveolar bone bending were observed. In the APS, a nearly equal separation was observed at both the ANS (R: 1.79 mm, L: 2.46 mm) and PNS (R: 1.85 mm, L: 2.49 mm), indicating a parallel split of the midpalatal suture. Furthermore, among the 36 pterygopalatine sutures examined, only three showed separation between the medial and lateral pterygoid processes.

Conclusion: MSE 2 application provides more favorable skeletal outcomes reduces dentoalveolar side effects, and results in a more parallel midpalatal suture split.

Keywords: Maxillary skeletal expander, MSE 2, midpalatal suture, cone beam computed tomography

INTRODUCTION

Maxillary transverse deficiency is a common skeletal anomaly that may present alone or alongside sagittal and vertical discrepancies.[1] Limited visibility of the posterior maxilla often results in a lower treatment demand for isolated transverse deficiency than for sagittal or vertical anomalies.[1,2] Nevertheless, this condition can significantly affect jaw function and facial appearance.[1]

Corresponding author: Assoc. Prof. Yeşim Kaya, **e-mail:** yesimkaya82@hotmail.com
Received: April 14, 2025 **Accepted:** October 10, 2025 **Publication Date:** 30.12.2025

The midpalatal and transpalatal sutures are the primary intermaxillary growth sites influencing transverse and anteroposterior maxillary development.[3] Orthopedic separation of these sutures using palatal expanders is the primary treatment for maxillary transverse deficiency.[1,3] The morphology of the sutures changes over time: it is broad and V-shaped in the infantile period, wavy in the juvenile period, and more tortuous with increasing interdigitation in the adolescent period.[4] In addition to the increasing resistance over time of the midpalatal and transpalatal sutures, the resistance of the circummaxillary sutures that articulate with the maxilla also affects palatal expander design and activation protocols.[5]

Rapid palatal expansion using conventional tooth-borne appliances that apply heavy orthopedic forces is one treatment option.[6] Although the primary goal is to maximize skeletal effects, dentoalveolar side effects, such as alveolar bone bending and dental tipping, are frequent.[6,7] To minimize these side effects, various mini-screw-assisted rapid palatal expanders (MARPE)-tooth-bone-borne (hybrid) and bone-borne-have been developed.[8]

The skeletal and dentoalveolar effects of MARPE vary according to miniscrew position and whether monocortical or bicortical anchorage is used.[9-11] A more parallel sutural opening can be achieved by inserting bicortically engaged miniscrews as posteriorly and as deeply into the palate as possible.[11-13] The maxillary skeletal expander (MSE), a type of MARPE, achieves bicortical engagement by inserting four miniscrews into the cortical bone of the palate and the nasal floor. These screws are positioned in the posterior maxilla, beneath the zygomatic buttress, adjacent to the midpalatal suture, and at the deepest point of the palate.[12,13] As a purely bone-borne device, the MSE produces more pronounced skeletal changes with minimal dentoalveolar effects.[7,13]

MSE 2, a type of MSE, is an effective non-surgical option for late adolescents and young adults when sutural rigidity is increased.[13] Its clinical utility extends beyond conventional orthodontic expansion, encompassing broader indications, including airway volume enhancement, management of facial asymmetry, and preparation for orthognathic surgery.[14,15] Recent studies have highlighted its capacity to reduce age-dependency and to extend the therapeutic window for skeletal expansion, thereby establishing its distinct role in contemporary orthodontics.[13,16]

Numerous studies have examined the skeletal and dental effects of MSE, using cone-beam computed tomography (CBCT), particularly in the coronal and axial planes.[5,7,10-13,17-21] These studies included subjects spanning wide age ranges, combining growing and non-growing individuals. McMullen et al.[5] found that MSE produced significantly greater skeletal and dental changes in growing patients than in nongrowing patients, highlighting the importance of growth stage in treatment outcomes. Based on these findings, this study investigated the skeletal and dental effects of MSE 2 in subjects aged 12-16 years, a transitional growth period encompassing the pubertal growth spurt, using CBCT to obtain coronal zygomatic and axial palatal sections (APS). By narrowing the age range and targeting this critical developmental window, our study addresses an important gap in the current literature and provides clinically relevant 3D data that may improve the understanding of age-specific skeletal responses to MSE 2 during adolescence. We hypothesized that MSE 2 would produce significant skeletal expansion with minimal dentoalveolar compensation in adolescents aged 12-16 years.

METHODS

This retrospective study was approved by the Ankara Yıldırım Beyazıt University Ethics Committee of the Health Sciences Institute (approval no: 19/1230, date: 08.12.2022). CBCT images of 18 subjects (10 females, mean age 14.26±1.36 years; 8 males, mean age 14.29±0.72 years; age range: 12-16 years) were selected from the redords of the Department of Oral and Maxillofacial Radiology, Faculty of Dentistry at Ankara Yıldırım Beyazıt University. Baseline orthodontic records indicated that the sample included four normodivergent individuals with mild skeletal Class II malocclusion (ANB: 4.95±0.39°; SN/GoGn: 35.17±1.62°), four normodivergent individuals with mild skeletal Class III malocclusion (ANB: -1.08±0.57°; SN/GoGn: 31.93±4.69°), and ten normodivergent individuals with skeletal Class I relationships (ANB: 1.77±1.22°; SN/GoGn: 31.87±2.12°). Additionally, overjet was increased in 3 individuals (mean 5.13±1.01 mm), was decreased in 4 individuals (mean -0.15±0.60 mm), and was within the ideal range in 11 individuals (mean 2.75±0.70 mm). Furthermore, bilateral posterior crossbite was observed in 14 individuals, while unilateral posterior crossbite was present in 4 individuals. Skeletal maturation assessment of available hand-wrist radiographs revealed that eight individuals were at the MP3cap stage, five at the DP3u stage, and five at the Ru stage. Informed written consent forms, routinely collected at the onset of treatment, included permission to use patient records in scientific research. These forms were signed by each patient and, in the case of those under the age of eighteen, by their parents.

The inclusion criteria were as follows: no previous orthodontic treatment, no systemic disease, and no history of trauma or craniofacial surgery; pre- and post-expansion CBCT images with a broad field of view (FOV) including the anterior cranial base; a maxillomandibular bone width discrepancy of more than 5 mm (corresponding to a total expansion activation between 50 and 90 turns) diagnosed using the maxillomandibular differential index;[22] treatment with the MSE 2 appliance (MSE 2, BioMaterials Korea Inc., Seoul, Korea) as described by Cantarella et al.;[20] and successful separation of the midpalatal suture. Poor-quality CBCT images with movement artifacts were excluded from the study.

Previously published studies demonstrated that the standard deviations (σ) for the split of the anterior and posterior nasal spines (PNS) and for maxillary molar inclinations ranged from 0.9 to 2.913, and from 2.20 to 2.38,10, respectively. Based on these findings, standard deviations of 1.9 for linear measurements and 2.0 for angular measurements were assumed. With a Type I error rate of 0.05, an effect size (d) of 0.9, and a Z value of 1.96, the minimum required sample size was calculated using the formula $n=Z^2\sigma^2/d^2$. The resulting sample sizes were 17.12 (rounded to 17) for linear measurements and 18.97 (rounded to 19) for angular measurements. G*Power software (version 3.1; Heinrich-Heine-University, Düsseldorf, Germany) was used to perform the calculations.

The MSE 2 appliance consisted of two molar bands (3M Unitek, Bradford, England) attached to the maxillary first molars, four mini-screw tubes soldered to the expansion screw, and two soft supporting arms connecting these components (Figure 1). Each tube, measuring 1.8 mm in diameter and 2 mm in length, served as a guide for the insertion of four mini-screws. Mini-screws with a diameter of 1.8 mm and a preferred length of 11-13 mm were used to achieve stable bicortical anchorage. The soft supporting arms stabilized the expansion screw, which was positioned on the hard palate between the zygomatic buttresses during miniscrew insertion.[12,20]

After bands were placed on the maxillary molars, an alginate impression was taken and a plaster model was prepared with the bands in proper positions. The expansion screw was positioned according to the manufacturer's guidelines-centered between the second premolars and second molars, aligned with the nasal septum, and placed close to the palatal mucosa. Two long arms on one side of the screw were spot-welded to the molar bands (Lampert Werktechnik GmbH, PUK 5, Germany). The appliance was fitted intraorally and cemented with glass-ionomer band cement (3M Unitek, Monrovia, CA, USA). Four miniscrews were inserted manually with the provided driver. The recommended expansion rate was 0.5-0.8 mm per day until a diastema was observed; thereafter, 0.25 mm per day was used until adequate expansion was achieved. After completion of the expansion, the MSE 2 appliance was left in place to provide retention for at least three months without activation.[20] A detailed evaluation of the patient files revealed a mean expansion of 64.55 tours (minimum: 50; maximum: 90) and a mean retention duration of 4.16 months (minimum: 3; maximum: 6) in this study.

Pre- and post-expansion CBCT images were acquired at the start of expansion and at the end of retention, respectively. The use of the same 3D imaging device (Promax 3D, Planmeca, Helsinki) and scanning procedures (84 kVp, 6 mAs, 8.5 s exposure time, 0.32-mm voxel, 150×110×80 mm large FOV) was also ensured.

All CBCT images were exported as digital ımaging and communications in medicine files and stored. OnDemand3D software (CyberMed Inc., Seoul, Korea) was used to superimpose the pre- and post-expansion CBCT images , using the anatomical structures of the anterior cranial base as a reference. The superimposition method is based on automated matching of grayscale voxel patterns (Figure 2).

After successfully superimposing the pre- and post-expansion CBCT images using OnDemand3D software, two reference planes were identified. Upper interzygomatic distance (UID), lower interzygomatic distance (LID), orbital distance (OD), alveolar bone distance, and dental distance (DD), nasal cavity width (NCW), and maxillary basal bone angle were measured in the coronal zygomatic section (CZS), which passes through the uppermost point of the frontozygomatic sutures and the lowest point of the zygomaticomaxillary sutures (Figure 3). The separation of the anterior and PNS and the articulation between the pyramidal process of the palatine bone and the pterygoid notch, located between the medial and lateral plates of the pterygoid process, were evaluated in the APS. The APS

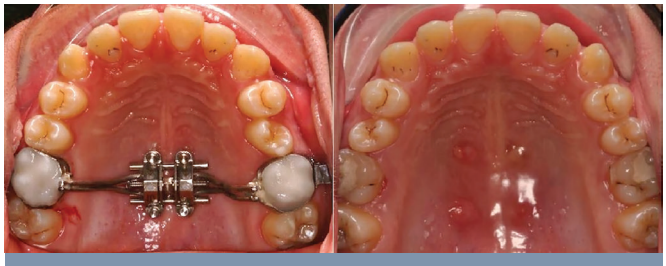

Figure 1. Pre- and post-expansion images of the MSE 2 appliance. MSE, maxillary skeletal expander.

Figure 2. Pre- and post-expansion superimposed CBCT images. CBCT, cone beam computed tomography.

passes through the anterior and PNS and is perpendicular to the midsagittal plane defined by the anterior nasal spine (ANS), the PNS and the nasion (Figure 4). The skeletal linear and angular measurements used in this study, along with their definitions, are presented in Table 1.

Statistical Analysis

A maxillofacial radiologist (AA) with over 10 years of experience in CBCT image analysis conducted all skeletal and linear measurements. To evaluate the intra-observer error, eight randomly selected pre- and post-expansion CBCT images were re-superimposed and re-traced four weeks after the initial tracing. To assess the measurement precision, intra-examiner reliability was calculated and found to be high (intraclass correlation coefficient: 0.890; $p<0.001$). Additionally, to assess inter-observer reliability, a second maxillofacial radiologist (BÇ) independently repeated the measurements on the same images and a similarly level of inter-observer agreement was observed (intraclass correlation coefficient: 0.820; $p<0.001$). Random measurement error was calculated using Dahlberg's formula, and it was observed that the error values ranged from 0.14° to 0.19° for the one angular measurement and from 0.032 to 0.046 mm for the eight linear measurements.

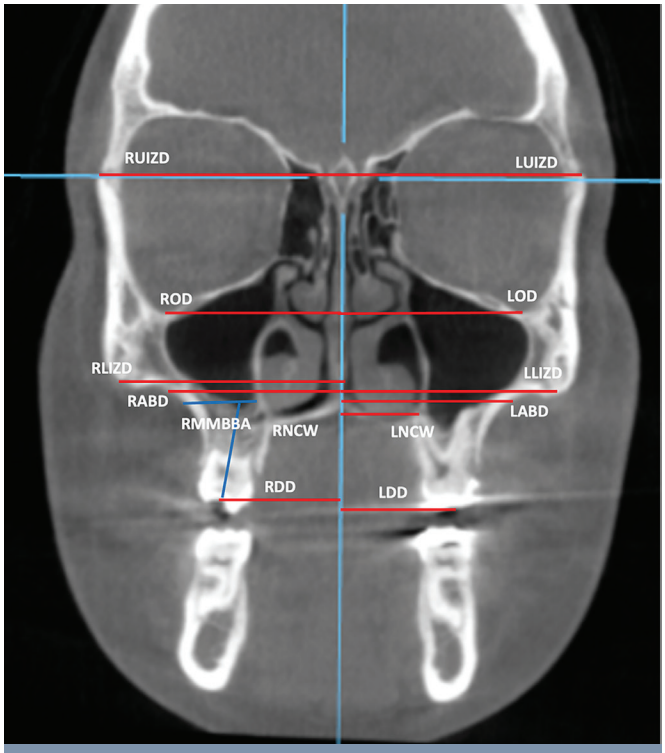

Figure 3. Coronal zygomatic section. Red lines represent linear measurements, and blue lines indicate angular measurements.

RUIZD, right upper interzygomatic distance; LUIZD, left upper interzygomatic distance; ROD, right orbital distance; LOD, left orbital distance; RLIZD, right lower interzygomatic distance; LIIZD, left lower interzygomatic distance; RABD, right alveolar bone distance; LABD, left alveolar bone distance; RNCW, right nasal cavity width; LNCW, left nasal cavity width; RDD, right dental distance; LDD, left dental distance; RMMBBA, right maxillary molar basal bone angle; LMMBBA, left maxillary molar basal bone angle.

Descriptive statistics for the continuous variables were presented as means and standard deviations. The normality assumption for the continuous variables was tested using the Kolmogorov-Smirnov test. A paired t-test was used to compare the means of pre- and post-expansion changes, as well as the right and left sides, for normally distributed variables. The statistical significance level was set at 5%, and analyses were performed using SPSS (version 21; Chicago, IL).

RESULTS

Skeletal linear and angular measurements in the CZS, except for NCW, did not differ significantly between the left and right sides in both pre- and post-expansion CBCT images. The left NCW (2.28 mm) was greater than the right (1.66 mm) (Table 2).

The treatment changes were as follows: 0.40 and 0.67 mm in the UID, 0.42 and 0.56 mm in the OD, 1.48 and 1.92 mm in the LID, 1.66 and 2.28 mm in the NCW, 1.63 and 1.97 mm in the alveolar bone distance, 2.83 and 3.18 mm in the DD, and 3.06 and 2.70° in the molar basal bone angle (MBBA) for the right and left sides, respectively. The increased expansion in the superior-inferior direction confirms the pyramidal pattern of skeletal expansion.

While LID represents pure skeletal expansion, alveolar bone distance represents skeletal expansion combined with alveolar bone bending, and DD represents skeletal expansion combined with alveolar bone bending and dental tipping. Based on this, the amounts of skeletal expansion, alveolar bone bending, and dental tipping for the right and left sides were calculated to be 1.48 and 1.92 mm, 0.15 and 0.05 mm, and 1.20 and 1.21 mm, respectively. These results indicate greater skeletal expansion, slightly less dental tipping, and negligible alveolar bone bending. The increase in the maxillary MBBA also confirms the presence of dental tipping (Table 2).

Figure 4. Axial palatal section showing anatomical landmarks.

RANS, right anterior nasal spine; LANS, left anterior nasal spine; RPNS, right posterior nasal spine; LPNS, left posterior nasal spine; R Lat Pter, lateral plate of the right pterygoid process; R Med Pter, medial plate of the right pterygoid process; L Med Pter, medial plate of the left pterygoid process; L Lat Pter, lateral plate of the left pterygoid process.

In the APS, the treatment changes at the anterior and PNSs were 1.79 and 2.46 mm for the right side, and 1.85 and 2.49 mm for the left side.

Because the amounts in the anterior and posterior regions of the maxilla were nearly equal, a parallel split of the midpalatal suture was observed. On the other hand, an asymmetry in the midpalatal suture split was observed, with greater separation on the left than on the right (Table 3). Moreover, only three of the 36 pterygopalatine sutures showed separation between the medial and lateral pterygoid processes.

A consistent asymmetry was observed in several measurements, with greater expansion noted on the left side compared to the right. This was evident in reduced interzygomatic distance (p=0.047), NCW (p=0.001), and ANS separation (p=0.002), as detailed in Tables 2 and 3.

DISCUSSION

In the CZS, the results of this study demonstrated greater skeletal expansion, slightly less dental tipping, and negligible alveolar bone bending. Moreover, a pyramidal skeletal expansion pattern was determined by the greatest increase in DD, followed by increases in alveolar bone distance, NCW, LID, and OD. In the APS, a parallel split of the midpalatal suture was observed. Based on these findings, our hypothesis was supported.

The reliability of CBCT-based 3D analysis for assessing skeletal and dentoalveolar changes has been confirmed in recent studies.[23,24] CBCT combined with multiplanar reorientation techniques enabled precise landmark localization at a voxel size of 0.32 mm, ensuring high-resolution imaging while maintaining acceptable radiation exposure.[23] Landmark

Table 1. Skeletal linear and angular mesurements investigated in the coronal zygomatic and axial palatal sections

	Measurements	Definitions
Coronal zygomatic section	**Right upper interzygomatic distance**	Distance of the outermost point of the right frontozygomatic suture to the midsagittal plane
	Left upper interzygomatic distance	Distance of the outermost point of the left frontozygomatic suture to the midsagittal plane
	Right orbital distance	Distance of the lowest point on the right inferior orbital margin to the midsagittal plane
	Left orbital distance	Distance of the lowest point on the left inferior orbital margin to the midsagittal plane
	Right lower interzygomatic distance	Distance of the outermost point of the right zygomaticomaxillary suture to the midsagittal plane
	Left lower interzygomatic distance	Distance of the outermost point of the left zygomaticomaxillary suture to the midsagittal plane
	Right alveolar bone distance	Distance of the alveolar bone point at the level of the apical of the maxillary right first molar root to the midsagittal plane
	Left alveolar bone distance	Distance of the alveolar bone point at the level of the apical of the maxillary left first molar root to the midsagittal plane
	Right nasal cavity width	Distance of the most anterior portion of the inferior contour of the right nasal cavity to the midsagittal plane
	Left nasal cavity width	Distance of the most anterior portion of the inferior contour of the left nasal cavity to the midsagittal plane
	Right dental distance	Distance of the occlusal contact point located at the central fossa of the right maxillary first molar to the midsagittal plane
	Left dental distance	Distance of the occlusal contact point located at the central fossa of the left maxillary first molar to the midsagittal plane
	Right maxillary molar basal bone angle	The angle formed between the line connecting the most lateral point of the right maxillary bone and the merge point of cortical bones of the nasal floor and maxillary sinus, and the line connecting the central pit of the right maxillary first molar crown to the furcation of the roots
	Left maxillary molar basal bone angle	The angle formed between the line connecting the most lateral point of the left maxillary bone and the merge point of cortical bones of the nasal floor and maxillary sinus, and the line connecting the central pit of the left maxillary first molar crown to the furcation of the roots
Axial palatal section	**Right anterior nasal spine**	Distance of the right anterior nasal spine to the midsagittal plane
	Left anterior nasal spine	Distance of the left anterior nasal spine to the midsagittal plane
	Right posterior nasal spine	Distance of the right posterior nasal spine to the midsagittal plane
	Left posterior nasal spine	Distance of the left posterior nasal spine to the midsagittal plane
	Right lateral-medial pterygoid process	The split of the right lateral and medial pterygoid process
	Left lateral-medial pterygoid process	The split of the left lateral and medial pterygoid process

identification was performed by calibrated observers, showing high intra- and inter-observer agreement. These findings are consistent with previous literature supporting the reproducibility and diagnostic accuracy of CBCT-based measurements in orthodontics.[23,24]

In light of the observed skeletal changes, our findings should be interpreted within the context of existing expansion-based orthopedic protocols. Previous studies, particularly those involving alternating expansion and constriction, have demonstrated that such approaches effectively disarticulate the circummaxillary sutures and facilitate maxillary displacement.[25,26] Despite variations in appliance design and treatment timing, these protocols share a common biomechanical principle whereby sutural loosening enhances the orthopedic response to protraction forces. In line with this rationale, the present results obtained with the MSE 2 appliance confirm that transverse expansion can induce clinically meaningful skeletal changes in adolescents, likely by operating through sutural disarticulation mechanisms similar to those described in previous protocols.

Since the treatment changes may vary depending on the location of the miniscrew and the design of the appliance,

Table 2. Skeletal angular and linear measurements investigated in the coronal zygomatic section

		Pre-expansion (Mean±SD)	Post-expansion (Mean±SD)	Treatment change (Mean±SD)	p
Upper interzygomatic distance	**Right**	50.13±2.55	50.54±2.55	0.40±0.36	0.001
	Left	50.18±2.43	50.86±2.49	0.67±0.54	0.001
	p	0.809	0.141		
Orbital distance	**Right**	30.52±1.96	30.94±1.96	0.42±1.96	0.001
	Left	30.87±2.09	31.43±2.18	0.56±2.13	0.001
	p	0.410	0.289		
Lower interzygomatic distance	**Right**	43.53±2.53	45.01±2.62	1.48±1.20	0.001
	Left	43.79±3.02	45.72±2.85	1.92±0.88	0.001
	p	0.422	0.047		
Nasal cavity width	**Right**	12.97±1.73	14.63±2.01	1.66±1.87	0.001
	Left	14.02±1.51	16.30±1.89	2.28±1.7	0.001
	p	0.001	0.001		
Alveolar bone distance	**Right**	29.83±1.85	31.46±1.83	1.63±1.33	0.001
	Left	30.22±2.51	32.20±2.60	1.97±1.41	0.001
	p	0.337	0.139		
Dental distance	**Right**	22.46±1.54	25.30±1.50	2.83±1.52	0.001
	Left	22.61±2.59	25.80±1.90	3.18±1.49	0.001
	p	0.789	0.250		
Maxillary molar basal bone angle	**Right**	90.40±6.83	93.47±5.46	3.06±2.67	0.001
	Left	92.07±4.85	94.78±3.50	2.70±2.08	0.001
	p	0.319	0.322		

p<0.05, Paired t-test was perfomed.
SD, standard deviation.

Table 3. Skeletal linear measurements investigated in the axial palatal section

		Pre-expansion (Mean±SD)	Post-expansion (Mean±SD)	Treatment change (Mean±SD)	p
Anterior nasal spine	**Right**	-	1.79±0.69	1.79±0.69	0.001
	Left	-	2.46±0.89	2.46±0.89	0.001
	p	-	0.002		
Posterior nasal spine	**Right**	-	1.85±0.67	1.85±0.67	0.001
	Left	-	2.49±0.85	2.49±0.85	0.001
	p	-	0.003		

p<0.05, Paired t-test was perfomed.
SD, standard deviation.

the skeletal expansion patterns produced by different MSEs have been examined in many previous studies.[5,10,11,18-20,27] Among those studies using CZSs from CBCT images, Chun et al.[28] investigated a tooth-bone-borne MARPE appliance that included four miniscrews inserted medial to the first premolars and distal to the first molars. A sequential increase in transverse measurements was reported from the upper interzygomatic region to the dental arch, reflecting a pyramidal skeletal expansion pattern with the apex near the frontonasal area and the base at the dentoalveolar level.[28]

Moon et al.[10] compared tooth-bone-borne (MSE 2) and tissue-bone-borne (C-Expander) appliances and reported comparable increases in maxillary and dental widths. In another study,[11] MSE 2 was compared with bone-borne expanders in which two miniscrews were inserted in the anterior palate at the level of the third rugae, and two were placed between the second premolar and the first molar. Both groups demonstrated similar increases in the lower interzygomatic and intermolar distances; however, the bone-borne group showed greater increases in OD and NCW.[11] Collectively, these studies indicate that MSE 2 and bone-borne expanders yield nearly identical skeletal effects, with MSE 2 potentially preferable in clinical situations requiring efficient skeletal expansion with less impact on the upper midface.

Among studies that specifically investigated MSE2 expanders, Cantarella et al.,[20] Paredes et al.,[7] McMullen et al.,[5] and Tang et al.[19] consistently reported significant skeletal and dentoalveolar changes, including increases in interzygomatic, alveolar, intermolar, and nasal cavity dimensions. The treatment changes observed in our study were generally in line with these findings, with minor differences likely related to variations in age ranges and in the total amount of expansion among study groups.[5,7,10,11,19,20]

Furthermore, the pyramidal skeletal expansion pattern observed in our sample, characterized by progressive displacement from the orbital and zygomatic regions toward the dentoalveolar level, was consistent with the expansion gradient described in prior MSE-based research.[5,11,19] Similarly, Ding et al.[16] demonstrated that MSE 2 appliances produce stable long-term skeletal and dentoalveolar expansion, with preservation of the pyramidal expansion pattern even after the retention phase. This consistent pattern across studies highlights the reliable biomechanical effect of the MSE 2 appliance and its potential predictability for clinical planning.

Tipping of the anchor teeth is a common side effect of MSE 2 expanders, because the gap between the miniscrews and their surrounding holes results in the anchor teeth being loaded primarily during initial activation.[5] In the present study, a significant amount of dental tipping was observed consistent with the study results of Paredes et al.[7] and Moon et al.[10] On contrary, our maxillary MBBA results, which confirms the dental tipping, generally agreed with the studies of Moon et al.[10] and Cantarella et al.[20] while lower than Paredes et al.[7] study. We also determined lower alveolar bone bending results compared to Paredes et al.[7] study. The discrepancy observed in dental tipping and alveolar bone bending between Paredes et al.[7] results and ours might result from the measurement method and age range of the study groups, respectively. Taken together, these findings emphasize the need to monitor early tipping forces carefully during MSE 2 treatment, particularly in growing patients. Moreover, recent reports indicate that maxillary transverse discrepancies should also be assessed in relation to molar rotations[29] and by employing different CBCT-based diagnostic methods that account for skeletal patterns,[30] as these factors may further influence treatment outcomes and long-term stability.

Most recently, Elawady et al.[31] conducted a randomized controlled trial using CBCT in young adults to evaluate MSE with and without micro-osteoperforations (MOP). They reported that MOP-assisted MSE resulted in significantly greater increases in nasal cavity and interzygomatic widths compared with standard MSE, whereas dental tipping and alveolar bending were comparable between groups.[31] These findings suggest that MOP can enhance the skeletal efficiency of expansion without causing dental side effects, complementing our results and providing practical insights into adjunctive techniques that may optimize treatment outcomes.

Previous studies have shown that during maxillary expansion, the inferior part of the pterygoid process tends to displace laterally with the hemimaxillae, whereas the superior part remains largely stable.[18,32] Age-related increases in sutural interdigitation have also been reported to make disarticulation of the palatal bone from the pterygoid process more difficult, thereby influencing the overall expansion pattern.[12,33] Despite these limitations, several MSE studies have demonstrated a parallel midpalatal suture split.[5,12,13,18] In the present study, we likewise observed a parallel split, with a nearly equal separation between the anterior and posterior regions of the maxilla. However, of the 36 pterygopalatine sutures examined, only three showed separation between the medial and lateral pterygoid processes.

Notably, an asymmetrical expansion pattern was detected, with greater skeletal and dental changes on the left side. This left-dominant expansion may reflect underlying anatomical asymmetries, variations in screw placement, or differences in initial molar inclination. Similar asymmetry has been noted in previous studies of MSE and MARPE appliances, which have reported unequal expansion patterns potentially associated with morphological differences in the maxilla, asymmetry in bone density, or uneven force distribution during screw activation.[21,27]

In contrast to prior studies that included broad age ranges, the present study focused solely on adolescents, allowing for a more controlled assessment of skeletal and dentoalveolar changes associated with MSE 2. This targeted approach enhances the interpretability of expansion outcomes in growing patients and helps establish a consistent reference point for future

clinical and radiographic research. By integrating multiplanar CBCT analysis with age-specific evaluation, the study addresses a notable gap in the literature regarding the skeletal effects of MSE 2 during adolescence. Furthermore, the demonstrated ability of MSE 2 to achieve significant skeletal expansion with minimal dentoalveolar side effects, particularly for borderline surgical cases, reinforces its clinical utility and supports its value in treatment planning and growth-phase-specific decision-making.

Study Limitations

The main limitations of this study included its retrospective design, relatively small sample size, mixed sample of male and female participants, limited age range, and short follow-up periods. It is therefore recommended that future studies be designed as prospective, randomized trials involving both males and females across various age groups, with standardized appliance activation protocols, controlled operator variability, and long-term follow-up periods, including CBCT scans at least one year post-expansion, to further validate and generalize the findings. Additionally, the absence of an untreated control group or of a matched cohort treated with conventional RPE or other MARPE designs limits the ability to assess the relative efficacy of MSE 2. Future research should aim to incorporate well-matched comparative groups to enable a more comprehensive evaluation of different maxillary expansion protocols.

Despite these limitations, the use of CBCT-based three-dimensional imaging enabled high-resolution evaluation of skeletal and dentoalveolar structures, enhancing both the precision and reproducibility of the measurements. Additionally, the inclusion of both coronal and axial evaluation planes contributed to a more comprehensive and spatially accurate analysis.

CONCLUSION

A pyramidal skeletal expansion pattern was observed in the coronal section of the zygoma. Expansion resulted in greater skeletal displacement, slightly reduced dental tipping, and negligible alveolar bending. A parallel split of the midpalatal suture was observed in the APS. Collectively, these findings support MSE 2 as a favorable treatment option for patients nearing the end of their growth period, producing predominantly skeletal expansion with limited dentoalveolar side effects.

Ethics

Ethics Committee Approval: This retrospective study was approved by the of Ankara Yıldırım Beyazıt University Ethics Committee of the Health Sciences Institute (approval no: 19/1230, date: 08.12.2022).

Informed Consent: Written and informed consents were previously signed by the participants or a legal guardian for those under 18 years old.

Footnotes

Author Contributions: Surgicial and Medical Practices - F.V., Y.K.; Concept - Y.K.; Design - Y.K.; Data Collection and/or Processing - F.V., Y.K.; Analysis and/or Interpretation - Y.K., Ö.A.; Literature Search - F.V., Y.K., Ö.A.; Writing - F.V., Y.K.

Conflict of Interest: The authors have no conflicts of interest to declare.

Financial Disclosure: The authors declared that this study received no financial support.

REFERENCES

1. Bin Dakhil N, Bin Salamah F. The diagnosis methods and management modalities of maxillary transverse discrepancy. *Cureus.* 2021;13(12):e20482. [CrossRef]
2. Reyneke JP, Conley RS. Surgical/orthodontic correction of transverse maxillary discrepancies. *Oral Maxillofac Surg Clin North Am.* 2020;32(1):53-69. [CrossRef]
3. Carlson DS, Buschang PH. Craniofacial growth and development: evidence-based perspectives. In: Graber LW, ed. Orthodontics: Current principles and techniques. 5th ed. Elsevier, PA: Mosby, 2011:215-246. [CrossRef]
4. Festa F, Festa M, Medori S, et al. Midpalatal suture maturation in relation to age, sex, and facial skeletal growth patterns: a CBCT study. *Children (Basel).* 2024;11(8):1013. [CrossRef]
5. McMullen C, Al Turkestani NN, Ruellas ACO, et al. Three-dimensional evaluation of skeletal and dental effects of treatment with maxillary skeletal expansion. *Am J Orthod Dentofacial Orthop.* 2022;161(5):666-678. [CrossRef]
6. Jia H, Zhuang L, Zhang N, Bian Y, Li S. Comparison of skeletal maxillary transverse deficiency treated by microimplant-assisted rapid palatal expansion and tooth-borne expansion during the post-pubertal growth spurt stage. *Angle Orthod.* 2021;91(1):36-45. [CrossRef]
7. Paredes N, Colak O, Sfogliano L, et al. Differential assessment of skeletal, alveolar, and dental components induced by microimplant-supported midfacial skeletal expander (MSE), utilizing novel angular measurements from the fulcrum. *Prog Orthod.* 2020;21(1):18. [CrossRef]
8. Lin L, Ahn HW, Kim SJ, Moon SC, Kim SH, Nelson G. Tooth-borne vs bone-borne rapid maxillary expanders in late adolescence. *Angle Orthod.* 2015;85(2):253-262. [CrossRef]
9. Li N, Sun W, Li Q, Dong W, Martin D, Guo J. Skeletal effects of monocortical and bicortical mini-implant anchorage on maxillary expansion using cone-beam computed tomography in young adults. *Am J Orthod Dentofacial Orthop.* 2020;157(5):651-661. [CrossRef]
10. Moon HW, Kim MJ, Ahn HW, et al. Molar inclination and surrounding alveolar bone change relative to the design of bone-borne maxillary expanders: a CBCT study. *Angle Orthod.* 2020;90(1):13-22. [CrossRef]
11. Bazzani M, Cevidanes LHS, Al Turkestani NN, et al. Three-dimensional comparison of bone-borne and tooth-bone-borne maxillary expansion in young adults with maxillary skeletal deficiency. *Orthod Craniofac Res.* 2023;26(2):151-162. [CrossRef]
12. Colak O, Paredes NA, Elkenawy I, et al. Tomographic assessment of palatal suture opening pattern and pterygopalatine suture disarticulation in the axial plane after midfacial skeletal expansion. *Prog Orthod.* 2020;21(1):21. [CrossRef]
13. Cantarella D, Dominguez-Mompell R, Mallya SM, et al. Changes in the midpalatal and pterygopalatine sutures induced by micro-

implant-supported skeletal expander, analyzed with a novel 3D method based on CBCT imaging. *Prog Orthod.* 2017;18(1):34. [CrossRef]

14. Moon W. Class III treatment by combining facemask (FM) and maxillary skeletal expander (MSE). *Seminars in Orthodontics.* 2018;24(1):95-107. [CrossRef]
15. Combs A, Paredes N, Dominguez-Mompell R, et al. Long-term effects of maxillary skeletal expander treatment on functional breathing. *Korean J Orthod.* 2024;54(1):59-68. [CrossRef]
16. Ding C, Paredes N, Wu B, Moon W. Long term skeletal, alveolar, and dental expansion effects of the midfacial skeletal expander. *Applied Sciences.* 2023;13(17):9569. [CrossRef]
17. Lee DW, Park JH, Moon W, Seo HY, Chae JM. Effects of bicortical anchorage on pterygopalatine suture opening with microimplant-assisted maxillary skeletal expansion. *Am J Orthod Dentofacial Orthop.* 2021;159(4):502-511. [CrossRef]
18. Song KT, Park JH, Moon W, Chae JM, Kang KH. Three-dimensional changes of the zygomaticomaxillary complex after mini-implant assisted rapid maxillary expansion. *Am J Orthod Dentofacial Orthop.* 2019;156(5):653-662. [CrossRef]
19. Tang H, Liu P, Liu X, et al. Skeletal width changes after mini-implant-assisted rapid maxillary expansion (MARME) in young adults. *Angle Orthod.* 2021;91(3):301-306. [CrossRef]
20. Cantarella D, Dominguez-Mompell R, Moschik C, et al. Midfacial changes in the coronal plane induced by microimplant-supported skeletal expander, studied with cone-beam computed tomography images. *Am J Orthod Dentofacial Orthop.* 2018;154(3):337-345. [CrossRef]
21. Cantarella D, Dominguez-Mompell R, Moschik C, et al. Zygomaticomaxillary modifications in the horizontal plane induced by micro-implant-supported skeletal expander, analyzed with CBCT images. *Prog Orthod.* 2018;19(1):41. [CrossRef]
22. Ye G, Li Q, Guo Z, et al. Comparative evaluation of transverse width indices for diagnosing maxillary transverse deficiency. *BMC Oral Health.* 2024;24(1):808. [CrossRef]
23. Lisboa Cde O, Masterson D, da Motta AF, Motta AT. Reliability and reproducibility of three-dimensional cephalometric landmarks using CBCT: a systematic review. *J Appl Oral Sci.* 2015;23(2):112-119. [CrossRef]
24. Gribel BF, Gribel MN, Frazão DC, McNamara JA Jr, Manzi FR. Accuracy and reliability of craniometric measurements on lateral cephalometry and 3D measurements on CBCT scans. *Angle Orthod.* 2011;81(1):26-35. [CrossRef]
25. Liou EJ, Tsai WC. A new protocol for maxillary protraction in cleft patients: repetitive weekly protocol of alternate rapid maxillary expansions and constrictions. *Cleft Palate Craniofac J.* 2005;42(2):121-127. [CrossRef]
26. Borzabadi-Farahani A, Lane CJ, Yen SL. Late maxillary protraction in patients with unilateral cleft lip and palate: a retrospective study. *Cleft Palate Craniofac J.* 2014;51(1):e1-e10. [CrossRef]
27. Park JJ, Park YC, Lee KJ, Cha JY, Tahk JH, Choi YJ. Skeletal and dentoalveolar changes after miniscrew-assisted rapid palatal expansion in young adults: a cone-beam computed tomography study. *Korean J Orthod.* 2017;47(2):77-86. [CrossRef]
28. Chun JH, de Castro ACR, Oh S, et al. Skeletal and alveolar changes in conventional rapid palatal expansion (RPE) and miniscrew-assisted RPE (MARPE): a prospective randomized clinical trial using low-dose CBCT. *BMC Oral Health.* 2022;22(1):114. [CrossRef]
29. Özden S, Cicek O. Analysis of the effect of maxillary transverse deficiencies on permanent maxillary first molar rotations using 3D digital models. *BMC Oral Health.* 2025;25(1):879. [CrossRef]
30. Chen Z, Guo R, Qin Q, Feng J, Zheng Y, Li W. Transverse analysis of maxillary transverse deficiency and sagittal skeletal patterns: a cone-beam computed tomography study. *Am J Orthod Dentofacial Orthop.* 2025;168(3):317-326.e3. [CrossRef]
31. Elawady AR, Abd Alfatah EB, Mohamed RE, Hussein FA, Ali MM, Shendy MA. Evaluation of maxillary skeletal expander (MSE) assisted by two techniques of microoste operforations in young adults using CBCT, a randomised controlled trial. Afr J Bio Sc. 2024;6(7):4192-4206. [CrossRef]
32. Jafari A, Shetty KS, Kumar M. Study of stress distribution and displacement of various craniofacial structures following application of transverse orthopedic forces--a three-dimensional FEM study. *Angle Orthod.* 2003;73(1):12-20. [CrossRef]
33. Savoldi F, Wong KK, Yeung AWK, Tsoi JKH, Gu M, Bornstein MM. Midpalatal suture maturation staging using cone beam computed tomography in patients aged between 9 to 21 years. *Sci Rep.* 2022;12(1):4318. [CrossRef]

DOI: 10.4274/TurkJOrthod.2025.2025.37

TURKISH JOURNAL OF
ORTHODONTICS

Original Article

3D Assessment of the Relationship of the Mandibular Buccal Shelf with the Mandibular Canal: A CBCT Retrospective Study

Jéssica Feliciano[1], Pedro Mariano Pereira[1,2], Luis Proença[2,3], Joana Borga[1], Iman Bugaighis[1,2,4]

[1]Egas Moniz School of Health & Science, Department of Orthodontics, Monte de Caparica, Portugal
[2]Egas Moniz Center for Interdisciplinary Research (CiiEM); Egas Moniz School of Health & Science, Caparica, Almada, Portugal
[3]Egas Moniz School of Health & Science, Quantitative Methods for Health Research Unit, Monte de Caparica, Portugal
[4]The Libyan Authority for Scientific Research, Tripoli, Libya

Cite this article as: Feliciano J, Pereira PM, Proença L, Borga J, Bugaighis I. 3D assessment of the relationship of the mandibular buccal shelf with the mandibular canal: a CBCT retrospective study. *Turk J Orthod.* 2025; 38(4): 199-205

Main Points

- The site on the mandibular buccal shelf (MBS) adjacent to the distal surface of the second molar is the safest point for micro-implant (MI) insertion in the absence of impacted third molars.
- The wide variation in the distance and angulation between the MBS and the mandibular canal (MC) indicates that the MBS is not entirely safe for MI insertion, regardless of specific locations, recommending analysis of each case individually.
- There is a significant sexual dimorphism in the distance between the MBS and MC, with females exhibiting significantly smaller measurements than males.
- Given the significant anatomical variability, cone-beam computed tomography might be employed as a complementary diagnostic tool to precisely assess the MC position and determine the optimal MI insertion angulation.

ABSTRACT

Objective: This study aimed to evaluate the micro-implant safest insertion site on the mandibular buccal shelf (MBS) without compromising the integrity of the mandibular canal (MC).

Methods: This retrospective investigation included cone-beam computed tomography (CBCT) of 96 Portuguese patients (58 females and 38 males, average age of 25.5±10.2 years). Measurements were taken in four bilateral MBS sites buccal to the mandibular second molar; tangent to the distal surface (7D), distobuccal cusp tip (7CD), buccal groove (7S) and mesiobuccal cusp tip (7CM). The transversal MBS midpoint was also determined, and the maximum angulation from the transversal MBS midpoint was extracted relative to the true vertical plane. Subsequently, the distance from the MBS midpoint to the MC was calculated at this angulation. Descriptive and inferential statistical analyses were performed at $p<0.05$

Results: Significant correlations were observed among several variables and age, sex and bilateral asymmetry ($p<0.05$). The MBS transversal width and the distance from the MBS midpoint to the MC progressively increased in the posterior direction while the angulation decreased.

Conclusion: The most appropriate micro-implant insertion location compared to the other MBS investigated sites, in the absence of impacted third molars, is adjacent to the distal surface of the second molar. This finding is consistent across all age groups, sexes, and insertion sides. However, due to the demonstrated variability, taking a CBCT scan prior to mini-implant insertion might be considered to minimize the risk of injury to the inferior alveolar nerve.

Keywords: CBCT, mandibular buccal shelf, mandibular canal, mini-implants

Corresponding author: Asst. Prof. Iman Bugaighis, **e-mail:** isbugaighis@yahoo.com
Received: February 27, 2025 **Accepted:** August 01, 2025 **Publication Date:** 30.12.2025

INTRODUCTION

Contemporary orthodontics continuously encounters the challenge of developing and implementing novel techniques, materials, and approaches to enhance the effectiveness of orthodontic treatment.[1] Over the years, emerging innovations of orthodontic anchorage systems have been notable, allowing significant advancements therapeutic possibilities. Traditionally, orthodontic anchorage could be achieved using intra-oral and extra-oral modalities. However, both approaches have limitations that might cause anchorage loss, ultimately compromising treatment objectives.[2,3] To reinforce anchorage and achieve predictable treatment results, temporary anchorage devices have emerged in clinical practice, making it possible to obtain a maximum anchorage with no or minimal movement of the anchorage unit.[4] Micro-implants (MIs) have become increasingly prevalent for their ease of placement and removal, low cost, and minimal or no requirement for patient compliance.[5]

The mandibular buccal shelf (MBS) is the vestibular posterior area of the mandible, buccal to the roots of the molars. This platform typically provides adequate bone volume and density for MI placement.[1] The MI is generally inserted nearly vertically, parallel to the molar roots; therefore, an angulated insertion technique may be necessary.[4] However, MBS bone height and thickness variation could compromise MI placement and primary stability. Numerous factors might influence the success and/or failure of MI, including aspects related to the patient (age, sex, skeletal pattern, insertion site, oral hygiene status, and smoking) or linked to the MI used (diameter, insertion technique, angulation, and force applied).[1,6]

Evaluating the approximation of the mandibular canal (MC) to a future MI position is critical to avoid injuring the inferior alveolar nerve (IAN).[7] Since the MC is an intra-osseous canal, radiographs are an essential diagnostic modality to determine the estimated position of an MI relative to the MC. Cone-beam computed tomography (CBCT) allows the determination of the MC location three-dimensionally, reducing the likelihood of causing injuries at the IAN level.[8,9]

Several investigations analysed the most appropriate MBS site for MI placement.[7,10,11] Gandhi et al.[11] compared MBS parameters, among American growing and non-growing patients, concluding that the MBS transversal width increased while its height progressively decreased from the distal root of the first molar to the distal root of the second molar in all three facial patterns without interfering with the MC, regardless of sex and age. In a Brazilian study, Eto et al.[7] reported a similar observation, concluding that the ideal MI placement site in the MBS faces the second molar's distal root, regardless of facial pattern, sex, and age. In a CBCT investigation, Elshebiny et al.[10] virtually placed an MI in MBS and digitally traced the IAN. The authors noted that the cortical bone thickness, MBS transversal width, and MI insertion depth were most favourable vestibular to the distobuccal cusp of the mandibular second molar. Despite these comparable findings, further investigations are necessary due to variations in craniofacial forms, including the MBS, among populations;[11-13] none of the performed studies have sufficiently addressed the potential MI insertion angle that can be employed without risking damage to the MC. Therefore, the primary aim of this study was to evaluate the safest insertion site for MI without compromising the integrity of the MC. Within this context, the following null hypotheses were tested:

- The MBS bone width and the location of the MC in the same region do not vary with respect to patients' age.

- The MBS bone width and the location of the MC in the same region do not vary considering the patients' sex.

- The bone width of the MBS and the location of the MC are symmetrical on both the right and left mandibular sides.

METHODS

This retrospective three-dimensional quantitative investigation was performed at Egas Moniz University Clinic. The research protocol was secured by the Ethics Committee of the Egas Moniz School of Health & Science (approval no.: PT-288/23, date: 30.11.2023), and written consents were obtained from the participants before administering the CBCT scans. This investigation, adhering to the Strengthening the Reporting of Observational Studies in Epidemiology guidelines for observational studies, was performed exclusively on Portuguese patients.[14,15]

Sample Size Calculation

The sample size was determined using the G*Power (v. 3.1.9.7, H.H.U.D., Düsseldorf, Germany). This calculation was informed by the findings of Matias et al.[13] and utilized a significance level of 5% (α=0.05) alongside an 80% power to detect a Cohen's d effect size of 0.6 in the cross-sectional width of the MBS. The sample size calculation indicated that, under these conditions, a minimum of 90 patients were required (n=45 per group for a two-group stratification).

Sample Description and Exclusion/Inclusion Criteria

A total of 1,431 patient records from individuals who attended the Egas Moniz University Clinic between January 2023 and March 2024, and underwent CBCT (exclusively for diagnostic purposes) were reviewed. Portuguese individuals who had CBCT scans showing complete bilateral MBS and mental foramen with full permanent lower dentition were selected. Patients exhibiting syndromes, apparent asymmetry, having a history of previous orthodontic treatment, or radiographic signs of periodontal disease were excluded from the study. Poor-quality CBCT scans were also excluded.

A total of 96 CBCT scans fulfilled the inclusion and exclusion criteria used in this study. Subsequently, the cohort was stratified for age and sex.

Image Acquisition and Processing

The CBCT scans were acquired using Planmeca Viso G7 (Planmeca, Helsinki, Finland) with 120 kV, 5 mA, a large field of view (20x17 cm), an exposure duration of 30 seconds, and a slice thickness of 0.45 mm. Following the protocol of As Low As Diagnostically Acceptable, the CBCT field of view adhered to being indication-oriented and patient-specific.[16] Each CBCT was constructed utilizing the Planmeca Romexis Viewer, V 6.0 software (Planmeca, Helsinki, Finland). The mandible was initially oriented in the three orthogonal planes, with the mental foramen used as a reference point to ensure that the axial plane remained parallel to the occlusal plane. Bilateral measurements were performed in four specific regions of the MBS at the level of the lower second molars (Figure 1): tangent to the distal surface, distobuccal cusp, buccal groove, and mesiobuccal cusp. In cases where the third molar was present in the MBS region, the tangent dimension to the distal surface of the second lower molar could not be obtained.

The superficial transverse midpoint of the MBS was first identified, and then the maximum insertion angle of this point was determined relative to the mandibular canal in the vertical plane. Using this angle, the distance between the midpoint of the MBS and the MC was measured (Figure 2). The transverse width of the MBS was defined as the buccolingual distance from the most buccal bony point of the shelf to the nearest bony point of the adjacent tooth. In cases where the precise position of the MC was unclear, the canal was manually traced using the Planmeca Romexis® 5 software to confirm its location.

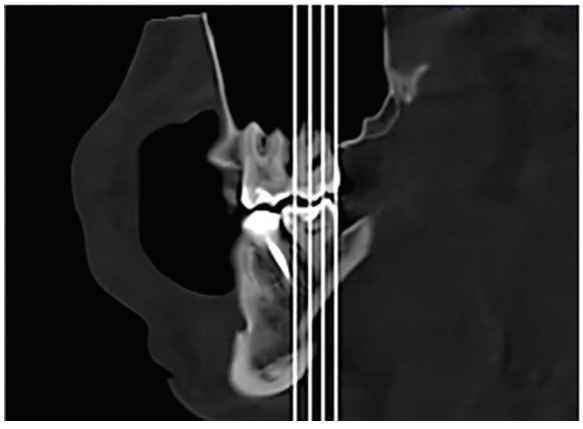

Figure 1. Sagittal view of the CBCT illustrating the four zones analyzed
CBCT, cone-beam computed tomography.

Statistical Analysis

Data analyses were performed using the SPSS software (IBM, SPSS Inc,. Chicago USA) v29.0. The normality and homogeneity of variance in the data obtained from the measurements across the different points were investigated using the Shapiro-Wilk and Levene's tests, respectively. Descriptive and inferential statistical methods were applied. In the latter, Student's t-tests were performed. The mean, standard deviation (SD), and 95% confidence intervals (95%) were computed for each variable. The significance level was established at 5% ($p<0.05$).

Reproducibility Study

Around 10% of the cohort (10 cases) was re-examined by the same operator at two-week intervals. Twenty-four measurements on each CBCT (240 measurements in total) were evaluated. The Intraclass Correlation Coefficient (ICC) showed excellent intra-examiner reproducibility between the repeated corresponding measurements (ICC=0.927-0.996).

RESULTS

The total cohort comprised 96 individuals aged 25.5 (±10.2) years, 58 females (60.4%) and 38 males (39.6%) of the total sample. The cohort was stratified into two age groups: ≤22 years old: comprising 49% and >22 years old: encompassing 51%. Table 1 presents the mean, SD, minimum and maximum values of each variable. These mean measurements indicate the progressively increasing transversal width of the MBS in the posterior direction (7CM <7S <7CD <7D), on both the right (7.2 mm <7.3 mm <7.3 mm <7.6 mm) and left sides (6.7 mm <6.9 mm <7.1 mm <7.3 mm) respectively. The maximum value found for the transverse width of the MBS was 12 mm in the area tangent to the distal surface of the second lower right molar, and the minimum value was 2.9 mm in the area adjacent to the mesial cusp of the second lower right molar.

Similarly, the mean distance from the midpoint of the MBS to the closest point of the MC increased progressively towards the posterior region on the right side (12.7 mm <12.9 mm <13.0 mm <13.7 mm) and the left side (12.6 mm <12.8 mm <13.1 mm <13.7 mm). The maximum value observed was 19.6 mm, corresponding to the tangent of the distal surface of the mandibular second molar, and the minimum value was 6.3 mm in the area of the distal cusp of the lower right second molar.

In contrast, the mean insertion angle measurements showed a progressive decrease in the posterior direction, on sides, both the right (10.9°>9.4°>7.0°>4.4°) and left (9.4°>7.9°>6.2°>4.9°). The minimum angulation value was the same at all sites analyzed and was zero degrees. It was noted that the SD for all the angular measurements was high, indicating their disparity and variation compared to the mean values.

Measurement Differences Among Males and Females

The mean MBS transversal width corresponding to the mesial cusp of the mandibular second molar was significantly greater in males (7.8±1.91 mm) compared to females (6.8±1.5 mm) at $p=0.011$. No statistically significant sexual dimorphism was found ($p>0.05$) regarding the angulation possible without interfering with the CM. Regarding the distance from the midpoint of the MBS to the closest point of the CM, statistically significant differences ($p\leq0.05$) were found in all locations, and the average was higher in males than in females (Table 2).

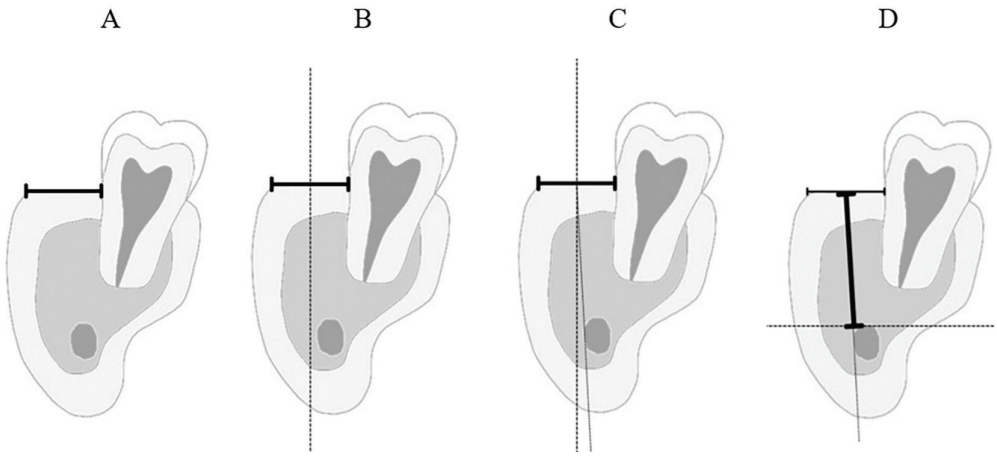

Figure 2. Illustration of the data collection method for the study sample. A: Superficial transverse width of the MBS; B: Midpoint of the initial measurement; C: Maximum angle from the anterior point to the mandibular canal relative to true vertical; D: Distance from the midpoint of the MBS to the nearest point of the mandibular canal

MBS, mandibular buccal shelf

Table 1. Descriptive and comparative measurements of the eight analyzed zones: four zones on the right side and four zones on the left side

		Width of the MBS (mm)		Angle to canal (graus)		Distance to the MC (mm)	
		Mean±SD	Max.-Min.	Mean±SD	Max.-Min.	Mean±SD	Max.-Min.
R	7D	7.6±1.6	12-5.0	4.4±4.9	17.0-0	13.7±2.3	19.4-8.6
	7CD	7.3±1.7	11.78-3.6	7.0±6.1	19.9-0	13.0±2.3	18.9-6.3
	7S	7.3±1.7	11.74-4.5	9.4±6.7	23.7-0	12.9±2.11	18.1-9.1
	7CM	7.2±1.8	11.9-2.9	10.9±7.0	29.7-0	12.7±2.02	17.6-9.0
L	7D	7.3±1.3	11.7-4.2	4.9±4.3	17.6-0	13.7±2.48	19.6-9.5
	7CD	7.1±1.2	9.1-4.0	6.2±5.3	21.8-0	13.1±2.31	17.6-9.5
	7S	6.9±1.2	10.2-4.5	7.9±6.0	12.4-0	12.8±2.33	17.3-6.8
	7CM	6.7±1.5	10.6-3.6	9.4±6.7	25.3-0	12.6±2.40	17.4-10.2

MBS, mandibular buccal shelf; MC, mandibular canal; R, right; L, left; SD, standard deviation; Max., maximum; Min., minimum; 7D, tangent to the distal surface; 7CD, distobuccal cusp tip; 7S, buccal groove; 7CM, mesiobuccal cusp tip.

Table 2. Measurement differences of the eight evaluated sites among males and females (p<0.05)

		Right								Left							
		7D		7CD		7S		7CM		7D		7CD		7S		7CM	
	Sex	F	M	F	M	F	M	F	M	F	M	F	M	F	M	F	M
MBS	Mean	7.7	7.3	7.2	7.1	6.9	7.5	6.8	7.8	7.3	7.3	6.6	6.8	6.8	7.0	6.6	7.2
	P	0.305		0.088		0.053		0.011		0.924		0.560		0.583		0.073	
Angle	Mean	3.7	5.1	6.1	8.2	8.5	10.3	9.5	12.1	3.9	3.6	5.3	6.1	6.9	7.3	8.3	8.4
	P	0.214		0.090		0.146		0.056		0.812		0.463		0.724		0.932	
Distance	Mean	13.2	14.8	13.2	14.6	12.9	14.1	12.6	13.8	13.3	14.7	13.5	14.5	12.9	13.9	12.7	13.7
	P	0.003		0.005		0.006		0.003		0.032		0.047		0.041		0.028	

MBS, mandibular buccal shelf; 7D, tangent to the distal surface; 7CD, distobuccal cusp tip; 7S, buccal groove; 7CM, mesiobuccal cusp tip.

Measurement Differences Between Age Groups

The mean possible insertion angle in relation to the true vertical plane was not influenced by age (p>0.05) except at three locations adjacent to the mandibular left second molar, the mesial cusp (p=0.035), the distal cusp (p=0.049), and the sulcus (p=0.048), which were significantly greater in the older age group than in the younger age group (22 years or younger). Among these values, the minimum noticed angulation was zero in both age groups, and the maximum was 25.3° in the older age group. The MBS transversal width and the distance to the MC were not influenced by age (Table 3).

Measurement Differences Between the Right and Left MBS

There were statistically significant discrepancies between the paired MBS transverse width (right and left sides) in the zones adjacent to the distal (p=0.002) and mesial (p=0.043) cusps of the lower second molars. Furthermore, there were statistically significant differences between the right and left sides of the lower second molars in the zones of the distal cusp (p=0.009), the sulcus (p<0.001), and the mesial cusp (p<0.001) concerning the possible angulation in relation to the true vertical without interfering with the CM. No statistically significant discrepancies were noted on the right and left side corresponding to the distance from the midpoint of the MBS to the closest point to the CM at p>0.05 (Table 4).

DISCUSSION

The primary objective of this retrospective 3D radiographic investigation was to identify the safest sites for MI insertion on an MBS, considering both the MI length and insertion angle to avoid interference with the MC. Additionally, this study aimed to assess the influence of sex, age, and symmetry on an MI insertion site. Understandably, the anatomy and variation of the MBS are of utmost significance for determining the optimal insertion site for an MI; therefore, avoiding iatrogenic complications.

Four distinct vestibular sites in the lower second molar region were explored bilaterally. Previous research has indicated that the lower first molar area has a less favorable bone height relative to the MC, and a narrower MBS width than the lower second molar region. Therefore, it was excluded from this study.[11] Simultaneously, the area tangent to the distal surface of the lower second molars was considered worth investigating since it had not been previously analyzed.[7,11] However, this area was often unclear in cases involving impacted third molars.

For a safe MI placement, the MBS should ideally have a minimum buccal bone width of 5 mm.[17] Our investigation observed a progressive increase in the MBS transverse width bilaterally in a posterior direction, aligning with the

Table 3. Measurement differences of the eight evaluated sites between the two age groups (p<0.05)

		Right								Left							
		7D		7CD		7S		7CM		7D		7CD		7S		7CM	
	Age	≤22	>22	≤22	>22	≤22	>22	≤22	>22	≤22	>22	≤22	>22	≤22	>22	≤22	>22
MBS	Mean	7.6	7.5	7.0	7.3	7.0	7.3	7.0	7.3	7.0	7. 5	6.7	6.6	6.9	7.0	6.7	6.9
	p	0.890		0.267		0.358		0.417		0.185		0.638		0.707		0.551	
Angle	Mean	3.4	4.8	6.1	7.6	8.1	10.3	9.3	11.7	2.7	4.6	4.6	6.7	5.9	8.1	7.0	9.6
	p	0.209		0.179		0.083		0.072		0.075		0.049		0.048		0.035	
Distance	Mean	14.2	13.5	14.2	13.3	13,6	13.0	13.4	12.7	14.0	13.5	14.4	13.4	13.7	13.0	13.4	12.8
	p	0.147		0.082		0.259		0.086		0.256		0.051		0.159		0.144	

MBS, mandibular buccal shelf; 7D, tangent to the distal surface; 7CD, distobuccal cusp tip; 7S, buccal groove; 7CM, mesiobuccal cusp tip.

Table 4. Measurement differences between the right and left MBS (p≤0.05)

		7D		7CD		7S		7CM	
	Side	R	L	R	L	R	L	R	L
MBS	Mean	7.6	7.3	7. 4	6.7	7.3	6.9	7.2	6.7
	p	0.085		0.002		0.084		0.043	
Angle	Mean	4.37	3.71	7.04	6.19	9.36	7.9	10.9	9.4
	p	0.244		0.009		<0.001		<0.001	
Distance	Mean	13.7	13.7	13.0	13.1	12.9	12.8	12.7	12.6
	p	0.977		0.477		0.776		0.925	

MBS, mandibular buccal shelf; 7D, tangent to the distal surface; 7CD, distobuccal cusp tip; 7S, buccal groove; 7CM, mesiobuccal cusp tip.

findings reported in the literature.[7,10,11,18-20] Furthermore, the distance from the MBS midpoint to the closest margin of the MC continuously increased towards the posterior direction, contradicting Gandhi et al.[11] and Eto et al.[7] observations of a lessening in bone height relative to the MC in the posterior direction. On the other hand, Elshebing et al.[10] noted a closer distance of a virtually inserted MI perpendicular to their occlusal plane in a more posterior position corresponding to an approximately vertical orientation, which support our findings that in further posterior regions, the MC is positioned more vertically. Additionally, our study found that female patients demonstrated a shorter distance to the MC in all the examined locations, which aligns with the findings of Eto et al.[7]

Determining the accurate insertion angle is critical for MI's stability and for avoiding contact with the anatomical structures in its vicinity, such as MC. Our analysis revealed significant variability in the angular values obtained, ranging from 29.7° at the vestibular mesiobuccal cusp of the right second molar to zero, the minimum value found across all locations. Although the average values suggest that the MI insertion angle is safer in more anterior regions, the finding of a minimum angle of zero degrees in all locations does not allow us to infer the possible angular capacity for MI insertion in either site. This suggests that each case must be assessed individually.

The MBS undergoes anatomical changes throughout the growth process.[21] Gandhi et al.[11] reported that growing females and males exhibited significantly wider MBS than their corresponding non-growing groups. In the older age group (>22 years), the angular capacities for MI insertion were found to be significantly greater along the mesiobuccal cusp, sulcus, and distobuccal cusp of the left second molar, with a similar corresponding distance available before reaching the MC in both age cohorts. Eto et al.[7] observed that patients aged between 20 and 40 years had significantly greater bone height relative to the MC when compared to other age groups. Gandhi et al.[11] bone height was significantly lower in growing females and males compared to their non-growing counterparts in the three locations studied (distal root of the first molar, mesial root of the second molar, and distal root of the second molar).

Our study noted that the transverse width of the MBS was significantly greater in males only at the mesial cusp of the right second lower molar. Regarding the distance to the CM, females exhibited significantly smaller measurements than males, suggesting the presence of sexual dimorphism associated with these variables. Minor asymmetry is a natural phenomenon present in individuals, influenced by genetic, environmental, or even random factors.[22] This study showed a significantly wider right MBS, vestibular to the mesial and distal lower second molar buccal cusps, than those on the equivalent left side. Furthermore, the possible MI insertion angulation without interfering with the MC was significantly greater at the distal cusp area, buccal groove, and mesiobuccal cusp of the right lower second molar than at the left corresponding sites. However, the distance from the midpoint of the MBS to the closest point of the MC was similar on both mandibular sides.

To maintain hygiene and minimize irritation to the surrounding soft tissue, an MI head should remain at least 5 mm above the level of the soft tissue.[23] In this context, the proposed size for the MI to be inserted into the MBS is 2x12, with a length of 15.8 mm. Based on this recommendation, an MI of approximately 9 to 10 mm in length would be inserted at the bone level. In the present study, the distance between the MI and the MC exhibited significant variability, ranging from 19.6 mm in the area tangent to the distal surface of the left lower second molars to 6.3 mm from the vestibular to the distobuccal cusp of the right lower second molar. The minimum measured values varied from 6.30 mm at the distobuccal cusp of the right second molars to 10.2 mm at the mesiobuccal cusp of the left lower second molars, indicating that the MBS is not entirely safe for MI insertion, regardless of the specific location.

Interestingly, in the absence of impacted third molars, the area tangent to the distal surface of the second molar appears to be the safest area for mini-implant insertion, demonstrating higher average distance values from the MC. This site also presents a more favorable average MBS transverse width. However, the minimum values noticed in this area were 8.6 mm on the right and 9.5 mm on the left, which do not allow it to be considered a completely safe zone, given that the typical bone level insertion length is 10 mm. Due to the above-reported reasons, it might be advisable to obtain a CBCT before MI insertion. However, the patient has to be informed about the increased CBCT radiation hazard and cost and contribute to the decision before inserting an MI, which relies on a 2D orthopantograph, accepting a small risk of possible iatrogenic injury to the MC.

Study Limitations

This study was performed at one center with limitations embedded in its retrospective design. More prospective multicenter investigations are recommended to consolidate the findings of our study.

CONCLUSION

Based on the analyzed data, the optimal location for MI insertion in the MBS, in the absence of impacted third molars, is the area adjacent to the distal surface of the second molar. This holds regardless of age, sex, or side of insertion. Our results indicate that this region not only has a greater MBS transverse width but also a longer distance to the MC. Nonetheless, given the observed variability in results, it is advisable to utilize CBCT as an adjunctive diagnostic tool for an MI insertion on MBS. CBCT enables a thorough examination of the MC position and aids in determining the feasible angulation across various mandibular bone structure regions, thereby mitigating the risk of injuries to the IAN.

Ethics

Ethics Committee Approval: The research protocol was secured by the Ethics Committee of the Egas Moniz School of Health & Science (approval no.: PT-288/23, date: 30.11.2023).

Informed Consent: Written consents were obtained from the participants before administering the CBCT scans.

Footnotes

Author Contributions: Concept - P.M.P., I.B.; Design - P.M.P., L.P., I.B.; Data Collection and/or Processing - J.F., L.P., J.B.; Analysis and/or Interpretation - J.F., I.B.; Literature Search - J.F., J.B.; Writing - J.F., P.M.P., L.P., I.B.

Conflict of Interest: The authors have no conflicts of interest to declare.

Financial Disclosure: This study did not receive any specific grant from funding agencies in the public, commercial, or not-for-profit sectors.

REFERENCES

1. Escobar-Correa N, Ramírez-Bustamante MA, Sánchez-Uribe LA, Upegui-Zea JC, Vergara-Villarreal P, Ramírez-Ossa DM. Evaluation of mandibular buccal shelf characteristics in the Colombian population: a cone-beam computed tomography study. *Korean J Orthod*. 2021;51(1):23-31. [CrossRef]
2. Alkadhimi A, Al-Awadhi EA. Miniscrews for orthodontic anchorage: a review of available systems. *J Orthod*. 2018;45(2):102-114. [CrossRef]
3. Mohammed H, Wafaie K, Rizk MZ, Almuzian M, Sosly R, Bearn DR. Role of anatomical sites and correlated risk factors on the survival of orthodontic miniscrew implants: a systematic review and meta-analysis. *Prog Orthod*. 2018;19(1):36. [CrossRef]
4. Park JH, ed. Temporary anchorage devices in clinical orthodontics. 1st ed. Wiley; 2020. [CrossRef]
5. Landin M, Jadhav A, Yadav S, Tadinada A. A comparative study between currently used methods and small volume-cone beam tomography for surgical placement of mini implants. *Angle Orthod*. 2015;85(3):446-453. [CrossRef]
6. Alharbi F, Almuzian M, Bearn D. Miniscrews failure rate in orthodontics: systematic review and meta-analysis. *Eur J Orthod*. 2018;40(5):519-530. [CrossRef]
7. Eto VM, Figueiredo NC, Eto LF, Azevedo GM, Silva AIV, Andrade I. Bone thickness and height of the buccal shelf area and the mandibular canal position for miniscrew insertion in patients with different vertical facial patterns, age, and sex. *Angle Orthod*. 2023;93(2):185-194. [CrossRef]
8. Velasco-Torres M, Padial-Molina M, Avila-Ortiz G, Garcia-Delgado R, Catena A, Galindo-Moreno P. Inferior alveolar nerve trajectory, mental foramen location and incidence of mental nerve anterior loop. *Med Oral*. 2017;22(5):e630-e635. [CrossRef]
9. Karatas OH, Toy E. Three-dimensional imaging techniques: a literature review. *Eur J Dent*. 2014;8(1):132-140. [CrossRef]
10. Elshebiny T, Palomo JM, Baumgaertel S. Anatomic assessment of the mandibular buccal shelf for miniscrew insertion in white patients. *Am J Orthod Dentofacial Orthop*. 2018;153(4):505-511. [CrossRef]
11. Gandhi V, Upadhyay M, Tadinada A, Yadav S. Variability associated with mandibular buccal shelf area width and height in subjects with different growth pattern, sex, and growth status. *Am J Orthod Dentofacial Orthop*. 2021;159(1):59-70. [CrossRef]
12. Nookala H, Sreenivasagan S, Sivakumar A, S AK. Computed tomographic evaluation of buccal shelf dimensions in South Indian patients with sagittal skeletal class III malocclusion: a retrospective study. *Cureus*. 2023;15(8):e43883. [CrossRef]
13. Matias M, Flores-Mir C, Almeida MRD, et al. Miniscrew insertion sites of infrazygomatic crest and mandibular buccal shelf in different vertical craniofacial patterns: a cone-beam computed tomography study. *Korean J Orthod*. 2021;51(6):387-396. [CrossRef]
14. Von Elm E, Altman DG, Egger M, Pocock SJ, Gøtzsche PC, Vandenbroucke JP. The strengthening the reporting of observational studies in epidemiology (STROBE) statement: guidelines for reporting observational studies. *Int J Surg*. 2014;12(12):1495-1499. [CrossRef]
15. Bruggesser S, Stöckli S, Seehra J, Pandis N. The reporting adherence of observational studies published in orthodontic journals in relation to STROBE guidelines: a meta-epidemiological assessment. *Eur J Orthod*. 2023;45(1):39-44. [CrossRef]
16. Oenning AC, Jacobs R, Pauwels R, et al. Cone-beam CT in paediatric dentistry: DIMITRA project position statement. *Pediatr Radiol*. 2018;48(3):308-316. [CrossRef]
17. Aleluia RB, Duplat CB, Crusoé-Rebello I, Neves FS. Assessment of the mandibular buccal shelf for orthodontic anchorage: influence of side, gender and skeletal patterns. *Orthod Craniofacial Res*. 2021;24(S1):83-91. [CrossRef]
18. Mohan R, Jain RK. Mandibular buccal shelf characteristics of South Indian population with different skeletal patterns- a retrospective cone beam computed tomographic study. *JCDR*. 2023;17(4):ZC19-ZC23. [CrossRef]
19. Vargas EOA, Lopes De Lima R, Nojima LI. Mandibular buccal shelf and infrazygomatic crest thicknesses in patients with different vertical facial heights. *Am J Orthod Dentofacial Orthop*. 2020;158(3):349-356. [CrossRef]
20. Kolge NE, Patni VJ, Potnis SS. Tomographic mapping of buccal shelf area for optimum placement of bone screws: a three-dimensional cone-beam computed tomography evaluation. *APOS*. 2019;9:241-245. [CrossRef]
21. Arango E, Plaza-Ruíz SP, Barrero I, Villegas C. Age differences in relation to bone thickness and length of the zygomatic process of the maxilla, infrazygomatic crest, and buccal shelf area. *Am J Orthod Dentofacial Orthop*. 2022;161(4):510-518.e1. [CrossRef]
22. Wang Y, Metoki A, Smith DV, et al. Multimodal mapping of the face connectome. *Nat Hum Behav*. 2020;4(4):397-411. [CrossRef]
23. Chang CH, Lin LY, Roberts WE. Orthodontic bone screws: a quick update and its promising future. *Orthod Craniofacial Res*. 2021;24(S1):75-82. [CrossRef]

TURKISH JOURNAL OF
ORTHODONTICS

DOI: 10.4274/TurkJOrthod.2025.2025.44

Original Article

Evaluation of Bracket Positioning; A Customized System Versus the Conventional Method

Kübra Sucu[1], Mete Özer[2]

[1]Vocational School of Health Services, University of Health Sciences, İstanbul, Türkiye
[2]Ondokuz Mayıs University Faculty of Dentistry, Department of Orthodontics, Samsun, Türkiye

Cite this article as: Sucu K, Özer M. Evaluation of bracket positioning; a customized system versus the conventional method. *Turk J Orthod.* 2025; 38(4): 206-215

Main Points

- Bracket placement varies in vertical position on the clinical crown depending on the method used, with differences observed among the Insignia system, the Kalange method, and Andrews' bracket-positioning approach.
- In both the Insignia system and the Kalange method, brackets tend to be positioned more incisally or occlusally relative to the facial axis point.
- In the Insignia system and Kalange method, anterior brackets are positioned more incisally than posterior brackets.

ABSTRACT

Objective: To evaluate the positioning of brackets in customized and conventional bonding methods in accordance with Andrews' approach to bracket placement.

Methods: Twenty-six patients were enrolled; 11 were treated with the Insignia system and 15 with Kalange's method. Crown length was measured on a digital diagnostic model and the facial axis (FA) point was calculated. After leveling and alignment, a new digital model was created, and the bracket position was measured along the vertical axis. The distance between the bracket position and the FA point was calculated, and the deviation was determined according to Andrews' method. Teeth with significant deviation (TSD), i.e., >0.5 mm, were identified. Frequencies and percentages of TSD were calculated.

Results: The TSD percentage was 56.65% in the Insignia group and 69.5% in the modified Kalange group; the difference between groups was significant (p=0.003). The anterior and posterior regions differed significantly within groups: in the Insignia group, this difference was observed in the maxilla (p=0.002), whereas in the modified Kalange group it was observed in both the mandible and maxilla (P < 0.001). In both groups, the anterior TSD percentage was higher than the posterior TSD percentage in both the maxilla and the mandible. The deviation was predominantly occlusal or incisal: Insignia group, 86.9%; modified Kalange group, 97.6%.

Conclusion: In the Insignia system and Kalange's method, brackets are positioned more incisally/occlusally relative to Andrews' FA point. In both methods, anterior brackets are positioned more incisally than posterior brackets.

Keywords: Bracket placement, Insignia, Kalange, Andrews

INTRODUCTION

The straight-wire appliance (SWA) is widely used in orthodontic treatment. In this technique, accurate bracket placement is the most crucial stage of treatment. If the bracket is not ideally placed, unplanned tooth movement occurs, leading to changes in the tip, torque, and rotation of the tooth. To rectify this error, archwire bending or bracket repositioning is usually necessary to achieve the desired outcome.[1,2]

Corresponding author: Lec. Kübra Sucu, **e-mail:** kubra.sucu@sbu.edu.tr
Received: April 10, 2025 **Accepted:** October 28, 2025 **Publication Date:** 30.12.2025

As a pioneer of the SWA technique, Andrews introduced two concepts related to bracket placement: the facial axis of the clinical crown (FACC) and the facial axis (FA) point. The FACC is defined as the long axis passing through the center of the facial surface of the clinical crown. The FA point is the midpoint of the FACC. Andrews identified the FA point as the optimal location for bracket placement and emphasized that the bracket's wings should be parallel to the FACC.[3-5]

Kalange introduced an indirect bonding method in which brackets were positioned on the teeth using millimetric measurements. He traced vertical lines indicating the long axes of the teeth and horizontal lines passing through the mesial and distal marginal edges of the posterior teeth on the study models. Brackets were positioned with reference to these lines.[6,7]

With the advancement of digital technologies, human errors in dentistry have been minimized. The Insignia™ Advantage System (Ormco, Brea, CA, USA), which incorporates self-ligating appliances and customized bracket slots, is among these developments. Using computer-assisted technology, a virtual design of the final alignment and occlusion can be obtained through reverse-engineered archwires and brackets. Bracket bases are standard; bracket slots are custom-produced to achieve the desired tooth movement through archwire progression, resulting in a straight finishing archwire. In the Insignia™ Advantage System, bracket-positioning points are determined virtually, and customized brackets are bonded using indirect-bonding transfer jigs.[8-13]

In the present study, the null hypothesis was that there would be no significant difference in the vertical bracket position on the clinical crown among the Insignia system, Kalange's method, and Andrews' bracket-positioning approach. The aim of the present study was to evaluate bracket positioning using customized and conventional bonding methods according to Andrews' approach to bracket placement.

METHODS

Ethical approval was obtained from the Ethics Committee of Ondokuz Mayıs University Medical Faculty (approval number: B.30.2.ODM.020.08/496, date: 14.06.2019). Since no study with the same design as the present one was found in the literature, the sample size was calculated based on the study by Koo et al.,[14] which was deemed most similar in design. With 80% power, a two-tailed significance level of 0.05, and transfer error means±standard deviations of 0.41±0.23 mm and 0.18±0.12 mm for the first and second groups, respectively, the minimum sample size calculated for the present study to detect a significant difference was 26 patients (13 per group). To compansate for possible dropout, the sample size was increased to 15 patients per group.

A total of 30 patients who presented to the Department of Orthodontics, Ondokuz Mayıs University Faculty of Dentistry were enrolled in the study. Written informed consent was obtained from all patients or their parents. The inclusion criteria were: (1) permanent dentition from the first molar to the first molar; and (2) Little's Irregularity Index[15] ≤3 mm (minimal crowding). The exclusion criteria were: (1) systemic diseases; (2) dentition that precludes ideal bracket placement; (3) dentition with shape or size anomalies, attrition, or abrasion; and (4) unhealthy gingival tissue. Based on the inclusion and exclusion criteria, the patients were allocated to two groups to undergo nonextraction fixed orthodontic treatment. The Insignia™ Advantage system was used in Group 1, and Kalange's method was used in Group 2.

Group 1 (Insignia)

- For each patient, an alginate impression (Zetalgin, Zhermack SpA, Badia Polesine, Italy) and a type C-polysiloxane impression (Zetaplus, Zhermack SpA) were taken. Two plaster models were obtained: a diagnostic model [T(0)] from the alginate impression and a treatment model from the C-polysiloxane impression.
- The treatment model was sent to the manufacturer (Ormco).
- Model scanning, digital modeling, and the initial setup were performed by a technician at Ormco.
- An orthodontist adjusted the ideal treatment plan using Insignia's Approver software (a trademark of Ormco).
- Custom-fabricated custom self-ligating brackets (Damon Q, Ormco), archwires, and transfer jigs were used.
- The orthodontist bonded the brackets using transfer jigs.

Group 2 (Modified Kalange)

- Two alginate impressions (Zetalgin, Zhermack SpA, Badia Polesine, Italy) were taken from each patient.
- Plaster models were obtained from these impressions: a diagnostic model [T(0)] and a treatment model.
- The treatment model was sent to a private orthodontic laboratory in Türkiye (Digital Ortodonti Laboratuvarı).
- Model scanning was performed using a 3D scanner (3Shape R-700 Desktop Orthodontic Scanner; 3Shape, Copenhagen, Denmark).
- Virtual brackets (Damon Q, Ormco) were placed on the teeth by a technician using Onyxceph³™ Dental Imaging Software (Chemnitz, Germany) in accordance with Kalange's method.
- The orthodontist verified the accuracy of the bracket placement and performed indirect bonding using the transfer tray fabricated from this setup. A virtual model with brackets was 3D-printed using a methacrylate-based resin (IMPRIMO® LC Model, Scheu-dental GmbH, Iserlohn, Germany).
- A transfer tray was fabricated from a double-layer, vacuum-formed viscoelastic plate (INDIVIDUA® Foil, Scheu-Dental GmbH) using the virtual model with brackets.

- The brackets were placed in the transfer tray.
- And the orthodontist performed indirect bonding using this tray.

All patients in both groups were treated by the same orthodontist. Four patients in the Insignia™ group who failed to attend scheduled appointments regularly were excluded from the study. In cases of bracket debonding, the teeth involved were excluded from the analysis.

In both groups, the leveling and aligning stages were completed with a 0.019″×0.025″ stainless-steel archwire, which remained in place for at least 1 month. After this period, the archwire was removed, an alginate impression was taken, and a plaster model with brackets, T(1), was obtained.

Measurement Technique

The T(0) and T(1) models were digitized using the 3D scanner (3Shape R700, 3Shape, Copenhagen, Denmark). Bracket positions were evaluated using the Ortho Analyzer software (3Shape) according to the FA point defined by Andrews.

Step 1: The crown lengths of anterior and premolar teeth were measured on virtual T(0) models as the linear distance between the gingival zenith and the incisal edge or cusp tip, parallel to the long axis of each tooth (Figure 1).

Step 2: On the virtual T(1) models, horizontal planes passing through the mesial and distal contact points of the premolars were defined on virtual T(1) models (Figure 2).

Step 3: For the anterior teeth, horizontal planes passing through the centers of the bracket slots were created for the anterior teeth on virtual T(1) models (Figure 3).

***All planes shown in Figure 2 and Figure 3 were created perpendicular to the teeth.

Step 4: The value a was calculated by dividing each crown length by two, and the ideal bracket positioning points were determined according to Andrews (Figure 1). For the anterior teeth, the value b was measured as the distance from the horizontal plane to the incisal edge or cusp tip (Figure 3). For the posterior teeth, value b was calculated by summing the distance from the bracket center and from the cusp tips to the horizontal plane, and then summing these distances (Figure 4). Finally, the value c was obtained by subtracting value a from value b to quantify the deviation from the ideal bracket position.

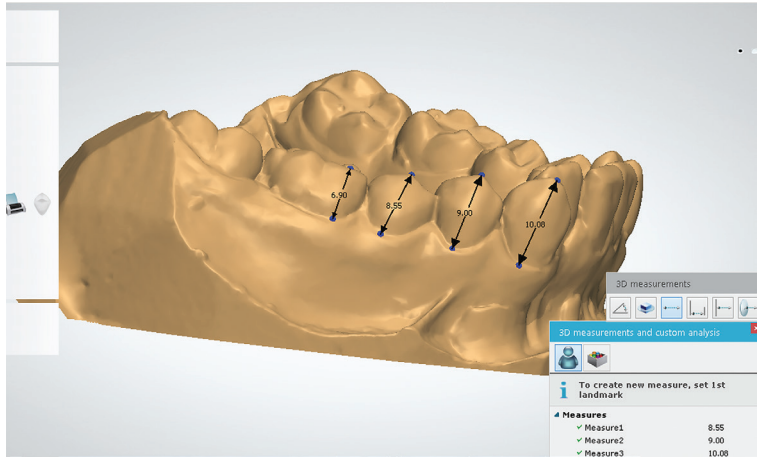

Figure 1. Measurement of the crown length.

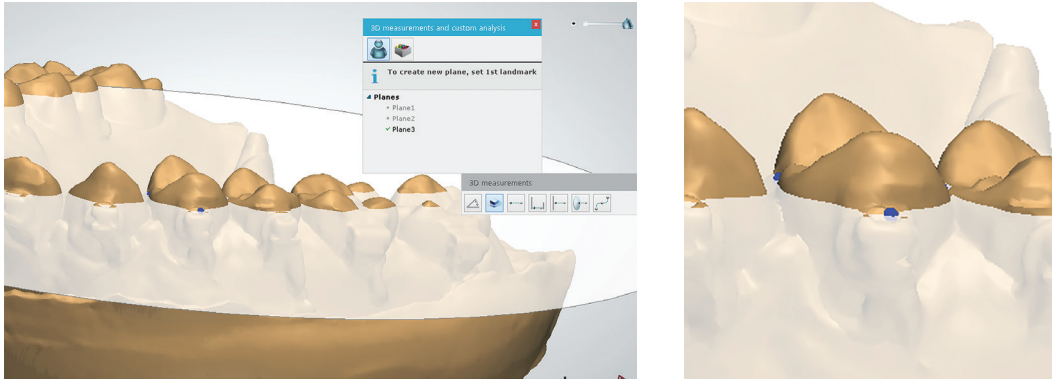

Figure 2. A horizontal plane passing through the mesial and distal contact points of the premolar tooth.

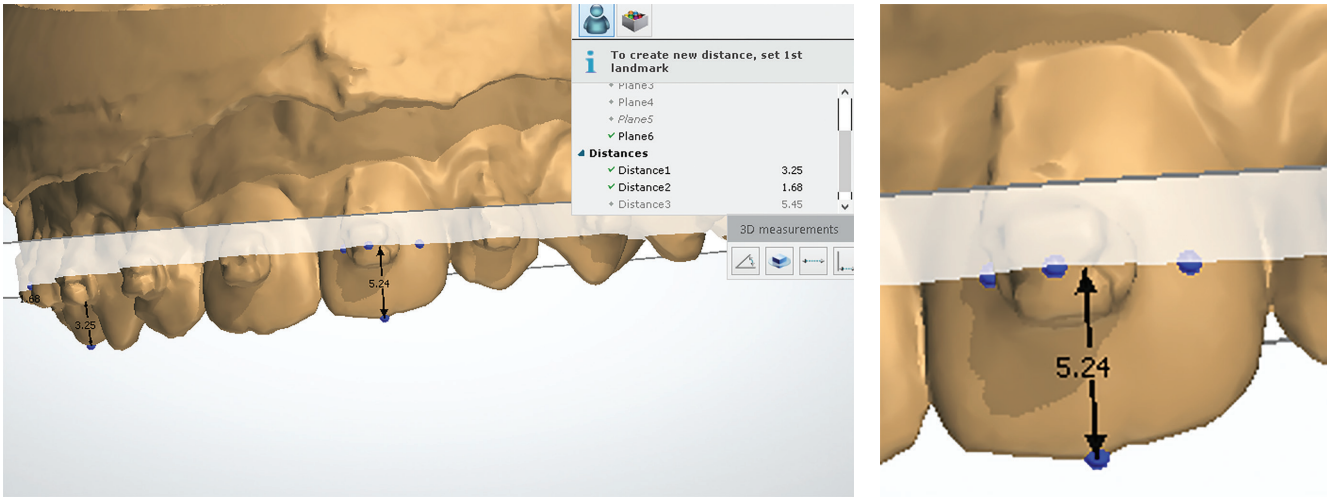

Figure 3. A horizontal plane passing through the center of the slot of the central bracket.

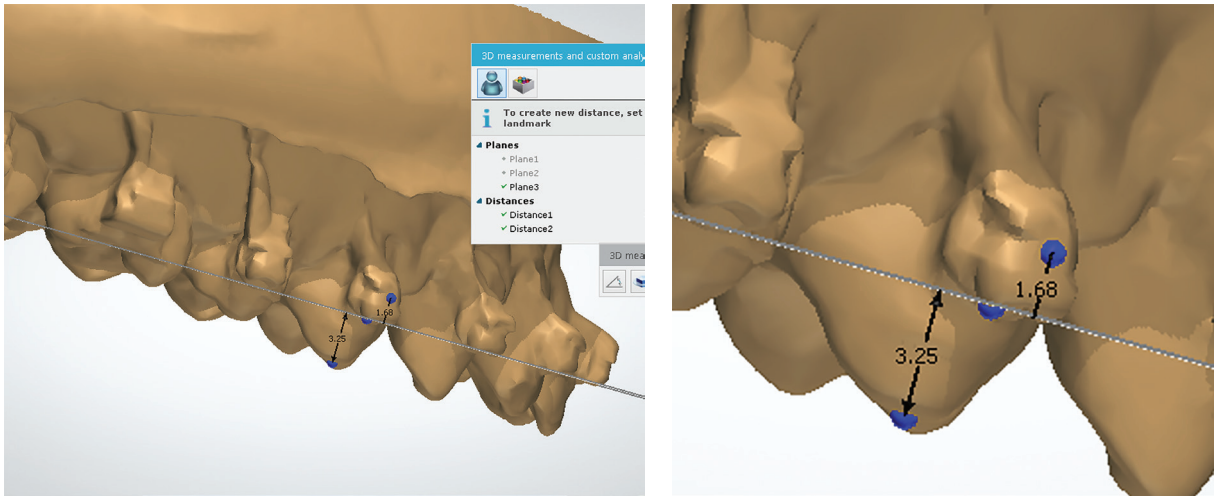

Figure 4. The distances from the center of the bracket and the tip of the cusp to the horizontal plane.

Assessment of Bracket Positions

The deviation of each bracket from its ideal position was calculated using the following formula:

(value b) - (value a) = (value c)

If value c=0, the bracket was positioned ideally.

If value c<0, the bracket was positioned gingivally.

If value c>0, the bracket is positioned incisally or occlusally.

According to Andrews, an acceptable error limit for bracket positioning accuracy is 0.5 mm or less.[16] Therefore, the the deviations were classified as follows:

If |value c| >0.5 mm, the deviation was considered significant.

If |value c| ≤0.5 mm, the deviation was considered not significant.

Statistical Analysis

SPSS 26.0 for Windows 64-bit software (SPSS, Chicago, IL, USA) was used for the statistical analyses. The Kolmogorov-Smirnov and Shapiro-Wilk tests were performed to assess whether continuous variables followed a normal distribution, and skewness and kurtosis values were examined. Variables with a p-value ≥0.05 in the normality tests were considered to follow a normal distribution. The consistency between observers was confirmed using Pearson's correlation coefficient calculated from bivariate analysis. Categorical variables were described as frequencies and percentages and compared using the chi-squared test. Mean differences between independent groups were analyzed using Student's t-test. Power analysis was performed using G*Power 3.1.

RESULTS

The power of the present study was calculated to be 86% for the overall measurement at the 95% confidence level. To determine the intraclass correlation, seven models were selected and measurements were repeated by a second practitioner. The correlation coefficients ranged from 0.90 to 1.00, indicating excellent agreement between observers.

Table 1 presents the demographic data for the modified Kalange and Insignia groups. The Insignia group consisted of 11 patients (216 teeth) whereas the modified Kalange group included 15 patients (295 teeth). The study included 7 female participants in the Insignia group and 12 female participants in the modified Kalange group. The mean age was 15.5 years (standard deviation 1.4) in the modified Kalange group and 15.2 years (standard deviation 2.2) in the Insignia group.

Table 2 shows the comparison of crown lengths across groups, with no significant differences observed for any tooth. Table 3 presents the percentages of teeth with significant deviation (TSD) for each group and the p-values. A significant difference between the groups was observed for all lower anterior teeth [p<0.001 (L3), p=0.003 (L2), and p=0.001 (L1)]. The overall percentage of TSD was 56.6% and 69.5% in the Insignia and modified Kalange groups, respectively. The difference between the groups was significant (p=0.003).

Table 4 presents the percentage of TSD by region. In the Insignia group, the percentage of TSD was 66.2% for the anterior maxilla and 34.1% for the posterior maxilla, indicating a significant difference between these regions (p=0.002). The percentage of TSD was 66.2% in the anterior mandible and 50.0% in the posterior mandible, with no significant differences observed between these regions. In the modified Kalange group, the percentage of TSD was 78.9% in the anterior maxilla and 15% in the posterior maxilla, indicating a significant difference between these regions (p<0.001). In the mandible, TSD occurred in 100% of the anterior region and 64.3% of the posterior region, again showing a significant difference (p<0.001).

Tables 5 and 6 show the directions of deviation. In the Insignia group, all anterior TSDs exhibited incisal deviation. Among the maxillary posterior TSDs, 86.7% deviated gingivally. For the mandibular posterior TSD, 85.7% deviated in the occlusal direction. In the modified Kalange group, all anterior TSDs also showed incisal deviation. Moreover, among the maxillary posterior TSDs, 66.7% showed occlusal deviation, while 94.4% of the mandibular posterior TSDs showed occlusal deviation. Overall, 86.9% of TSDs in the Insignia group and 97.6% in the modified Kalange group deviated occlusally or incisally.

Figure 5 illustrates the percentage of TDS alongside the direction of deviation for each group.

Table 1. Demographic data for the Insignia and Modified Kalange groups

	Insignia	Modified Kalange	Overall
Number of patients (n, %)	11 (42.3%)	15 (57.7%)	26 (100%)
Female (n, %)	7 (63.6%)	12 (80%)	19 (73.1%)
Age (mean±SD)	15.55±1.44	15.27±2.25	15.38±1.92
Number of teeth (n, %)	216 (42.3%)	295 (57.7%)	511

SD, standard deviation.

Table 2. Comparison of crown lengths between the groups

	Insignia		Modified Kalange		
Tooth	**N**	**Mean±SD (mm)**	**N**	**Mean±SD (mm)**	**p-value**
U5	22	6.61±0.69	30	6.71±0.65	0.595
U4	22	7.38±0.73	30	7.5±0.57	0.526
U3	22	9.63±1.33	30	9.68±0.66	0.869
U2	22	8.49±0.95	30	8.37±0.66	0.62
U1	21	10.16±1.18	30	10.36±0.81	0.470
L5	21	7.21±0.76	27	7.31±0.5	0.586
L4	21	8.2±0.99	29	8.31±0.43	0.596
L3	22	10.03±1.46	30	10±0.58	0.862
L2	21	9.04±1.12	30	9.23±0.43	0.431
L1	22	8.75±0.8	29	9.04±0.5	0.128

p-values calculated by Student's t-test, significance level, p≤0.05.
N, total number of teeth; SD, standard deviation.

Table 3. Comparison between the percentages of teeth with significant deviation for each group

	Insignia			Modified Kalange			
Tooth	N	n	n (%)	N	n	n (%)	p-value
U5	22	7	31.8	30	4	13.3	0.169
U4	22	8	36.4	30	5	16.7	0.195
U3	22	13	59.5	30	21	70	0.602
U2	22	12	54.5	30	23	76.7	0.167
U1	21	18	85.7	30	27	90	0.680
L5	21	9	42.9	27	17	63	0.274
L4	21	12	57.1	29	19	65.5	0.759
L3	22	13	59.1	30	30	100	<0.00*
L2	21	15	71.4	30	30	100	0.003*
L1	22	15	68.2	29	29	100	0.001*
Overall	216	122	56.5	295	205	69.5	0.003*

*Statistically significant difference, significance level, p≤0.05.
N, total number of teeth; n, number of teeth with significant deviation; p-values calculated by the chi-squared test.

Table 4. Comparison between the percentages of teeth with significant deviation by region

	Maxillary anterior region			Maxillary posterior region			
	N	n	n (%)	N	n	n (%)	p
Insignia	65	43	66.2	44	15	34.1	0.002*
Modified Kalange	90	71	78.9	60	9	15.0	<0.00*
	Mandibular anterior region			Mandibular posterior region			
	N	n	n (%)	N	n	n (%)	p
Insignia	65	43	66.2	42	21	50.0	0.144
Modified Kalange	89	89	100	56	36	64.3	<0.00*

*Statistically significant difference, significance level, p≤0.05.
N, total number of teeth; n, number of teeth with significant deviation; p-values calculated by the chi-squared test.

Table 5. Number/percentage of teeth with significant deviation positioned occlusally/incisally or gingivally

	Insignia					Modified Kalange				
		O/I		G			O/I		G	
Tooth	N	n	n (%)	n	n (%)	N	n	n (%)	n	n (%)
U5	7	1	14.3	6	85.7	4	2	50	2	50
U4	8	1	12.5	7	87.5	5	4	80	1	20
U3	13	13	100	0	0	21	21	100	0	0
U2	12	12	100	0	0	23	23	100	0	0
U1	18	18	100	0	0	27	27	100	0	0
L5	9	9	100	0	0	17	16	94.1	1	5.9
L4	12	9	75	3	25	19	18	94.7	1	5.3
L3	13	13	100	0	0	30	13	100	0	0
L2	15	15	100	0	0	30	15	100	0	0
L1	15	15	100	0	0	29	15	100	0	0
Overall	122	106	86.9	16	13.1	205	200	97.6	5	2.4

N, total number of teeth with significant deviation; n, number of teeth with significant deviation; O, occlusally; I, incisally; G, gingivally.

DISCUSSION

Accurate bracket placement is a crucial part of treatment using the SWA technique. To achieve the desired tooth movement, ideal bracket positioning is required.[17] Andrews emphasized that the bracket should be positioned at the midpoint of the clinical crown and on the long axis of the tooth to achieve accurate expression of the bracket prescription. This study aimed to evaluate the bracket positions obtained by two different methods, using this concept as a reference. The findings revealed significant differences between the groups in both overall and regional deviations; therefore, the null hypothesis was rejected.

The Insignia™ Advantage system positions brackets digitally on a 3D model. This system aims to control tooth positions and arch form in 3D, ensure occlusal contacts, and achieve an excellent smile design.[8,18] The system uses the reverse-engineering principle and determines the positions and occlusal relationships of the teeth at the end of the treatment using 3D simulation. Bracket placement is performed according to this virtual setup.

Table 6. Number/percentage of teeth with significant deviation positioned occlusally/incisally or gingivally by region

	Insignia					Modified Kalange				
		O/I		G			O/I		G	
Region	N	n	n (%)	n	n (%)	N	n	n (%)	n	n (%)
Maxillary anterior	43	43	100	0	0	71	71	100	0	0
Maxillary posterior	15	2	13.3	13	86.7	9	6	66.7	3	33.3
Mandibular anterior	43	43	100	0	0	89	89	100	0	0
Mandibular posterior	21	18	85.7	3	14.3	36	34	94.4	2	5.6

N, total number of teeth; n, number of teeth with significant deviation; O, occlusally; I, incisally; G, gingivally.

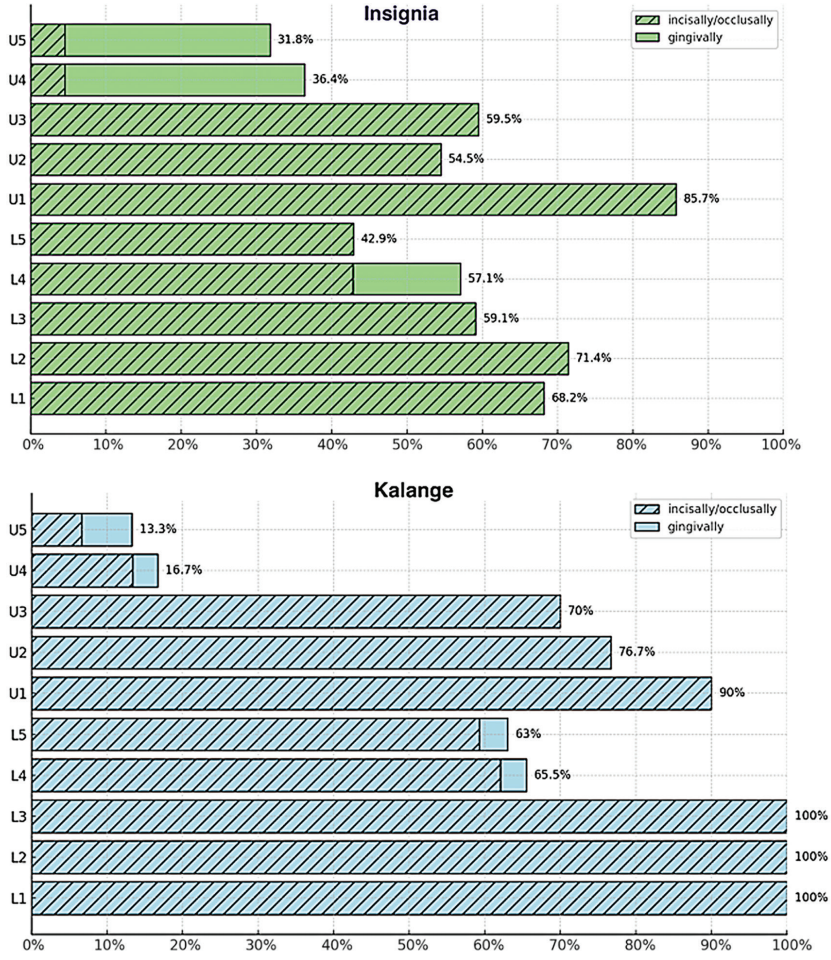

Figure 5. Percentages of teeth with significant deviation and directions of deviation.

In Kalange's method, a conventional indirect bonding technique, the brackets are placed on vertical lines indicating the long axes of the teeth and on horizontal lines parallel to the mesial and distal marginal ridges of the posterior teeth. These lines are customized for each patient and serve as a guide for bracket placement. The method aims to achieve aesthetic harmony, fulfill the treatment objectives, and ensure proper function with leveled marginal ridges, canine guidance, and incisor guidance.[7] In the present study, Kalange's technique was modified so that brackets were positioned digitally on 3D virtual models rather than manually on plaster casts. This modification allowed both the Insignia and the modified Kalange methods to be implemented within a standardized digital workflow. Consequently, bracket positioning was conducted in a computer environment for both Kalange's method and the Insignia system, achieving standardization between the two methodologies.

Treatment models in the Insignia and modified Kalange groups were produced using two impression materials: polyvinyl siloxane and alginate. Previous studies by Petrović et al.[19] and Bud et al.[20] have demonstrated that plaster models produced from silicone impressions are more accurate than plaster models produced from alginate. However, Torassian et al.[21] reported that plaster models produced from a traditional color-change alginate and stored for up to one week exhibited dimensional deviations of less than 0.5 mm, which are clinically insignificant. Similarly, Vogel et al.[22] concluded that alginate-derived plaster models are reliable for orthodontic use. In the present study, although the impression materials differed between the two groups, the discrepancy remained within acceptable limits and was considered negligible in both groups.

The effect of transfer trays on bracket positioning in indirect bonding methods has been investigated in previous studies. Gündoğ et al.,[23] Schmid et al.,[24] and Niu et al.[25] reported clinical acceptability rates for double vacuum-formed trays of 95%, 94%, and 91.4%, respectively. The mean deviations were 0.23 mm, 0.10 mm, and 0.23 mm; the first and third values (0.23 mm) include molars, where most deviations occurred. Gündoğ et al.[23] and Niu et al.[25] found that 3D-printed transfer trays demonstrated higher accuracy than vacuum-formed trays; however, the data obtained from both methods were clinically comparable. Furthermore, in a study comparing CAD-CAM systems, Albertini et al.[26] reported that the mean vertical deviation of the Insignia system was 0.28 mm. Dr. Leon Verhagen stated that the Insignia system achieved a bracket-transfer accuracy of 98% based on more than 105 Insignia SL cases.[27] In the present study, although the bracket transfer methods differed between the two groups, bracket accuracy was judged-based on previous research-to be within clinically acceptable limits and was therefore considered unlikely to have introduced bias into the outcomes.

In the Insignia group, the percentage of TSD was over 50% for all teeth except U4s, U5s, and L5s (which showed deviations of 36.4%, 31.8%, and 42.8%, respectively), resulting in an overall deviation ratio of 56.5%. This difference may be attributed to the approach used for bracket placement. While Andrews conventionally places brackets directly on the patient in a clinical setting based on clinical crown length, the Insignia system, as claimed by the manufacturer, evaluates all morphological characteristics of each tooth individually for bracket placement. It is claimed that the system takes into account arch form and pretreatment in-out, tip, and torque values, with the stated aim of achieving a more precise treatment plan and more accurate bracket placement.[28]

Kalangeon the other hand, argues that although Andrews' FA point concept provides a solid theoretical foundation, it presents several limitations in certain clinical situations. Kalange indicates that, in patients with large anterior and small posterior teeth, extrusion of the anterior teeth and intrusion of the posterior teeth would be expected, whereas the opposite pattern would occur in patients with small anterior and large posterior teeth. When both methods are compared, the Kalange approach results in bracket placement that is more incisal/occlusal on large teeth and more gingival on small teeth compared to the FA point. Kalange suggests that this individualized bracket placement strategy may help prevent clinical complications associated with the Andrews method.[7]

German et al.[29] synthesized data from studies on anterior crown length conducted by Chu[30], Chu and Okubo[31] and presented mean values in a summary chart. Consistent with these findings, Volchansky et al.[32] comprehensively reported the clinical crown lengths of the maxillary and mandibular teeth. The measurements in our study were consistent with those reported in previous research. Moreover, no significant differences were found in crown length values between the modified Kalange and Insignia groups. In the present study, except for U4 and U5 (13.3% and 16.7%, respectively), the percentage of TSD exceeded 50% for all teeth, resulting in an overall percentage of 69.5% in the modified Kalange group. Considering the directions of bracket deviations, 97.6% of TSD were oriented in the incisal/occlusal direction. Our findings suggest that the deviation observed in the Kalange group is not due to individual variation in crown length but is directly attributable to Kalange's methodology.

In Kalange's method, posterior brackets are positioned 2 mm gingival to the horizontal line passing through the marginal ridges of the teeth. For anterior brackets, the reference point is the distance from the bracket position on the first premolar to the cusp tip of the same tooth. Given that the present study included teeth with average crown lengths, these findings indicate that the 2-mm reference value used in Kalange's method is insufficient for such teeth according to Andrews' concept. This results in the brackets being positioned incisal to the midpoint of the clinical crown.

In our study, the anterior and posterior regions were also compared. A significant difference in the number of TSDs between the anterior and posterior regions of the maxilla was observed in the Insignia group (p=0.002). In the modified

Kalange group, significant differences were observed between the anterior and posterior regions of both the mandible and the maxilla ($p<0.001$ for both regions). In both groups, deviation rates in the anterior regions of the maxilla and mandible were higher than those in the posterior regions. Examination of bracket direction showed that all anterior brackets in both groups were positioned incisally. This positioning of the brackets may result in intrusion of anterior teeth and, due to their more gingival placement, extrusion of posterior teeth. In both methods, these tooth movements may facilitate the flattening of the curve of spee and enable easier interdigitation, thereby reducing the need for a finishing stage in orthodontic treatment.

In the Insignia group, as mentioned above, in addition to differences between the anterior and posterior regions of the maxilla, the deviation ratio of U1 was higher (85.7%) than that of U2 and U3 (54.5% and 59.5%, respectively). It may be considered that both of these factors lead to an increased compensating curve and a flat smile arc characterized by a maxillary incisal arc line that is flatter than the curvature of the lower lip on smile.[33-35] That similar results were observed in the modified Kalange group-where bracket positions are determined using the incisal edge or cusp tip as reference points and millimetric adjustments are made to ensure esthetic alignment-calls into question the Andrews approach. These results should be corroborated by comparative studies that evaluate the impact of bracket-positioning methods on the smile arc at treatment completion.

In the SWA technique, bracket position is the primary factor affecting the tip, torque, and rotation of the tooth. Variations in bracket placement methods can significantly affect treatment outcomes by causing differences in tooth movement. Although digital treatment planning within the Insignia system facilitates accurate results, the potential for errors in bracket positioning remains a concern.[12] In addition, estimation of the midpoint of the clinical crown using Andrews' method may be subject to human error. Conducting two-dimensional measurements within a three-dimensional environment may compromise standardization in Kalange's method. Our study focuses on determining differences in bracket position among the methods mentioned, using measurements. In light of the results obtained, future studies evaluating the impact of differences in bracket placement on the effectiveness of orthodontic treatment will complement the present research.

Study Limitations

Certain limitations inherent to the study design should be acknowledged. Although all patients were enrolled within the same time period and both the methodology and the examiner were consistent, prospective randomization was not implemented. Although any resulting bias is likely negligible, its potential influence on the outcomes cannot be entirely excluded.

In order to enhance the statistical power of our study, the initial sample size was expanded. However, several patients in the Insignia group were excluded due to follow-up issues, which reduced the final sample size. This limitation should be considered within the scope of the study.

CONCLUSION

In both the Insignia system and Kalange's method, brackets were positioned more incisally or more occlusally relative to Andrews' FA point. In both systems, anterior brackets were positioned more incisally than posterior brackets.

Ethics

Ethics Committee Approval: Ethical approval was obtained from the Ethics Committee of Ondokuz Mayıs University Medical Faculty (approval number: B.30.2.ODM.020.08/496, date: 14.06.2019).

Informed Consent: Informed consent was obtained from all participants or their legal guardians after all explanations and clarifications regarding the trial had been provided.

Footnotes

Author Contributions: Surgical and Medical Practices - K.S., M.Ö.; Concept - K.S., M.Ö.; Design - K.S., M.Ö.; Data Collection and/or Processing - K.S.; Analysis and/or Interpretation - K.S., M.Ö.; Literature Search - K.S.; Writing - K.S.

Conflict of Interest: The authors have no conflicts of interest to declare.

Financial Disclosure: The authors declare that this study has received no financial support.

REFERENCES

1. Carlson SK, Johnson E. Bracket positioning and resets: five steps to align crowns and roots consistently. *Am J Orthod Dentofacial Orthop.* 2001;119(1):76-80. [CrossRef]
2. Suárez C, Vilar T. The effect of constant height bracket placement on marginal ridge levelling using digitized models. *Eur J Orthod.* 2010;32(1):100-105. [CrossRef]
3. Andrews LF. The straight-wire appliance, origin, controversy, commentary. *J Clin Orthod.* 1976;10(2):99-114. [CrossRef]
4. Andrews LF. The straight-wire appliance. Explained and compared. *J Clin Orthod.* 1976;10(3):174-195. [CrossRef]
5. Andrews LF. The straight-wire appliance. *Br J Orthod.* 1979;6(3):125-143. [CrossRef]
6. Kalange JT. Ideal appliance placement with APC brackets and indirect bonding. *J Clin Orthod.* 1999;33(9):516-526. [CrossRef]
7. Kalange JT. Prescription-based precision full arch indirect bonding. *Seminars in Orthodontics.* 2007;13(1):25-36. [CrossRef]
8. Gracco A, Stellini E, Parenti SI, Bonetti GA. Individualized orthodontic treatment: the Insignia system. *Orthodontics (Chic.).* 2013;14(1):e88-e94. [CrossRef]
9. Kim E, Sherf N, Lamichane M, et al. A comparison of SureSmile, Insignia, and Invisalign in treating non-extraction cases of mild to moderate crowding: a prospective clinical trial. *Australas Orthod J.* 2022;38(2):290-306. [CrossRef]

10. Weber DJ, Koroluk LD, Phillips C, Nguyen T, Proffit WR. Clinical effectiveness and efficiency of customized vs. conventional preadjusted bracket systems. *J Clin Orthod.* 2013;47(4):261-266. [CrossRef]
11. Aldrees AM. Do customized orthodontic appliances and vibration devices provide more efficient treatment than conventional methods? *Korean J Orthod.* 2016;46(3):180-185. [CrossRef]
12. Grauer D, Wiechmann D, Heymann GC, Swift EJ Jr. Computer-aided design/computer-aided manufacturing technology in customized orthodontic appliances. *J Esthet Restor Dent.* 2012;24(1):3-9. [CrossRef]
13. Perri A, Gracco A, Siviero L, Parenti IS, Ippolito DR. Customized orthodontics: the Insignia system. *Int J Orthod Milwaukee.* 2014;25(4):17-20. [CrossRef]
14. Koo BC, Chung CH, Vanarsdall RL. Comparison of the accuracy of bracket placement between direct and indirect bonding techniques. *Am J Orthod Dentofacial Orthop.* 1999;116(3):346-351. [CrossRef]
15. Little RM. The irregularity index: a quantitative score of mandibular anterior alignment. *Am J Orthod.* 1975;68(5):554-563. [CrossRef]
16. Taylor NG, Cook PA. The reliability of positioning pre-adjusted brackets: an in vitro study. *Br J Orthod.* 1992;19(1):25-34. [CrossRef]
17. Balut N, Klapper L, Sandrik J, Bowman D. Variations in bracket placement in the preadjusted orthodontic appliance. *Am J Orthod Dentofacial Orthop.* 1992;102(1):62-67. [CrossRef]
18. Gracco A, Tracey S. The insignia system of customized orthodontics. *J Clin Orthod.* 2011;45(8):442-451; quiz 467-quiz 468. [CrossRef]
19. Petrović V, Šlaj M, Buljan M, Čivljak T, Zulijani A, Perić B. Comparison of tooth size measurements in orthodontics using conventional and 3D digital study models. *J Clin Med.* 2024;13(3):730. [CrossRef]
20. Bud ES, Bocanet VI, Muntean MH, et al. Extra-oral three-dimensional (3D) scanning evaluation of three different impression materials-an in vitro study. *Polymers (Basel).* 2022;14(17):3678. [CrossRef]
21. Torassian G, Kau CH, English JD, et al. Digital models vs plaster models using alginate and alginate substitute materials. *Angle Orthod.* 2010;80(4):474-481. [CrossRef]
22. Vogel AB, Kilic F, Schmidt F, Rübel S, Lapatki BG. Dimensional accuracy of jaw scans performed on alginate impressions or stone models: a practice-oriented study. *J Orofac Orthop.* 2015;76(4):351-365. [CrossRef]
23. Gündoğ H, Arman Özçırpıcı A, Pamukçu H. Transfer accuracy of three indirect bonding trays: an in vitro study with 3D scanned models. *Turk J Orthod.* 2023;36(1):1-9. [CrossRef]
24. Schmid J, Brenner D, Recheis W, Hofer-Picout P, Brenner M, Crismani AG. Transfer accuracy of two indirect bonding techniques-an in vitro study with 3D scanned models. *Eur J Orthod.* 2018;40(5):549-555. [CrossRef]
25. Niu Y, Zeng Y, Zhang Z, Xu W, Xiao L. Comparison of the transfer accuracy of two digital indirect bonding trays for labial bracket bonding. *Angle Orthod.* 2021;91(1):67-73. [CrossRef]
26. Albertini P, Tremaroli M, Cremonini F, Palone M. Comparison of bracket position accuracy with different CAD/CAM indirect bonding systems. *Pesqui Bras Odontopediatria Clín Integr.* 2021;21(supp1):e210028. [CrossRef]
27. Ormco. Insignia™ Advantage. Accessed August 28, 2025. [CrossRef]
28. Scholz RP, Sarver DM. Interview with an insignia doctor: David M. Sarver. *Am J Orthod Dentofacial Orthop.* 2009;136(6):853-856. [CrossRef]
29. German DS, Chu SJ, Furlong ML, Patel A. Simplifying optimal tooth-size calculations and communications between practitioners. *Am J Orthod Dentofacial Orthop.* 2016;150(6):1051-1055. [CrossRef]
30. Chu SJ. Range and mean distribution frequency of individual tooth width of the maxillary anterior dentition. *Pract Proced Aesthet Dent.* 2007;19(4):209-215. [CrossRef]
31. Chu SJ, Okubo S. Range and mean discordance of individual tooth width of the mandibular anterior dentition. *Pract Proced Aesthet Dent.* 2008;20(5):313-320. [CrossRef]
32. Volchansky A, Cleaton-Jones P, Fatti LP. A technique for computer plotting of clinical crown height derived from orthodontic study models. *J Dent.* 1981;9(2):150-156. [CrossRef]
33. Sarver DM. The importance of incisor positioning in the esthetic smile: the smile arc. *Am J Orthod Dentofacial Orthop.* 2001;120(2):98-111. [CrossRef]
34. Pitts TR. Bracket positioning for smile arc protection. *J Clin Orthod.* 2017;51(3):142-156. [CrossRef]
35. Alam MK, Abutayyem H, Almaslamani MJ, Odeh R. Bracket positioning has an impact on smile arc protection: a systematic review and meta-analysis. *Bangladesh Journal of Medical Science.* 2025;24(3):984-994. [CrossRef]

TURKISH JOURNAL OF
ORTHODONTICS

DOI: 10.4274/TurkJOrthod.2025.2025.16

Original Article

Measurement of Aligner Thickness and Gap Width in Two Types of Clear Aligner Sheets Manufactured Using Two Different Thermoforming Machines - A Nano-CT Pilot Study

Gowardhan S, Mahalakshmi Krishnakumaran, Balaji Krishnan, Shanthini Priya Arumugam, Aswini Soundharya Sekar, Subashree R

Tagore Dental College and Hospital, Clinic of Orthodontics, Chennai, India

Cite this article as: S G, Krishnakumaran M, Krishnan B, Arumugam SP, Sekar AS, R S. Measurement of aligner thickness and gap width in two types of clear aligner sheets manufactured using two different thermoforming machines - a nano-CT pilot study. *Turk J Orthod.* 2025; 38(4): 216-223

Main Points

- Aligner material type and tooth morphology (especially in the molar region) are important factors influencing aligner fit and thickness.
- Both thermoforming machines generated aligners that were clinically acceptable in terms of fit, particularly in the anterior region.
- Aligner thickness generally decreased from the posterior (molar) to the anterior (incisor) tooth structures. Conversely, adaptation was greater in the anterior region (smaller gap width) than in the posterior region.
- The results underscore the importance of appropriate material selection and thermoforming precision for effective anchorage and force delivery, especially in the posterior segments of the dental arch.

ABSTRACT

Objective: The aim of this study was to compare the effects of two thermoforming machines on the gap width and thickness of passive aligners with the same nominal thickness from different manufacturers by using nano-computed tomography (CT).

Methods: An intraoral scan of a patient with Angle's Class I malocclusion was conducted, and a 3D maxillary arch model was printed. The aligners (n=16) were fabricated using two thermoforming machines: Ministar machine (n=8) and a Plastpress machine (n=8). Each group was subdivided on the basis of aligner material: polyethylene terephthalate glycol (PET-G) (Group A) and thermoplastic polyurethane (TPU) (Group B). Sheets with a nominal thickness of 0.75 mm were used. Nano-CT was performed, and the rendered 3D models were sliced into central incisor, canine, and molar regions to assess gap width and aligner thickness in the buccal, incisal, and palatal regions.

Results: Comparing thermoforming machines, PET-G (p=0.010) and TPU (p=0.004) aligners showed significant differences in gap width in the molar region. Similar results were found for aligner thickness (TPU, p=0.05; PET-G, p=0.004). Comparing PET-G and TPU sheets thermoformed via the same machine, significant differences were observed only in the molar region (p=0.004), with no differences in the canine and incisor regions. Adaptation in the anterior region was greater than in that of the posterior region, whereas aligner thickness increased from posterior to anterior.

Conclusion: Aligner material type significantly affected gap width and thickness only in the molar region, whereas the specific thermoforming machine did not substantially affect these characteristics.

Keywords: Gap width, aligner thickness, thermoforming procedures, thermoforming machines

Corresponding author: Prof. Mahalakshmi Krishnakumaran, **e-mail:** mahakrishnasai@gmail.com
Received: January 30, 2025 **Accepted:** September 21, 2025 **Publication Date:** 30.12.2025

INTRODUCTION

Clear aligners (CAs) were initially introduced by Tooth Positioner Orthodontics in 1945,[1,2] facilitating tooth movement through the use of tooth positioners. They encompass a variety of devices, each with unique mechanisms, construction methods, and applicability in the treatment of malocclusions. Originally, CAs were designed to address minor tooth irregularities. While some aligner systems are effective in correcting minor malalignments, others are intended for more complex malocclusions.[3,4] However, there is a lack of published clinical evidence to substantiate these claims, and the available evidence is often of low scientific quality.[5] The integration of advanced transparent thermoplastic materials and computer technology, including computer-aided design (CAD)-computer aided manufacturing, stereolithography (STL), and tooth movement simulation software, has significantly enhanced the use of CA products in the correction of malocclusions. Materials such as polyethylene terephthalate glycol (PET-G) and thermoplastic polyurethane (TPU) are widely used in orthodontic aligners, and their properties influence clinical performance and patient satisfaction. Recent advancements in CA materials have prompted research into aligner properties, including temperature, humidity, thickness, elastic deformation duration, and thermoforming,[5,6] thereby validating the reliability of CAs in treating malalignment. These factors are linked to optical properties, force generation, retention, and movement predictability.[7,8] PET-G, a non-crystalline copolymer of PET modified with cyclohexanedimethanol, provides substantial strength and rigidity for effective tooth repositioning. Research has indicated that PET-G aligners exhibit decreased mechanical properties when exposed to extreme temperatures and high moisture exposure during use.[9] Nevertheless, they exhibit good mechanical behavior under cyclic loading with increased stiffness and low residual strain accumulation.[10] Although the thermoforming process and intraoral conditions reduce the thermomechanical properties of PET-G materials, they maintain greater stability than alternatives such as TPU.[11] The resistance of PET-G to deformation also aids in sustaining orthodontic forces, as well as superior resistance to staining and chemical changes compared with polyurethane, thereby preserving aligner aesthetics.[12] TPU aligners offer flexibility and consistent, gentle force delivery, which are beneficial for prolonged orthodontic treatment. They exhibit higher hardness and stiffness but are more susceptible to creep and stress relaxation, which affects longevity and force application.[13] Compared with PET-G aligners, TPU aligners are less resistant to staining. The biocompatibility and comfort of TPU provide a better patient experience, thereby improving treatment adherence and outcomes.[14]

The effectiveness of thermoformed aligners depends on several variables, including the manufacturing process (specifically, the temperature and pressure settings), modulus of elasticity of the materials used, presence of dimples and appendages, and hygroscopic swelling when the aligners are exposed to saliva or water.[15,16] The interplay between aligner thickness and adaptation is pivotal in determining the efficiency and range of movements achieved with CAs. Orthodontists strategically employ the aligner thickness to predict and precisely control the forces and torques applied to teeth, which are crucial for guiding bone remodeling outcomes, such as cell damage, hyalinization of the periodontal ligament, bone necrosis, and root resorption. Consequently, the inner surface of the aligner must fit accurately against the teeth to ensure effective delivery of the intended forces. Poor fit can also result in aligners detaching from the teeth, particularly during root movements that require torque, which interferes with establishing the force couple required for predictable tooth movement.[17] The thermoforming process may lead to a reduction in the thickness of the aligners compared with the original dimensions of the thermoplastic sheet.[18] Golkhani et al.[19] reported that thermoforming reduces material thickness and alters aligner geometry, thereby affecting force and torque delivery and diminishing mechanical strength. Conversely, Tamburrino et al.[20] reported that thermoforming PET-G increased its elastic modulus by 11% and yield strength by 9%, which was attributed to the alignment of the polymer chains ("drawing"). The authors further suggested that the thermal shock associated with thermoforming may modify the surface roughness, potentially influencing the optical and absorption characteristics of the material, thereby indirectly contributing to an increase in its optical density.

A consistent thickness is essential for applying the intended force necessary for precise tooth movement, whereas an appropriate thickness enhances aligner retention and patient comfort.[21-25] Furthermore, it affects an aligner's durability and resistance to deformation, ensuring uninterrupted treatment. Monitoring the thickness also aids in detecting manufacturing errors and ensures material consistency across different aligners. Various methodologies have been employed, ranging from non-destructive high-resolution micro-computed tomography (micro-CT), which provides intricate two-dimensional and three-dimensional evaluations of internal structures and thickness variations, to precise coordinate measuring machines for physical assessments and optical scanners that compare digital models with CAD schematics. Additional techniques include scanning electron microscopy of cross-sections, profilometers for surface and thickness evaluations, and less precise direct measurements via calipers. Collectively, these methods provide a comprehensive understanding of the physical dimensions of an aligner. Advanced techniques, such as nano-CT, are particularly beneficial in research and development for optimizing aligner design and materials, ultimately improving the clinical outcomes of patients. This technology allows highly detailed three-dimensional imaging at submicrometer resolution, significantly surpassing that of conventional micro-CT systems.[26]

Despite the widespread use of aligner systems with various materials in dentistry, studies addressing the reliability of thermoforming machines used in fabrication, which influences the properties of CAs, are lacking. Additionally, aligners from

different manufacturers recommend diverse methods for manufacturing CA, potentially affecting the quality of aligners. The impact of operating conditions on the mechanical properties also varies from polymer to polymer.[20] This study aims to assess and contrast the thermoforming machine-induced variations in gap width and aligner thickness for passive aligners sourced from two different manufacturers, with identical nominal material thicknesses.

METHODS

Ethics Committee Information

The design of the nano-CT study was approved by the Institutional Ethics Committee of Tagore Dental College and Hospital (protocol number IEC/TDC/120/2022, date: 26.10.2022).

Digital Model Creation

An intraoral scan was performed on a patient diagnosed with Angle Class I malocclusion, characterized by the absence of crowding or spacing in the maxillary arch. An Aoralscan 3 intraoral scanner [Shining 3D Tech Co., Ltd., China, field of view (FOV) 16×12 mm, depth 22 mm] was used. This non-contact scanner operates based on structured light principles. The STL files were transmitted to a single aligner manufacturer (Wero Aligners, Chennai, Tamil Nadu) for treatment planning and 3D model production. All model bases were constructed with a uniform height of 5 mm.

Sample Size Calculation

The sample size was determined based on a previous study.[8] An a priori power analysis was performed to ascertain the sample size required for statistical comparison between the two independent groups. Using a two-tailed hypothesis test with an alpha level (α) of 0.05 and a desired statistical power (1-β) of 0.80, the analysis aimed to identify a significant effect size (d=1.67). Assuming an equal distribution ratio (N2/N1=1), the computed non-centrality parameter (δ=3.12) and critical t value (tcrit=2.18) at 12 degrees of freedom indicate the necessity of seven participants per group, culminating in a total sample size of 14. The actual power for this sample size was calculated to be 0.82, slightly exceeding the target power, which implies that a high likelihood of detecting a true effect of the specified magnitude should exist in the population.

Sample Preparation

Sixteen samples were used for thermoforming. The aligners were divided into two groups. Group 1 (n=8): aligners thermoformed using the Ministar, Group 2 (n=8): aligners thermoformed using the Plastpress. Each group was subdivided according to the type of aligner material used: Group A-PET-G (Erkodur AL, Erkodent Erich Kopp, GmbH, Germany) and GROUP B-TPU (Zendura FLX, CA, USA).

Aligner sheets with a thickness of 0.75 mm were used fabrication. The models were positioned at the center of the platform, with their midline aligned at the 12:00 position. The sheets were molded in accordance with the manufacturer's instructions using the same operator to reduce bias. The thermoforming machines employed were the Ministar (SCHEU Dental GmbH) and the Plastpress (BIOART).

The Ministar uses positive-pressure thermoforming combined with vacuum assistance. Initially, a fast infrared heating element was used to warm one side of the material to a maximum temperature of 60 °C. The softened material was subsequently pressed against a mold inside a pressure chamber at 4 bar, adopting the desired form. The system maintained consistent heating through thermostatic control, and the barcode scanner facilitated precise material-specific programming of the heating and cooling cycles. In contrast, PlastPress uses positive air-pressure thermoforming.

Data Acquisition

The aligners were maintained in situ on the model at ambient temperature until the completion of nano-CT scanning (Bruker Multiscale NANO CT-2214, Bruker Corporation, Billerica, MA, USA) to minimize potential distortion. The scanner was equipped with a flat-panel camera featuring a 140 mm FOV and a pixel size of 74.800 µm. The image pixel size was 35.00068 µm, with a depth of 16 bits, an exposure time of 1800 ms, a rotation step of 0.300°, and a scanning position of -34 mm. Following the scan, the raw data were reconstructed using NRecon software (version 2.1.0.2, Sky Scan Microphotonics, Inc., Allentown, PA). The reconstructed image dimensions were 3072 pixels in width and height, with an angular step of 0.300 s and cone beam angles of 40.23° horizontally and 26.097° vertically. The rendered 3D models were visualized using CTVox (version 3.3.0), and measurements were performed using Adobe Data Viewer (version 1.5.6.2).

2D Analysis

The 3D models were virtually divided into three anatomical regions, each corresponding to the central incisor, canine, and first molar to assess aligner thickness and the air gap (gap width) between the aligner and the cast. This division was essential for assessing the aligner thickness and air volume (gap width) between the aligner and the cast. For each tooth, a tangent was established between the mesial and distal contact points. The midpoint of these tangents, which was aligned with the tooth's long axis, served as the vertical reference plane. A horizontal line was drawn to connect the centers of the buccal and palatal surfaces positioned perpendicular to this plane served as the horizontal reference plane.

These reference lines functioned as reference lines, with tangents to these lines offering multiple reference points on each two-dimensional grid, including the following:

Five points for the central incisor (Figure 1), five points for the canine (Figure 2), and six points for the first molar (Figure 3).

The 2D reference points and slice planes were identified on the building grid for the (A) incisor, (B) canine, and (C) molar.

1. Buccal gingival edge,
2. Buccal surface center,
3. Incisal edge, buccal cusp,
3a. Palatal cusp,
4. Palatal surface center,
5. Palatal gingival edge.

Statistical Analysis

Statistical analyses were performed using the IBM (Armonk, New York, USA) SPSS Statistics V20. Wilks' normality test was conducted to evaluate the distribution of the data, which demonstrated a deviation from normality. As a result, non-parametric tests were employed, as they are more appropriate for datasets that do not satisfy parametric assumptions. Asymp. Sig. (2-tailed) was used to compare two independent groups with non-normally distributed data. This test was applied to analyze the gap width and aligner thickness between aligners manufactured by Ministar and Plastpress machines as well as between two thermoforming sheets in three different tooth types: incisors, canines, and molars. Statistical analyses were performed with a 95% confidence interval, and the findings were considered statistically significant when $p<0.05$.

RESULTS

Table 1 presents descriptive statistics (median and interquartile range) for PET-G and TPU sheets thermoformed using Ministar and Plastpress across various regions, namely, molars, canines, and incisors.

Analysis of aligner thickness (Table 2) revealed no significant differences between PET-G and TPU sheets in the canine (p=0.810 Ministar and p=0.378 for Plastpress) and incisor regions (p=0.422 for Ministar and p=0.470 for Plastpress) for both thermoforming machines. However, a significant difference was detected in the molar region (p=0.004) across all the sheets, independent of the thermoforming machine.

For gap width, no significant differences were observed in the canine (Ministar: p=0.229; Plastpress: p=0.128) or incisor regions (Ministar: p=0.128; Plastpress: p=0.575). In contrast, the molar region showed significant differences for both machines (Ministar: p=0.010; Plastpress: p=0.004).

Table 3 demonstrates that comparisons of aligner thickness between the two machines (Ministar vs. Plastpress) revealed no significant differences in the canine (TPU: p=0.810; PET-G: p=0.171) or incisor (TPU: p=0.936; PET-G: p=0.936) regions. However, the molar region again exhibited significant differences in thickness for both PET-G (p=0.004) and TPU (p=0.050).

Similarly, gap width comparisons between machines showed no significant differences in the canine (TPU: p=0.065; PET-G: p=0.936) or incisor regions (TPU: p=0.378; PET-G: p=0.173). In contrast, the molar region showed significant differences in gap width for PET-G (p=0.010) and TPU (p=0.004).

DISCUSSION

The increasing demand for CAs has led to the development of novel thermoplastic materials for their production.[27-31] The aligner sheets used in this study are among the most versatile

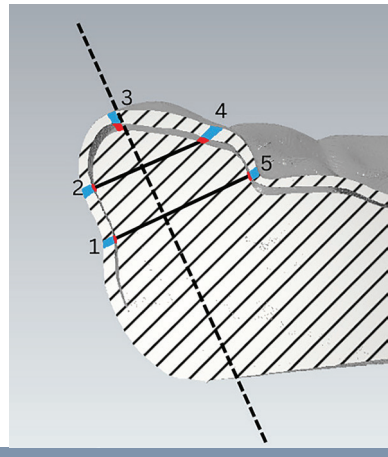

Figure 2. Measurement of aligner thickness and gap width in canines

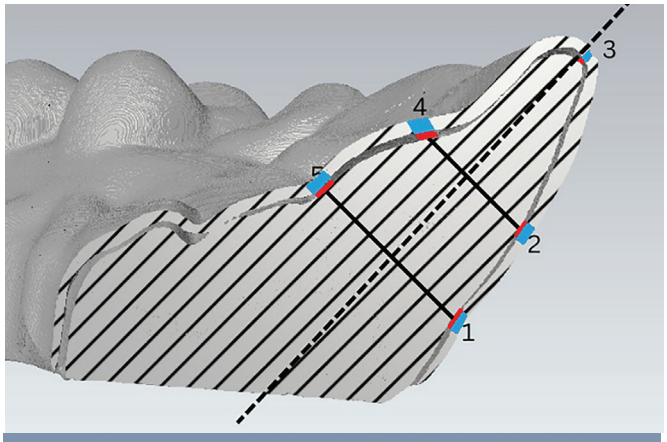

Figure 1. Measurement of aligner thickness and gap width in the central incisor

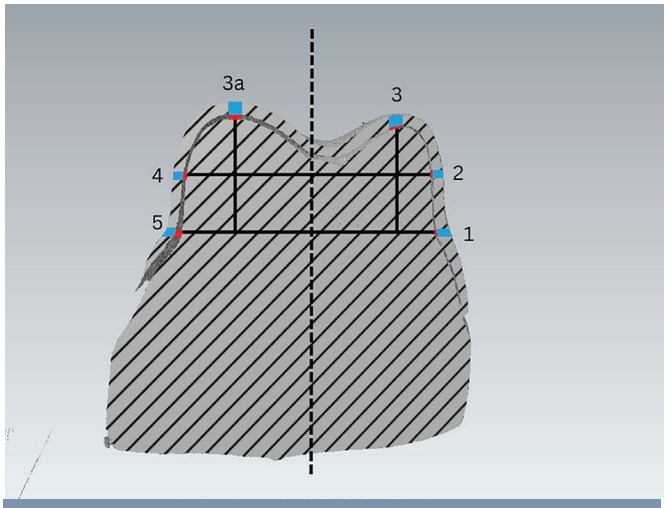

Figure 3. Measurement of aligner thickness and gap width in the first molar

Table 1. Frequency distribution of material thickness and gap width in three different tooth structures using different thermoforming machines and thermoforming sheets

Material	Tooth region	Thickness		Gap width	
		Median (mm)	IQR	Median (µm)	IQR
Ministar PET-G	Molar	0.303	0.083	146.5	97.5
	Canine	0.373	0.2191	182.0	103.25
	Incisor	0.358	0.302	127.125	109.31
Ministar TPU	Molar	0.538	0.0838	259.5	152.31
	Canine	0.325	0.251	228.667	282.25
	Incisor	0.403	0.2775	211.167	196.88
Plastpress PET-G	Molar	0.543	0.0484	263.125	159.31
	Canine	0.437	0.2391	173.375	129.43
	Incisor	0.337	0.1991	178.750	141.56
Plastpress TPU	Molar	0.45	0.0525	77.167	70.4
	Canine	0.273	0.3188	74.667	52
	Incisor	0.390	0.3687	143.000	107.33

PET-G, polyethylene glycol; TPU, thermoplastic polyurethane; IQR, interquartile range

Table 2. Comparison of material thickness and gap width between two thermoforming sheets in three different tooth structures

Tooth	Material	Mean rank	p-value
Material thickness			
Molar	Ministar PET-G	3.5	0.004*
	Ministar TPU	9.5	
Canine	Ministar PET-G	6.75	0.810
	Ministar TPU	6.25	
Incisor	Ministar PET-G	5.67	0.422
	Ministar TPU	7.33	
Molar	Plastpress PET-G	9.5	0.004*
	Plastpress TPU	3.5	
Canine	Plastpress PET-G	7.42	0.378
	Plastpress TPU	5.58	
Incisor	Plastpress PET-G	5.75	0.470
	Plastpress TPU	7.25	
Gap width			
Molar	Ministar PET-G	3.83	0.010*
	Ministar TPU	9.17	
Canine	Ministar PET-G	5.25	0.229
	Ministar TPU	7.75	
Incisor	Ministar PET-G	4.92	0.128
	Ministar TPU	8.08	
Molar	Plastpress PET-G	9.5	0.004*
	Plastpress TPU	3.5	
Canine	Plastpress PET-G	8.08	0.128
	Plastpress TPU	4.92	
Incisor	Plastpress PET-G	7.08	0.575
	Plastpress TPU	5.92	

Asymp. Sig. (2-tailed) test; 95% confidence interval
p<0.05, *statistically significant
PET-G, polyethylene glycol; TPU, thermoplastic polyurethane

Table 3. Comparison of material thickness and gap width between two thermoforming machines

	Material	Mean rank	p-value
TPU material thickness			
Molar	Ministar TPU	8.5	0.053
	Plastpress TPU	4.5	
Canine	Ministar TPU	6.75	0.810
	Plastpress TPU	6.25	
Incisor	Ministar TPU	6.42	0.936
	Plastpress TPU	6.58	
TPU Gap width			
Molar	Ministar TPU	9.50	0.004
	Plastpress TPU	3.50	
Canine	Ministar TPU	8.42	0.065
	Plastpress TPU	4.58	
Incisor	Ministar TPU	7.42	0.378
	Plastpress TPU	5.58	
PET-G material thickness			
	Material	**Mean rank**	**p-value**
Molar	Ministar PET-G	3.5	0.004
	Plastpress PET-G	9.5	
Canine	Ministar PET-G	5.08	0.171
	Plastpress PET-G	7.92	
Incisor	Ministar PET-G	6.58	0.936
	Plastpress PET-G	6.42	
PET-G Gap width			
Molar	Ministar PET-G	3.83	0.010
	Plastpress PET-G	9.17	
Canine	Ministar PET-G	6.42	0.936
	Plastpress PET-G	6.58	
Incisor	Ministar PET-G	5.08	0.173
	Plastpress PET-G	7.92	

Asymp. Sig. (2-tailed) test; 95% confidence interval
p<0.05, *statistically significant
PET-G, polyethylene glycol; TPU, thermoplastic polyurethane

elastomeric thermoplastics, such as TPU and PET-G, and consist of either amorphous or partially crystalline polymers with superior physical, chemical, abrasion, adhesion, and processing properties.[32] In CA fabrication, PET-G is frequently preferred owing to its superior transparency, robust fatigue resistance, and dimensional stability. TPU is a flexible and easily moldable elastomer that offers high elasticity and formability, providing comfortable wear and effective impact cushioning. Given the limitations of single-layer materials, innovations have led to the development of multilayer hybrid materials. These advanced materials have been engineered to integrate the advantageous properties of various materials. For example, layering a rigid outer material with a softer inner layer can improve tensile strength and reduce water absorption.[17] Aligner thickness and adaptation remain critical determinants of physiologic tooth movement, as they influence the magnitude and delivery of orthodontic forces. The transparency of aligner sheets is significantly influenced by their thickness, as structural deformation occurring at temperatures above the glass transition temperature and pressure leads to secondary bonding forces, transforming the amorphous structure into a crystalline structure.[33,34] The thermoforming process also results in a rough surface that can trap staining substances.[35]

Numerous studies have indicated that aligner thickness does not significantly affect the forces generated for movements such as tipping and rotation and that intraoral use or thermoforming does not produce clinically relevant changes in thickness or alter aligner shape. However, increases in aligner thickness may adversely affect labial and palatal tooth movements.[17,35,36] Iliadi et al.[37] reported that aligner thickness affects the rate of deflection under simulated intraoral conditions, with thicker materials generating greater force and moment on the tooth.

Several studies have indicated that CAs made from thicker sheets (0.75 mm or 0.8 mm) exert stronger forces than those made from thinner sheets (0.4-0.5 mm).[38-40] A study using finite element analysis (FEA) reported that aligners with different thicknesses affected the displacement tendency of teeth, particularly concerning incisor retraction and torque control.[41] Thicker aligners (0.75 mm) have been associated with enhanced torque control and palatal root torque, which are essential for achieving bodily retraction of the anterior teeth while minimizing the risk of root resorption. Li et al.[42] reported that increasing aligners thickness results in a more significant buccal displacement of the crowns and an increase in stress on the periodontal ligaments during expansion. Conversely, thinner aligners may provide less control but may be more comfortable for the patient.[43] Therefore, a thorough analysis of the aligner thickness is crucial in determining the predictability and success of orthodontic treatment.

The deformation of aligners in terms of thickness and gap width may be influenced by tooth morphology, the extent of intended tooth movement, and the thermoforming process. The aligner sheets were manufactured via vacuum-based thermoplastic molding and pressure-based thermoforming machines. Vacuum-based thermoforming is more time-consuming and technique-sensitive and may result in unpredictable changes in the mechanical and physical properties of the material Although pressure-forming machines are similar to vacuum-forming machines, they employ compressed air to heat aligner sheets, resulting in sharper and more precise details. Hahn et al.[33] reported that high-pressure thermoforming produces appliances with a more precise fit, leading to significantly stronger forces than those of vacuum-formed appliances.[44] As a result, pressure-forming systems have become widely adopted in clinical practice. Consequently, this study aimed to evaluate variations in the properties of CAs, such as gap width and thickness, using two different thermoforming machines, which are crucial in orthodontic tooth movement.

CA thickness can be evaluated using various methods, including non-invasive micro-CT, which is notable for its non-destructive and high-resolution capabilities in assessing the overall thickness distribution. We opted to use nano-CT because it is an emerging high-resolution, cross-sectional imaging technique that represents a technical advancement over micro-CT. Nano-CT achieves superior spatial resolution of up to 400 nm by utilizing a transmission target X-ray tube to achieve a focal spot size of less than 400 nanometers (nm), along with specific detectors and examination protocols. The enhanced resolution of this technique, achieved through a smaller focal spot of the transmission tube and closer sample positioning, enables more detailed imaging than typical micro-CT systems.[45] We employed a trim line positioned 1 mm above the gingival margin, as this design significantly affects the biomechanical efficacy of aligners in facilitating tooth movement. Evidence suggests that aligners with straight extended trim lines demonstrate greater force and provide superior control compared with scalloped designs. A FEA revealed that straight-cut trim lines produce greater forces than scalloped trim lines, which is crucial for effective tooth movement. The straight design optimizes the force distribution, thereby enhancing retention and reducing stress on the teeth during facial translation, distalization, and extrusion.[46,47]

In our study, the mean thickness of the aligner sheets was reduced to 0.5 mm, consistent with the findings of Min et al.[39] and Park et al.,[17] who reported a reduction in aligner thickness of approximately 57.5% following thermoforming. Moreover, TPU sheets exhibited superior adaptation in both thermoforming machines. This observation aligns with the study by Mantovani et al.,[15] who noted that during thermoforming, CA (PET-G) plastic sheets tend to thin at the gingival edge, resulting in reduced rigidity. Consequently, this thinning leads to a less optimal fit between the tooth and aligner at the gingival margin of clear CA aligners compared with the Invisalign material (SmartTrack material), which comprises multilayer aromatic thermoplastic aligners. Our study also demonstrated that the TPU experienced less thickness reduction than PET-G, corroborating Park et al.[17] (PET-G-504.68 µm, TPU-509.54 µm). This may be attributed to the copolyester-elastomer multilayer composition of TPU,

which offers superior tensile strength than the PET-G materials. Consequently, this multilayer structure may be more amenable to stretching during heating and pressure thermoforming, resulting in more precise fitt. The study also indicated that the thermoforming machine does not significantly reduce the thickness of the aligner sheets, potentially due to the minimum air pressure of 3-4 bar used by both systems. Our 2D research further revealed that the aligner fit (gap width) was generally superior in the gingival regions of the first molar than in the occlusal regions. Compared with other areas, the molar tooth exhibited increased gap width and thickness changes between Ministar and Plastpress. The aligner thickness also decreased from the posterior to the anterior tooth structures, possibly due to greater stretching of the aligner sheets in the anterior region. These findings are consistent with those of Palone et al.,[8] Mantovani et al.,[15] Bucci et al.,[18] and Lee et al.[48] This could be advantageous for tooth movement because a decreased or minimal gap width with increased thickness may counteract the vertical dislodging.

In summary, the statistical analysis indicated that significant differences in aligner thickness and gap width were observed only in the molar region, whereas the incisor and canine regions exhibited no statistically significant variations, irrespective of the material or machine employed. Compared with PET-G aligners, TPU aligners demonstrate superior adaptation and less thickness reduction. This study further revealed that Ministar, which provides automated control of heating and pressure, produced more consistent results than Plastpress, which relies on manual settings. Nonetheless, both machines generate clinically acceptable aligners in terms of fit, particularly in the anterior region. A posterior-to-anterior thickness gradient was identified, which may have biomechanical implications for tooth movement and alignment retention. This finding may facilitate future research on a broader range of aligner materials, thermoforming systems, and malocclusion severities.

Study Limitations

This study considered only minor deformities, and severe malocclusions could have affected the results. In addition, grip points, attachments, or divots were not considered. The results may not be representative and could have been adversely affected by unfavorable temperature and pressure settings because only a small sample size was evaluated for each aligner brand. Future studies should examine a wider range of materials and machine systems to enhance the clinical applicability of these findings.

CONCLUSION

This study demonstrated that while PET-G and TPU materials performed similarly in the anterior tooth regions when thermoformed using either Ministar or PlastPress, the molar region exhibited significant variations in aligner thickness and gap width, influenced by aligner material and tooth morphology.

Among the two thermoforming machines, Ministar yielded more consistent outcomes, likely due to its automated temperature and pressure regulation. These findings underscore the importance of material selection and thermoforming precision, both of which are critical for effective anchorage and force delivery.

Ethics

Ethics Committee Approval: The design of the nano-CT study was approved by the Institutional Ethics Committee of Tagore Dental College and Hospital (protocol number IEC/TDC/120/2022, date: 26.10.2022).

Informed Consent: Researchers ensured the patient gave informed consent before using their intra-oral scan for the study.

Footnotes

Author Contributions: Concept - G.S., M.K., B.K.; Design - G.S., M.K., B.K., S.P.A.; Data Collection and/or Processing - G.S., M.K.; Analysis and/or Interpretation - G.S., M.K., S.P.A, S.R.; Literature Search - G.S., M.K., A.S.S., S.R.; Writing - G.S., M.K., A.S.S.

Conflict of Interest: The authors have no conflicts of interest to declare.

Financial Disclosure: This study did not receive any specific grant from funding agencies in the public, commercial, or not-for-profit sectors.

REFERENCES

1. Kesling HD. The philosophy of the tooth-positioning appliance. *Am J Orthod Oral Surg.* 1945;31(6):297-304. [CrossRef]
2. Jeremiah HG, Bister D, Newton JT. Social perceptions of adults wearing orthodontic appliances: a cross-sectional study. *Eur J Orthod.* 2011;33(5):476-482. [CrossRef]
3. Boyd RL, Miller RJ, Vlaskalic V. The invisalign system in adult orthodontics: mild crowding and space closure cases. *J Clin Orthod.* 2002;36(10):592-602. [CrossRef]
4. Boyd RL, Vlaskalic V. Three-dimensional diagnosis and orthodontic treatment of complex malocclusions with the invisalign appliance. *Semin Orthod.* 2001;7(4):274-293. [CrossRef]
5. Weir T. Clear aligners in orthodontic treatment. *Aust Dent J.* 2017;62 Suppl 1:58-62. [CrossRef]
6. Chen SM, Huang TH, Ho CT, Kao CT. Force degradation study on aligner plates immersed in various solutions. *J Dent Sci.* 2023;18(4):1845-1849. [CrossRef]
7. Landel RF, Nielsen LE. Mechanical properties of polymers and composites. 2nd ed. Boca Raton, FL: CRC Press; 1993. [CrossRef]
8. Palone M, Longo M, Arveda N, et al. Microcomputed tomography evaluation of general trends in aligner thickness and gap width after thermoforming procedures involving six commercial clear aligners: an in vitro study. *Korean J Orthod.* 2021;51(2):135-141. [CrossRef]
9. Ihssen BA, Nimer A, Drescher D, Willmann JH. Effect of in vitro aging by water immersion and thermocycling on the mechanical properties of PETG aligner material. *J Orofac Orthop.* 2019;80(6):292-303. [CrossRef]
10. Cianci C, Casavola C, Ciavarella D, et al. Mechanical behavior of PET-G tooth aligners under cyclic loading. *Front Mater.* 2020;7. [CrossRef]
11. Dalaie K, Fatemi SM, Ghaffari S. Dynamic mechanical and thermal properties of clear aligners after thermoforming and aging. *Progress in Orthodontics.* 2021;22(1):15. [CrossRef]

12. Šimunović L, Čekalović Agović S, Bačić I, et al. Color and chemical stability of 3D-printed and thermoformed polyurethane-based aligners. *Polymers.* 2024;16(8):1067. [CrossRef]
13. Srinivasan B, Padmanabhan S, Srinivasan S. Comparative evaluation of physical and mechanical properties of clear aligners-a systematic review. *Evid Based Dent.* 2023;25(1):53. [CrossRef]
14. Katschnig M, Janics T, Holzer C, Burgstaller C, Wallner J, Zemann W. Biofunctional glycol-modified polyethylene terephthalate and thermoplastic polyurethane implants by extrusion-based additive manufacturing for medical 3D maxillofacial defect reconstruction. *Polymers.* 2020;12(8):1751. [CrossRef]
15. Mantovani E, Castroflorio E, Rossini G, et al. Scanning electron microscopy evaluation of aligner fit on teeth. *Angle Orthod.* 2018;88(5):596-601. [CrossRef]
16. Ryokawa H, Miyazaki Y, Fujishima A, Miyazaki T, Maki K. The mechanical properties of dental thermoplastic materials in a simulated intraoral environment. *Orthod Waves.* 2006;65:64-72. [CrossRef]
17. Park SY, Choi SH, Yu HS, et al. Comparison of translucency, thickness, and gap width of thermoformed and 3D-printed clear aligners using micro-CT and spectrophotometer. *Sci Rep.* 2023;13(1):10921. [CrossRef]
18. Bucci R, Rongo R, Levatè C, et al. Thickness of orthodontic clear aligners after thermoforming and after 10 days of intraoral exposure: a prospective clinical study. *Prog Orthod.* 2019;20(1):36. [CrossRef]
19. Golkhani B, Weber A, Keilig L, Reimann S, Bourauel C. Variation of the modulus of elasticity of aligner foil sheet materials due to thermoforming. *J Orofac Orthop.* 2022;83(4):233-243. [CrossRef]
20. Tamburrino F, D'Antò V, Bucci R, Alessandri-Bonetti G, Barone S, Razionale AV. Mechanical properties of thermoplastic polymers for aligner manufacturing: in vitro study. *Dent J (Basel).* 2020;8(2):47. [CrossRef]
21. Lagravère MO, Flores-Mir C. The treatment effects of Invisalign orthodontic aligners: a systematic review. *J Am Dent Assoc.* 2005;136(12):1724-1729. [CrossRef]
22. Simon M, Keilig L, Schwarze J, Jung BA, Bourauel C. Treatment outcome and efficacy of an aligner technique--regarding incisor torque, premolar derotation and molar distalization. *BMC Oral Health.* 2014;14:68. [CrossRef]
23. Upadhyay M, Arqub SA. Biomechanics of clear aligners: hidden truths & first principles. *J World Fed Orthod.* 2022;11(1):12-21. [CrossRef]
24. Alhasyimi AA, Ayub A, Farmasyanti CA. Effectiveness of the attachment design and thickness of clear aligners during orthodontic anterior retraction: finite element analysis. *Eur J Dent.* 2024;18(1):174-181. [CrossRef]
25. Tamer İ, Öztaş E, Marşan G. Orthodontic treatment with clear aligners and the scientific reality behind their marketing: a literature review. *Turk J Orthod.* 2019;32(4):241-246. [CrossRef]
26. Kampschulte M, Langheinirch AC, Sender J, et al. Nano-computed tomography: technique and applications. *Rofo.* 2016;188(2):146-154. [CrossRef]
27. Papadopoulou AK, Cantele A, Polychronis G, Zinelis S, Eliades T. Changes in roughness and mechanical properties of invisalign® appliances after one- and two-weeks use. *Materials (Basel).* 2019;12(15):2406. [CrossRef]
28. Jaggy F, Zinelis S, Polychronis G, et al. ATR-FTIR analysis and one-week stress relaxation of four orthodontic aligner materials. *Materials (Basel).* 2020;13(8):1868. [CrossRef]
29. Kwon JS, Lee YK, Lim BS, Lim YK. Force delivery properties of thermoplastic orthodontic materials. *Am J Orthod Dentofacial Orthop.* 2008;133(2):228-34; quiz 328.e1. [CrossRef]
30. Martina S, Rongo R, Bucci R, Razionale AV, Valletta R, D'Antò V. In vitro cytotoxicity of different thermoplastic materials for clear aligners. *Angle Orthod.* 2019;89(6):942-945. [CrossRef]
31. Schuster S, Eliades G, Zinelis S, Eliades T, Bradley TG. Structural conformation and leaching from in vitro aged and retrieved invisalign appliances. *Am J Orthod Dentofacial Orthop.* 2004;126(6):725-728. [CrossRef]
32. Hahn W, Engelke B, Jung K, et al. The influence of occlusal forces on force delivery properties of aligners during rotation of an upper central incisor. *Angle Orthod.* 2011;81(6):1057-1063. [CrossRef]
33. Hahn W, Fialka-Fricke J, Dathe H, et al. Initial forces generated by three types of thermoplastic appliances on an upper central incisor during tipping. *Eur J Orthod.* 2009;31(6):625-631. [CrossRef]
34. Seo JH, Eghan-Acquah E, Kim MS, et al. Comparative analysis of stress in the periodontal ligament and center of rotation in the tooth after orthodontic treatment depending on clear aligner thickness-finite element analysis study. *Materials (Basel).* 2021;14(2):324. [CrossRef]
35. Ryu JH, Kwon JS, Jiang HB, Cha JY, Kim KM. Effects of thermoforming on the physical and mechanical properties of thermoplastic materials for transparent orthodontic aligners. *Korean J Orthod.* 2018;48(5):316-325. [CrossRef]
36. Daniele V, Macera L, Taglieri G, Spera L, Marzo G, Quinzi V. Color stability, chemico-physical and optical features of the most common PET-G and PU based orthodontic aligners for clear aligner therapy. *Polymers (Basel).* 2021;14(1):14. [CrossRef]
37. Iliadi A, Koletsi D, Eliades T. Forces, and moments generated by aligner-type appliances for orthodontic tooth movement: a systematic review and meta-analysis. *Orthod Craniofac Res.* 2019;22(4):248-258. [CrossRef]
38. Elkholy F, Mikhaiel B, Schmidt F, Lapatki BG. Mechanical load exerted by PET-G aligners during mesial and distal derotation of a mandibular canine : an in vitro study. *J Orofac Orthop.* 2017;78(5):361-370. [CrossRef]
39. Min S, Hwang CJ, Yu HS, et al. The effect of thickness and deflection of orthodontic thermoplastic materials on its mechanical properties. *Korean J Orthod.* 2010;40(1):16-26. [CrossRef]
40. Kohda N, Iijima M, Muguruma T, Brantley WA, Ahluwalia KS, Mizoguchi I. Effects of mechanical properties of thermoplastic materials on the initial force of thermoplastic appliances. *Angle Orthod.* 2013;83(3):476-483. [CrossRef]
41. Cheng Y, Liu X, Chen X, et al. The three-dimensional displacement tendency of teeth depending on incisor torque compensation with clear aligners of different thicknesses in cases of extraction: a finite element study. *BMC Oral Health.* 2022;22(1). [CrossRef]
42. Li N, Li D, Yang M, et al. Effects of different tooth movement patterns and aligner thicknesses on maxillary arch expansion with clear aligners: a three-dimensional finite element study. *Front Bioeng Biotechnol.* 2024;12. [CrossRef]
43. Cengiz SM, Goymen M. The effectiveness of orthodontic treatment with clear aligners in different thicknesses. *Sci Rep.* 2025;15(1). [CrossRef]
44. Gao L, Wichelhaus A. Forces and moments delivered by the PET-G aligner to a maxillary central incisor for palatal tipping and intrusion. *Angle Orthod.* 2017;87(1):35-42. [CrossRef]
45. Staderini E, Chiusolo G, Guglielmi F, et al. Effects of thermoforming on the mechanical, optical, chemical, and morphological properties of PET-G: in vitro study. *Polymers (Basel).* 2024;16(2):203. [CrossRef]
46. Elshazly TM, Bourauel C, Chavanne P, Elattar H, Keilig L. Numerical biomechanical finite element analysis of different trimming line designs of orthodontic aligners: an in silico study. *J World Fed Orthod.* 2024;13(2):65-71. [CrossRef]
47. Elshazly TM, Bourauel C, Aldesoki M, et al. Effect of attachment configuration and trim line design on the force system of orthodontic aligners: a finite element study on the upper central incisor. *Orthod Craniofac Res.* 2024;27(Suppl 2):131-140. [CrossRef]
48. Lee SY, Kim H, Kim HJ, et al. Thermomechanical properties of 3D printed photocurable shape memory resin for clear aligners. *Sci Rep.* 2022;12(1):6246. [CrossRef]

TURKISH JOURNAL OF
ORTHODONTICS

DOI: 10.4274/TurkJOrthod.2025.2025.85

Original Article

Comparison of Mechanical, Surface, and Chemical Properties of Different Thermoplastic Retainer Materials before and after Thermoforming: Scanning Electron Microscopy and Fourier Transform Infrared Spectroscopy Analyses

Yasemin Tunca[1], Nihal Fahrzadeh[2], Murat Tunca[1], Yüksel Akınay[3]

[1]Kütahya Health Sciences University Faculty of Dentistry, Department of Orthodontics, Kütahya, Türkiye
[2]Van Yüzüncü Yıl University Faculty of Dentistry, Department of Orthodontics, Van, Türkiye
[3]Van Yüzüncü Yıl University Faculty of Engineering, Department of Mining Engineering, Van, Türkiye

Cite this article as: Tunca Y, Fahrzadeh N, Tunca M, Akınay Y. Comparison of mechanical, surface, and chemical properties of different thermoplastic retainer materials before and after thermoforming: scanning electron microscopy and fourier transform infrared spectroscopy analyses. *Turk J Orthod.* 2025; 38(4): 224-232

Main Points

- Thermoforming significantly increases surface roughness in some polyethylene terephthalate glycol-based retainers, potentially affecting long-term performance.
- Scanning electron microscopy and Fourier transform infrared spectroscopy analyses revealed that molecular structure remains stable despite morphological changes.
- Surface roughness may influence bacterial adhesion, making material selection critical for clinical outcomes.
- Thermoplastic materials based on polyethylene terephthalate glycol copolyester with high surface homogeneity exhibit improved long-term stability.

ABSTRACT

Objective: The aim of this study was to evaluate the surface hardness, surface roughness, and chemical structure changes of four vacuum-formed retainer (VFR) materials after thermoforming.

Methods: Four groups of VFR materials were evaluated: Taglus, Lumex-G, Atmos, and Duran. Each group consisted of 12 samples (n=12) that were thermoformed according to the manufacturer's guidelines. Surface roughness was measured using a high-precision profilometer, and hardness was assessed with a micro-Vickers hardness tester. Chemical structure analysis was conducted using Fourier transform infrared spectroscopy (FTIR), and surface morphology was examined using scanning electron microscopy (SEM).

Results: Hardness measurements demonstrated a general decrease across all groups following thermoforming. After thermoforming, surface roughness increased significantly in the Taglus and Lumex-G groups, whereas the Atmos and Duran groups maintained greater surface stability. FTIR demonstrated that all materials retained their chemical stability, and no significant changes in functional groups were detected. SEM results revealed more pronounced surface irregularities in the Taglus and Lumex-G groups.

Conclusion: Polyethylene terephthalate glycol copolyester-based materials with high surface homogeneity, such as Atmos and Duran, may be recommended for clinical use due to their superior surface stability and chemical resilience. By contrast, the surface irregularities observed in Taglus and Lumex-G may compromise their long-term clinical performance.

Keywords: Vacuum-formed retainer, surface hardness, surface roughness, Fourier transform infrared spectroscopy

Corresponding author: Asst. Prof. Yasemin Tunca, **e-mail:** dtyasemintunca@gmail.com
Received: July 25, 2025 **Accepted:** December 18, 2025 **Publication Date:** 30.12.2025

INTRODUCTION

After completion of orthodontic treatment, retainers are commonly used to stabilize newly aligned teeth.[1] Retainers are generally classified into two main categories: removable and fixed.[2] Compared with fixed retainers, removable retainers, made of thermoplastic materials and known as vacuum-formed retainers (VFRs), are preferred for their superior comfort and aesthetic appeal.[3,4] Although patient compliance is a limitation of VFRs, they are cost-effective, easy to insert and remove, and require minimal clinical time.[5] VFRs are primarily manufactured from a variety of thermoplastic polymers, each with unique properties that substantially affect the final product's performance.[6]

Commonly used thermoplastic materials include polyurethane, polypropylene (PP), and polycarbonate (PC).[7] The current literature indicates that the majority of commercial VFRs are polyethylene terephthalate glycol (PET-G)-based; fewer materials belong to the thermoplastic polyurethane (TPU) class, while PC- and PP/polyolefin-based systems are less commonly represented.[8-10] These materials soften upon heating, can be thermoformed, and then harden, retaining their shape upon cooling. This thermal process directly influences the materials' mechanical properties, causing changes in surface roughness, hardness, and porosity due to the rearrangement of polymer chains.[11,12] Surface hardness determines a material's resistance to deformation and scratching, contributing to its longevity and wear resistance.[13] Surface roughness affects tactile sensations, gloss, friction, and light reflection, which are critical for both functional and aesthetic purposes.[14]

Structural changes in these materials may lead to issues such as discoloration, abrasion, and increased bacterial retention over time.[15-18] Although the recommended usage period for VFRs varies, an average of 12 months is typical.[1,19] Over time, changes in the surface properties of thermoplastic materials, including hardness, roughness, and porosity, significantly affect their performance and aesthetics.[18] Although researchers have explored these properties in thermoplastic retainer materials,[8,11,20] comprehensive evaluations using scanning electron microscopy (SEM) and Fourier transform infrared spectroscopy (FTIR) are lacking in the literature.[21] The current study makes a key contribution by evaluating the mechanical properties of four commonly used VFR materials, using SEM and FTIR analyses, in their initial state and after thermal processing.

The null hypothesis (H_0) of our study is "There is no difference between VFR materials in terms of surface roughness, surface hardness, or chemical structure changes in the initial state and after thermoforming".

METHODS

Analyses of surface hardness and roughness were conducted at the Dentistry Research Laboratory of Van Yüzüncü Yıl University. As the study did not involve the use of human or animal materials, ethical approval was not required.

Sample Size

The sample size for this study was calculated to detect changes in two physical properties-surface hardness and surface roughness-through repeated measurements conducted before and after thermoforming. Assuming a medium effect size (f=0.25), a significance level of α=0.05, and a statistical power (1-β) of 80%, a sample size of 48 was required. This design involved repeated measurements of four thermoplastic retainer materials, with a minimum of 12 samples per group (n≥12).

Sample Selection Criteria

Four main VFR groups, each consisting of 12 samples from different commercial brands, were selected. The thermoplastic retainer appliances were Duran (125×125×1 mm; Scheu Dental GmbH, Iserlohn, Germany), Taglus (125×125×1 mm; Laxmi Dental Export Pvt. Ltd, Mumbai, India), Atmos (approximately 127×127×1.016 mm; American Orthodontics, Sheboygan, WI, USA), and Lumex-G (125×125×1 mm; Foamalite Ltd, Loch Gowna, Cavan, Ireland). These four thermoplastic retainer materials were selected because they are among the most widely used in clinical orthodontics. To ensure standardization, all materials were used in their original commercial dimensions as provided by the manufacturers, without cutting or reshaping, to avoid altering their physical properties. The brands, compositions, and thermal processing durations of the thermoplastic materials are presented in Table 1. All tests were conducted in a controlled laboratory environment (23 °C±2 °C, 50%±5% relative humidity) following a minimum 24-hour stabilization period to mitigate the potential impact of moisture and temperature on the thermoplastics. Specimens were handled in accordance with established protocols, with powder-free nitrile gloves used as a standard precaution. Additionally, the surfaces under consideration were meticulously cleaned with

Table 1. Thermoplastic material brands and contents and thermal processing times

VFR Brand	Content	Manufacturer	Heating time (s)	Cooling time (s)
Duran	Polyethylene terephthalate glycol copolyester (PET-G)	Scheu Dental GmbH, Iserlohn, Germany	30	60
Taglus	Polyethylene terephthalate glycol copolyester -polyethylene	Laxmi Dental Export Pvt. Ltd, Mumbai, India	70	40
Atmos	Copolyester	American Orthodontics, Sheboygan, WI, USA	40	30
Lumex G	Polyethylene terephthalate glycol copolyester	Foamalite Ltd, Loch Gowna, County Cavan, Ireland	30	25

lint-free wipes and isopropyl alcohol (≥99.5%), which is known for its effectiveness in removing contaminants and promoting a sterile environment.

Micro-Vickers Hardness Measurement

The micro-Vickers hardness of the VFR samples was measured using a micro-Vickers hardness tester (HMV-G 21D; Shimadzu, Japan). A square-pyramidal indentation was created on the sample surfaces using a Vickers diamond indenter. The device was calibrated with a certified reference hardness block before performing three repeated measurements on each sample. The instrument settings were configured with a Vickers load of HV 0.025 (245.2 mN) and a dwell time of 15 s. Indentations were then photographed at 40× magnification (Figure 1). The mean of three measurements, each taken from a different region of the sample, was calculated. The same procedure was repeated after thermoforming.

Surface Roughness Measurement

The most common surface roughness parameters were evaluated: Ra (average roughness), Rq (root mean square roughness), and Rz (maximum height of the profile). A high-precision manual profilometer (Surftest SJ-301, Mitutoyo, Kanagawa, Japan) equipped with a 5-µm diamond stylus tip was used for the measurements. The device scanned 2 mm in a linear motion across the top surface of each specimen to detect irregularities (Figure 2). Three readings were taken at different locations on each specimen, and the mean value was used for statistical analysis.

The instrument was calibrated with a manufacturer-supplied reference standard prior to each measurement session to ensure accuracy and reproducibility. A cut-off value of 0.8 mm and a scan speed of 0.5 mm/s were applied in accordance with international roughness measurement standards. The same procedure was repeated after thermoforming.

SEM, DSC, and FTIR Analyses

Morphological analyses of the VFR groups were conducted using field-emission SEM. All SEM images are presented at consistent magnifications with clearly visible scale bars (200 µm for low magnification and 100 µm for high magnification). The chemical bond types and thermal behaviors of the VFR groups were characterized by FTIR and differential scanning calorimetry (DSC). The thermal behavior and phase changes of the Taglus, Lumex-G, Atmos, and Duran groups were further investigated using DSC.

Thermoforming

Thermoforming was performed on VFR samples after pre-thermoforming measurements. To standardize the process, each sample was pressed into a metal mold with a flat, round surface, and a single doctor monitored the processing time. Thermoforming was performed using an Essix-type vacuum-forming device (Dentsply Sirona, USA), which operates within a heating range of 160 °C-200 °C. The device applies a negative pressure (vacuum) of approximately -0.8 bar to adapt the softened sheet to the dental model, with a heater-to-sheet distance of approximately 25 mm. After thermoforming, the same mechanical property measurements (surface hardness and roughness) were repeated under the same conditions.

Statistical Analysis

Statistical analyses were performed using IBM SPSS Statistics for Windows, version 23.0 (IBM Corp., Armonk, NY, USA) and the R statistical software (R Foundation for Statistical Computing, Vienna, Austria). A robust ANOVA was used to compare hardness and surface roughness measurements that were not normally distributed across brands and thermoforming conditions. Multiple comparisons following robust ANOVA were performed using robust pairwise t-tests, with Holm correction to control the family-wise error rate. Parameters that followed a normal distribution were compared across three or more groups using one-way ANOVA. Parameters that were not normally distributed were compared across three or more groups using the Kruskal-Wallis H test. Multiple comparisons

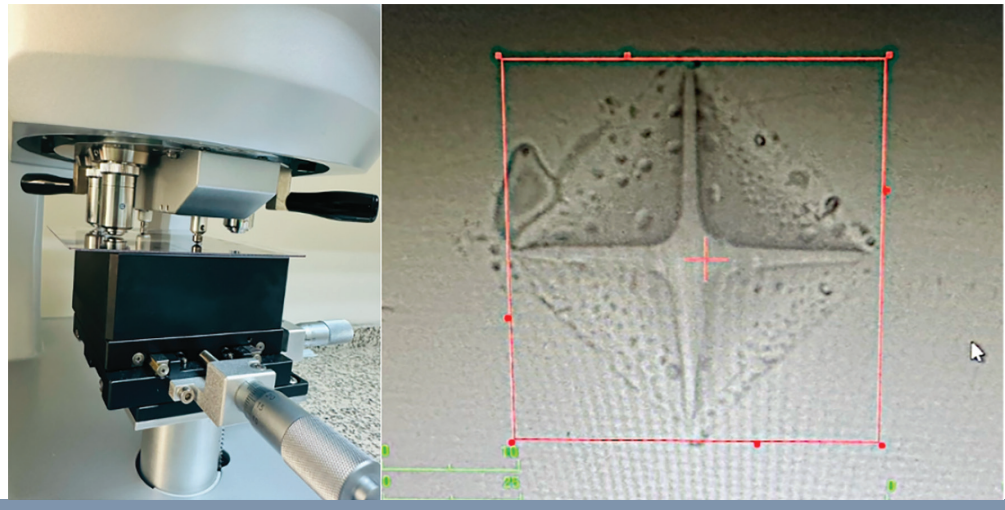

Figure 1. Micro-Vickers hardness of the vacuum-formed retainer samples.

were analyzed using Dunn's test. The results are presented as mean ± standard deviation and as the median (minimum-maximum). The significance level was set at $p<0.05$.

RESULTS

Surface hardness values before and after thermoforming, and the comparative statistics by brand and thermoforming are presented in Table 2. Differences in median surface hardness by brand were not statistically significant (p=0.212). However, the effects of thermoforming and thermoforming *brand factors on median hardness values were statistically significant (p<0.001). Comparative statistics for differences in surface hardness before and after thermoforming are presented. No statistically significant differences were observed among brands in mean hardness values (p=0.150).

Comparative statistics of the Ra, Rz, and Rq surface roughness values before and after thermoforming, by brand, are presented in Table 3. The main effect of brand on median Ra values was not statistically significant (p=0.054), whereas the main effect of thermoforming on median Ra values was statistically significant (p<0.001). Furthermore, the interaction between brand and thermoforming for Ra values was statistically significant (p=0.021). The highest median Ra value (0.12) was observed in the Taglus group after thermoforming, whereas the lowest median value (0.02) was found in the Duran, Atmos, Taglus, and Lumex-G groups before thermoforming. A statistically significant difference was observed in the median Ra values among brands (p=0.002). The median values were 0.03 for Duran, 0.02 for Atmos, 0.09 for Taglus, and 0.06 for Lumex-G. The median Ra value for Atmos was significantly lower than that for Taglus, but no significant difference was observed between Duran and Lumex-G.

The main effect of brand on median Rz values was not statistically significant (p=0.667), whereas the main effect of thermoforming on Rz values was statistically significant (p=0.037). However, the interaction effect between brand and thermoforming on Rz values was not statistically significant (p=0.300). For Rz surface roughness, the median values were: Duran 0.14 (0.10-0.52); Atmos 0.05 (0.32-0.4); Taglus 0.44 (0.11-2.57); and Lumex-G 0.3 (0.04-1.16). Median Rz values differed significantly among brands (p=0.004). The median Rz value for

Figure 2. Surface roughness measurement using Surftest SJ-301 (Mitutoyo, Kanagawa, Japan).

Table 2. Comparison of surface hardness values by brand and thermoforming

Brand	Thermoforming				Q	η^2	p
	Before Mean±SD Median (Min-Max)	After Mean±SD Median (Min-Max)	Difference Mean±SD Median (Min-Max)				
Duran	13.26±1.52 13.47 (10.07-15.23)^{A}	9.13±0.14 9.14 (8.85-9.38)^{B}	4.13±1.51 4.34 (1.08-6.09)	**B**	1.50	0.049	0.212
Atmos	12.35±0.56 12.25 (11.12-13.07)^{A}	9.22±0.18 9.22 (8.97-9.47)^{B}	3.12±0.6 3.21 (1.65-3.98)	**T**	173.55	0.664	<0.001
Taglus	12.38±1.23 12.67 (9.77-14.27)^{A}	9.30±0.39 9.34 (8.47-9.84)^{B}	3.08±1.37 3.24 (0.36-5.36)	**B*T**	18.06	0.381	<0.001
Lumex-G	12.00±1.80 11.9 (7.72-15.27)^{A}	9.10±0.21 9.02 (8.9-9.52)^{B}	2.90±1.85 2.82 (-1.4-6.29)				
Test statistics			1.860				
η^2			0.113				
p			0.150*				

^{A}: Groups sharing this superscript before thermoforming are not significantly different.
^{B}: Groups sharing this superscript after thermoforming are not significantly different
*One-way analysis of variance (ANOVA). Statistical significance: p<0.05.
Q, robust ANOVA test statistic; SD, standard deviation; η^2, effect sizes; B, brand; T, thermoforming; Min, minimum; Max, maximum.

Table 3. Comparison of average roughness, root mean square roughness, and maximum height of the profile values by brand and thermoforming

	Brand	Thermoforming		
		Before Mean±SD Median (Min-Max)	**After** Mean±SD Median (Min-Max)	**Difference** Mean±SD Median (Min-Max)
Ra	Duran	0.02±0.01 0.02 (0.02-0.04)^{AB}	0.06±0.02 0.06 (0.03-0.09)^{AC}	0.04±0.02 0.03 (0.01- 0.07)^{ab}
	Atmos	0.03±0.02 0.02 (0.02-0.10)^{B}	0.05±0.03 0.04 (0.02-0.13)^{ABC}	0.02±0.04 0.02 (0.06-0.11)^{b}
	Taglus	0.02±0.01 0.02 (0.02-0.04)^{B}	0.15±0.11 0.12 (0.05-0.4)^{ABC}	0.13±0.11 0.09 (0.01-0.38)^{a}
	Lumex-G	0.03±0.02 0.02 (0.02-0.10)^{B}	0.10±0.06 0.09 (0.05-0.26)^{C}	0.07±0.07 0.06 (0.05-0.24)^{ab}
		B	**T**	**B*T**
	Q	2.55	17.04	9.74
	Test statistics			14.761
	η^2	0.080	0.162	0.249
	p	0.054	<0.001	0.021
				0.002*
Rz	Duran	0.24±0.10 0.23 (0.14-0.49)	0.45±0.24 0.35 (0.25-0.67)	0.18±0.23 0.14 (0.10-0.52)^{ab}
	Atmos	0.28±0.09 0.26 (0.19-0.54)	0.34±0.16 0.3 (0.17-0.64)	0.06±0.19 0.05 (0.32-0.4)^{b}
	Taglus	0.18±0.05 0.16 (0.13-0.3)	0.96±0.88 0.6 (0.27-2.73)	0.82±0.86 0.44 (0.11-2.57)^{a}
	Lumex-G	0.25±0.10 0.23 (0.14-0.45)	0.65±0.30 0.54 (0.3-1.53)	0.38±0.35 0.3 (0.04 -1.16)^{ab}
		B	**T**	**B*T**
	Q	0.522	4.358	3.664
	Test statistics			13.355
	η^2	0.017	0.047	0.111
	p	0.667	**0.037***	0.300
				0.004*
Rq	Duran	0.04±0.02 0.03 (0.02-0.05)	0.08±0.02 0.07 (0.04-0.11)	0.04±0.03 0.03 (0-0.09)^{b}
	Atmos	0.03±0.01 0.03 (0.02-0.13)	0.06±0.04 0.06 (0.03-0.15)	0.03±0.05 0.02 (0.08-0.12)^{b}
	Taglus	0.03±0.01 0.03 (0.02-0.05)	0.33±0.23 0.19 (0.06-0.52)	0.18±0.14 0.16 (0.02-0.5)^{a}
	Lumex-G	0.04±0.02 0.03 (0.02-0.07)	0.13±0.07 0.12 (0.07-0.34)	0.1±0.08 0.08 (0.01-0.3)^{ab}
		B	**T**	**B*T**
	Q	2.00	15.57	7.25
	Test statistics			16.375
	η^2	0.064	0.150	0.198
	p	0.112	**<0.001**	0.064
				0.001*

*Kruskal-Wallis H Test. Statistical significance: p<0.05.
$^{A-B}$: Interactions with the same superscript letter are not significantly different.
$^{a-b}$: Interactions with the same superscript letter are not significantly different.
$^{A-C}$: Same uppercase superscripts in a column indicate no significant difference before thermoforming.
$^{a-b}$: Same lowercase superscripts in a column indicate no significant difference after thermoforming.
Q, robust ANOVA test statistics; Min, minimum; Max, maximum; η^2, effect sizes; B: brand; T, thermoforming.

Atmos was significantly lower than that for Taglus and did not differ significantly from those for Duran and Lumex-G.

The main effect of brand on median Rq values was not statistically significant (p=0.112). By contrast, the main effect of thermoforming on Rq values was statistically significant (p<0.001). However, the interaction effect of brand and thermoforming on Rq values did not reach statistical significance (p=0.064). A statistically significant difference was also observed in the median Rq values among brands (p=0.001). Furthermore, median Rq values for Duran, Atmos, Taglus, and Lumex-G were 0.03 (0-0.09), 0.02 (0.08-0.12), 0.16 (0.02-0.5), and 0.08 (0.01-0.3), respectively. The Rq value for Taglus was similar to that of Lumex-G, but was significantly different from those of Duran and Atmos.

The morphology of Taglus, Lumex-G, Atmos, and Duran after thermoforming was examined by SEM (Figure 3). Surface roughness measurements were obtained from the heat-treated centers. The Taglus and Lumex groups exhibited greater surface roughness than the Atmos and Duran groups.

Characteristic bond types in Taglus, Lumex-G, Atmos, and Duran were identified by FTIR analysis (Figure 4a). The peaks indicate that all groups have similar bond types, consistent with polyethylene (PE) terephthalate, as specified in the manufacturers' product datasheets.[22] The peaks observed at 1,712 and 1,238 cm^{-1} were attributed to the C=O and (C=O)-C functional groups, whereas CH_2, C-H, and C-C bond vibrations were detected at 1,095, 875, and 721 cm^{-1}, respectively. The FTIR spectra confirmed that the four materials have comparable chemical structures.

To evaluate thermal behavior, two complementary thermal analysis techniques were employed. DSC was used to assess the phase transition properties of the materials. The DSC results indicated that all materials had similar melting behavior, with the onset of melting occurring at around 370 °C-375 °C and peak melting temperatures reaching approximately 410 °C-415 °C. Thermogravimetric analysis (TGA) was performed to determine the thermal degradation characteristics. According to the TGA results, the onset of thermal degradation began at approximately 370 °C and was completed by 440 °C-445 °C, indicating that all the tested materials possessed high thermal stability before substantial decomposition occurred.

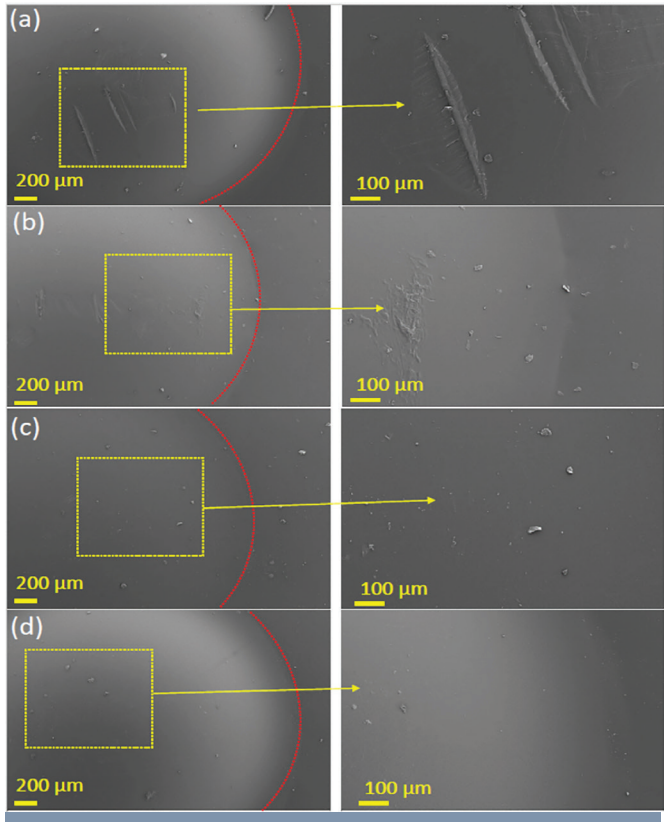

Figure 3. Scanning electron microscopy images of the vacuum-formed retainer materials: (a) Taglus, (b) Lumex-G, (c) Atmos, and (d) Duran.

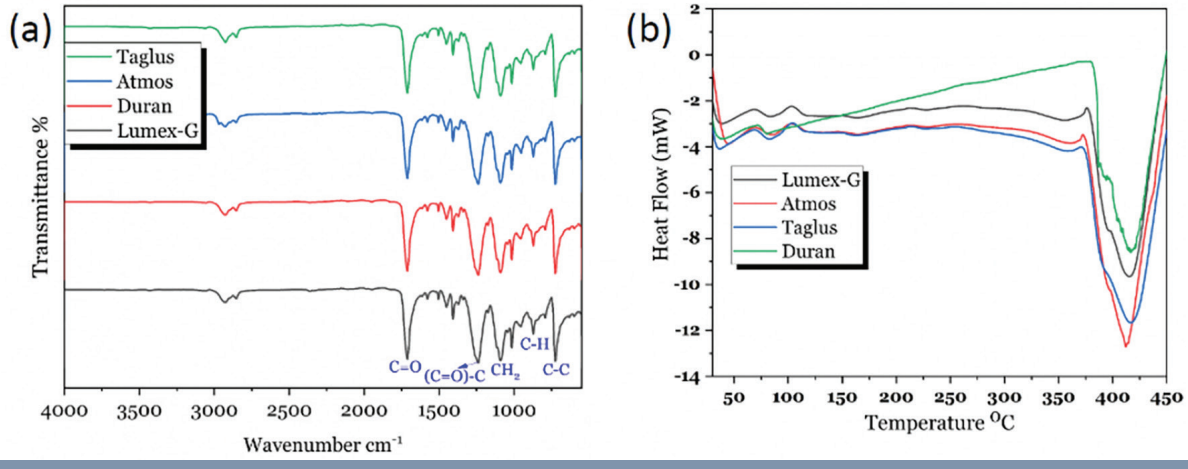

Figure 4. Fourier transform infrared spectroscopy analysis of the vacuum-formed retainer materials. materials. **(a)** FTIR spectra of the groups are presented. **(b)** DSC thermograms of the groups are presented.
FTIR, Fourier transform infrared spectroscopy; DSC, differential scanning calorimetry.

DISCUSSION

Maintaining the final tooth positions achieved through orthodontic treatment is critical for long-term treatment success. Although the duration of retention protocols varies with malocclusion type, an average retention period of one year is generally accepted. During this period, VFRs are exposed to masticatory forces and oral fluids, and their mechanical and surface properties play a key role in meeting aesthetic and functional expectations.[6,16] Therefore, analyzing changes in the surface hardness, roughness, and chemical structure of VFRs both in their initial state and after thermoforming is essential for evaluating their clinical effectiveness.[6,12] This study compared the mechanical properties of different VFR materials before and after thermoforming. Four thermoplastic retainer materials (Duran, Taglus, Atmos, and Lumex-G) were selected because they are among the most widely used in clinical orthodontics and represent different polymer types (PET-G, PET-G/ PE blend, PC, and copolyester, respectively). The findings of this study indicate that certain material properties are sensitive to thermoforming, resulting in a partial rejection of the null hypothesis.

Compositional analysis revealed that Duran and Lumex-G are primarily composed of PET-G, whereas Taglus contains both PET-G and PE. In contrast, Atmos is composed of copolyester. Differences in material composition may substantially affect mechanical stability, as PET-G has been reported to confer durability owing to its amorphous structure, chemical resistance, and thermal stability.[6-8,16] Albilali et al.[8] reported that PET-G-based materials maintained high hardness values even after thermal treatment. Although no statistically significant differences were observed between groups in the present study, hardness generally decreased following thermoforming. This reduction can be attributed to rearrangements of polymer chains in amorphous thermoplastics that compromise mechanical durability.[16] Furthermore, long-term exposure to oral fluids and prolonged water sorption may further accelerate reductions in hardness and elasticity, suggesting that *in vitro* thermoforming alone may underestimate the extent of clinical degradation.[23]

Additionally, the Taglus brand's PET-G and PE content may have contributed to its lower hardness values. PE is suggested to have lower hardness than PET-G, potentially reducing the blend's overall hardness. In contrast, the Atmos and Duran groups retained higher hardness values even after thermoforming. This finding may be attributed to the molecular homogeneity and thermal stability of pure copolyester and PET-G within their polymer structures. Our findings are largely consistent with the literature; however, the lower hardness values observed in the Taglus group may be related to its PE content and warrant further investigation.

The impact of thermoforming on the surface roughness of VFR materials is critical to both aesthetic performance and clinical application. Thermoforming may increase surface roughness due to the rearrangement of polymer chains. Such morphological alterations can lead to surface irregularities that ultimately reduce the long-term durability of orthodontic appliances.[8,11] Moreover, increased surface roughness values has been associated with increased bacterial adhesion and plaque accumulation on VFRs, increasing potential periodontal risk.[17] SEM analysis supported these findings, as the Taglus and Lumex-G surfaces exhibited greater surface irregularities than Atmos and Duran, consistent with the profilometry results. Recent studies have also investigated new thermoplastic materials, such as TPU and polyolefins, which may offer improved resistance to surface degradation compared with that of PET-G; however, clinical validation remains limited.[20]

In the present study, a significant increase in surface roughness was observed after thermoforming, particularly in the Taglus and Lumex-G groups. This finding suggests that the molecular homogeneity of these materials might be disrupted during thermal processing. Specifically, the PE content in Taglus, which is less hard than PET-G, may have contributed to this result by weakening the material's structural stability. Lumex-G, although PET-G-based, may be more susceptible to thermal rearrangement due to differences in polymer chain alignment or manufacturing processes.

These results align with previous studies indicating that thermoforming often leads to surface irregularities, which can reduce the long-term durability of orthodontic appliances. For example, Ahn et al.[16] demonstrated that thermal aging processes significantly altered the molecular structure and surface morphology of VFR materials, resulting in increased surface roughness. Furthermore, this roughness may serve as a site for bacterial adhesion, compromising the appliance's clinical effectiveness.[15-18] Gardner et al.[11] reported that rough surfaces could interact with oral fluids and food residues, leading to increased microbial plaque accumulation, which may negatively impact periodontal health. Therefore, minimizing the effects of thermoforming on surface roughness is critical for material selection and manufacturing process design.

In the present study, changes in surface and chemical structure of VFR materials after thermoforming were evaluated using SEM and FTIR. The SEM results revealed that the surfaces in the Taglus and Lumex-G groups exhibited greater irregularities than those of the Atmos and Duran groups. This finding is consistent with the observed increases in surface roughness and may be associated with disruptions in the Taglus and Lumex-G materials' molecular homogeneity. These surface irregularities are thought to result from microscopic rearrangements of polymer chains, and the SEM observations are consistent with the surface roughness results.

Moreover, FTIR analysis revealed that all materials shared similar functional groups, with characteristic peaks consistent with PET-G-based structures. Specifically, the peaks observed at 1,712 and 1,238 cm^{-1} correspond to the C=O and (C=O)-C functional groups, respectively. However, the surface and

thermal properties of materials can vary due to processing parameters such as time, temperature, and pressure as well as other physical effects. Using the same PET-G raw materials may produce identical bond types in FTIR analysis, whereas different processing parameters such as temperature, pressure, and duration may produce different thermal and physical properties. These minor differences were evident in the SEM and DSC results. Even if FTIR indicates chemical stability after thermoforming, small differences in surface roughness, hardness, and decomposition temperatures can be attributed to physical defects such as porosity. This observation also highlights a limitation of FTIR analysis: while it effectively detects major chemical structures, it may not capture subtle molecular-level differences, especially in copolymer blends. For example, the increase in surface roughness observed in the Taglus group could be due to microscopic rearrangements in amorphous regions induced by the presence of PE. Such minor chemical changes may not be detectable by FTIR, but can still manifest as alterations in surface morphology.

Study Limitations

The inability to evaluate, *in vivo*, the physical changes induced by chewing forces on VFR materials, the lack of long-term assessment of the effects of saliva and other oral fluids, and the fact that thermoforming was performed by a single operator represent the primary limitations of this study. In addition, no artificial aging procedures (e.g., thermal cycling, mechanical loading, or water sorption tests) were applied, limiting extrapolation of the findings to long-term clinical performance. Furthermore, the assessment of material properties was limited to Vickers hardness and two-dimensional profilometry. The absence of advanced characterization techniques, such as three-dimensional surface topography analysis or nanoindentation, may have restricted a more detailed understanding of microstructural changes. These limitations should be taken into consideration when interpreting the present findings, and future studies addressing these aspects would provide a more comprehensive evaluation of thermoplastic retainer materials.

CONCLUSION

Following thermoforming, a significant increase in surface roughness was observed in the Taglus and Lumex-G groups, whereas the Atmos and Duran groups largely maintained surface stability. DSC and FTIR analyses indicated that no major chemical or thermal degradation occurred in any of the materials, while SEM analysis confirmed surface-level morphological changes, particularly in the Taglus and Lumex-G groups. Within the limitations of this *in vitro* study, PET-G-based materials with high surface homogeneity appeared to demonstrate better surface stability.

Ethics

Ethics Committee Approval: As the study did not involve the use of human or animal materials, ethical approval was not required.

Informed Consent: Not applicable.

Footnotes

Author Contributions: Concept - Y.T., N.F.; Design - Y.T., M.T.; Data Collection and/or Processing - Y.T., M.T.; Analysis and/or Interpretation - M.T., Y.A.; Literature Search - Y.T., M.T.; Writing - Y.T., N.F.

Conflict of Interest: The authors have no conflicts of interest to declare.

Financial Disclosure: The authors declared that this study received no financial support.

REFERENCES

1. Johnston CD, Littlewood SJ. Retention in orthodontics. *Br Dent J.* 2015;218(3):119-122. [CrossRef]
2. Quinzi V, Carli E, Mummolo A, De Benedictis F, Salvati SE, Mampieri G. Fixed and removable orthodontic retainers, effects on periodontal health compared: a systematic review. *J Oral Biol Craniofac Res.* 2023;13(2):337-346. [CrossRef]
3. Ruyi W, Zhihe Z, Yu L. [Current situation and prospect for orthodontic thermoplastic materials]. *Hua Xi Kou Qiang Yi Xue Za Zhi.* 2018;36(1):87-91. [Chinese]. [CrossRef]
4. Ozeer KAA, David SA, Mohamed U, Sunil PC, Paul S, Paul P. An Innovative Approach to Retention: Thermoplastic Retainer. *J Contemp Dent Pract.* 2017;18(7):572-575. [CrossRef]
5. Manzon L, Fratto G, Rossi E, Buccheri A. Periodontal health and compliance: a comparison between Essix and Hawley retainers. *Am J Orthod Dentofacial Orthop.* 2018;153(6):852-860. [CrossRef]
6. Grünheid T, Bitner TF. Wear and fatigue resistance: an in-vitro comparison of three polyethylene terephthalate glycol and thermoplastic polyurethane materials for vacuum-formed retainers. *Int Orthod.* 2023;21(2):100748. [CrossRef]
7. Kwon JS, Lee YK, Lim BS, Lim YK. Force delivery properties of thermoplastic orthodontic materials. *Am J Orthod Dentofacial Orthop.* 2008;133(2):228-234; quiz 328.e1. [CrossRef]
8. Albilali AT, Baras BH, Aldosari MA. Evaluation of water sorption and solubility and FTIR spectroscopy of thermoplastic orthodontic retainer materials subjected to thermoforming and thermocycling. *Applied Sciences.* 2023;13(8):5165. [CrossRef]
9. Jaggy F, Zinelis S, Polychronis G, et al. ATR-FTIR analysis and one-week stress relaxation of four orthodontic aligner materials. *Materials (Basel).* 2020;13(8):1868. [CrossRef]
10. Dalaie K, Rafsanjan KT, Nojehdehian H, Namazi Z. Physical and chemical changes of clear aligners after thermoforming and intraoral exposure. *APOS-Trends Orthod.* 2024;14(4):235-247. [CrossRef]
11. Gardner GD, Dunn WJ, Taloumis L. Wear comparison of thermoplastic materials used for orthodontic retainers. *Am J Orthod Dentofacial Orthop.* 2003;124(3):294-297. [CrossRef]
12. Zhang N, Bai Y, Ding X, Zhang Y. Preparation and characterization of thermoplastic materials for invisible orthodontics. *Dent Mater J.* 2011;30(6):954-959. [CrossRef]
13. Riggio M, Piazza M. Hardness test. In: Kasal B, Tannert T, eds. In situ assessment of structural timber. Dordrecht, Netherlands: Springer; 2010:123-135. [CrossRef]
14. Hartcher-O'Brien J, Evers J, Tempelman E. Surface roughness of 3D printed materials: comparing physical measurements and human perception. *Materials Today Communications.* 2019;19(1):300-305. [CrossRef]

15. Alfadil L, Patel M, Pandis N, Fleming PS. Assessment of wear characteristics, longevity and stiffness of Essix-type retainers. *Clin Oral Investig.* 2024;28(3):185. [CrossRef]
16. Ahn HW, Ha HR, Lim HN, Choi S. Effects of aging procedures on the molecular, biochemical, morphological, and mechanical properties of vacuum-formed retainers. *J Mech Behav Biomed Mater.* 2015;51:356-366. [CrossRef]
17. Al Groosh DH, Bozec L, Pratten J, Hunt NP. The influence of surface roughness and surface dynamics on the attachment of Methicillin-Resistant Staphylococcus aureus onto orthodontic retainer materials. *Dent Mater J.* 2015;34(5):585-594. [CrossRef]
18. Pascual AL, Beeman CS, Hicks EP, Bush HM, Mitchell RJ. The essential work of fracture of thermoplastic orthodontic retainer materials. *Angle Orthod.* 2010;80(3):554-561. [CrossRef]
19. Littlewood SJ, Millett DT, Doubleday B, Bearn DR, Worthington HV. Retention procedures for stabilising tooth position after treatment with orthodontic braces. *Cochrane Database Syst Rev.* 2016;2016(1):CD002283. [CrossRef]
20. Asefi S, Nejatifard M, Kayyal S, Shahabi S. Investigation of the mechanical properties of thermoplastic materials influenced by different chemicals. *Turk J Orthod.* 2024;37(2):91-97. [CrossRef]
21. Alexandropoulos A, Al Jabbari YS, Zinelis S, Eliades T. Chemical and mechanical characteristics of contemporary thermoplastic orthodontic materials. *Aust Orthod J.* 2015;31(2):165-170. [CrossRef]
22. Lumex G Information Sheet. PPB Ltd. Published May 2020. Accessed December 25, 2025. [CrossRef]
23. Ryu JH, Kwon JS, Jiang HB, Cha JY, Kim KM. Effects of thermoforming on the physical and mechanical properties of thermoplastic materials for transparent orthodontic aligners. *Korean J Orthod.* 2018;48(5):316-325. [CrossRef]

DOI: 10.4274/TurkJOrthod.2025.2025.79

TURKISH JOURNAL OF
ORTHODONTICS

Original Article

Evaluation of in Vivo Effects of Low-Intensity Pulsed Ultrasound and Low-Level Laser Therapy on Premaxillary Suture During Rapid Maxillary Expansion

Esra Erkan[1], Şeniz Karaçay[2], Esra Çikler[3], İlayda Özge Polat[3]

[1]Private Practice, İstanbul, Türkiye
[2]University of Health Sciences Faculty of Dentistry, Department of Orthodontics, İstanbul, Türkiye
[3]University of Health Sciences Faculty of Medicine, Department of Histology and Embryology, İstanbul, Türkiye

Cite this article as: Erkan E, Karaçay Ş, Çikler E, Polat İÖ. Evaluation of in vivo effects of low-intensity pulsed ultrasound and low-level laser therapy on premaxillary suture during rapid maxillary expansion. *Turk J Orthod.* 2025; 38(4): 233-243

Main Points

- During rapid maxillary expansion, low-intensity pulsed ultrasound (LIPUS) application is more effective than low-level laser therapy (LLLT) in terms of the suture width, newly formed bone areas, and vascular endothelial growth factor (VEGF) expression in the suture.
- LLLT and LIPUS do not affect the number of osteoblasts in the suture when they are applied alone, while their combined therapy significantly increases osteoblast numbers.
- Combined therapy triggers angiogenesis and osteogenesis more by increasing the expressions of bone morphogenetic protein-2, osteopontin, and VEGF in the suture compared with monotherapies.
- Combined therapy has a synergistic effect and strengthens the effects of LLLT and LIPUS on premaxillary sutural ossification.

ABSTRACT

Objective: To evaluate and compare the effects of low-intensity pulsed ultrasound (LIPUS), low-level laser therapy (LLLT), and their combined effects on sutural bone regeneration during rapid maxillary expansion (RME) of rats.

Methods: Twenty-eight Sprague-Dawley rats were randomly assigned to four groups: LLLT group, LIPUS group, combination group, and control group. RME was performed on all groups for 11 days. The Both LLLT and LIPUS groups received their respective therapies (30 J/cm^2), while the combination group received both therapies, each at 30 J/cm^2. All treated rats received their doses on days 0, 4, and 8 and were sacrificed on day 11. Numbers of osteoblasts, capillaries, and osteoclasts were counted, and suture widths and areas of newly formed bone were measured histomorphometrically. General and cellular immunoreactivity of bone morphogenetic protein-2 (BMP-2), vascular endothelial growth factor (VEGF), and osteopontin (OPN) was evaluated by immunohistochemistry.

Results: The number of osteoblasts was significantly higher in the combination group than in the control group ($p<0.05$). The combination group showed the highest general BMP-2 immunoreactivity and cellular VEGF immunoreactivity among all groups, and exhibited increased cellular OPN immunoreactivity compared with the control group ($p<0.05$). Both the area of newly formed bone ($p<0.05$) and suture width ($p<0.01$) were significantly greater in the LIPUS group than in the LLLT group.

Conclusion: LIPUS is a more effective adjuvant therapy than LLLT for increasing sutural bone formation during RME. Combined therapy with LIPUS and LLLT has a synergistic effect and accelerates sutural bone regeneration by enhancing cellular activation more than either LIPUS or LLLT alone.

Keywords: Low-level laser therapy, low-intensity pulsed ultrasound, maxillary expansion, rat

Corresponding author: Esra Erkan, MD, **e-mail:** dr.esraerkan@gmail.com
Received: July 20, 2025 **Accepted:** December 22, 2025 **Publication Date:** 30.12.2025

INTRODUCTION

Rapid maxillary expansion (RME) has been used in the treatment of transverse maxillary deficiencies for over a century, since Angell first described the procedure in the 1860's.[1] The primary disadvantage of RME is the prolonged retention period required to permit new bone deposition in the expanded suture. Therefore, researchers have studied many alternative methods, such as various pharmacological agents (vitamin E, propolis, topical ozone, osthole, and simvastatin), to accelerate new bone formation, reduce relapse, and shorten the retention period by increasing the regenerative capacity of the midpalatal suture during the expansion and retention periods.[2-6] Additionally, low-intensity pulsed ultrasound (LIPUS) and low-level laser therapy (LLLT) are among the newer methods introduced in recent years to accelerate bone regeneration.[7-10]

LLLT irradiation is reported to be absorbed by cytochrome c oxidase in the inner mitochondrial membrane, stimulating the cellular energy cycle and metabolic activity.[11] Secondary mediators that arise in response to photobiomodulation activate transcription factors and signaling pathways. Many transcription factors associated with osteogenesis have been reported to be activated by laser light. In recent studies, LLLT has been used to reduce orthodontic pain and orthodontically induced root resorption, to accelerate tooth movement, and to promote bone regeneration during expansion.[8,10,12]

When low-intensity ultrasound waves are absorbed by tissue, non-thermal effects, including cavitation and acoustic streaming occur, resulting in increased cell membrane ion permeability and enhanced cellular activity.[13] Because of these properties, LIPUS is used for tissue regeneration and bone healing.[7,14]

Despite the growing literature supporting their individual effectiveness, comparative studies examining the effects of LLLT and LIPUS on bone formation remain limited. Lirani-Galvão et al.[15] performed osteotomies in rats to compare the in vivo effects of LLLT and LIPUS on bone repair. Their study concluded that LLLT promoted bone formation, while LIPUS facilitated bone resorption. Subsequently, another study investigating bone defect healing in rats reported that LLLT had positive effects on new bone formation, while LIPUS had no significant effects.[16] Babuccu et al.[14] compared the effects of LLLT, LIPUS, and their combined application on tibial osteotomies in rats. The study demonstrated that vascularization and new bone formation were higher, and inflammation was lower, in the combination group than in the other groups. Mahmoud et al.[17] reported that, in patients with dental implants, LIPUS significantly reduced post-implant marginal bone loss compared with LLLT, whereas LLLT was more effective for soft tissue healing, and combined therapy reduced pain intensity. However, the potential synergistic effect of combined LLLT and LIPUS therapy has not been investigated for RME.

The first hypothesis of this study was that LIPUS would be more effective than LLLT in stimulating cellular activation and new bone formation when applied to the premaxillary suture at equal doses during RME. The second hypothesis was that combined therapy would enhance sutural activation and increase areas of newly formed bone more effectively than monotherapies due to their distinct mechanisms of action at the cellular level.

METHODS

This animal study was carried out in year 2021. All animal study procedures were approved by the University of Health Sciences Hamidiye Local Ethics Committee for Animal Experiments (approval no.: 2020-03/05, date: 25.06.2020). Twenty-eight female Sprague-Dawley rats, aged 9-10 weeks and weighing between 100-160 g, were used in the study. Experimental animals were housed in separate plastic cages in their respective groups at 23 °C under fluorescent lighting with a 12-hour light/dark cycle. Throughout the study period, the animals were fed a standard pellet diet and provided with tap water ad libitum.

According to the power analysis (G*Power, version 3.1; effect size 0.5, α 0.05, and power 80%), seven animals were required in each experimental group, and the sample size was approved by the ethics committee. The rats were assigned to four groups (i.e., three experimental groups and a control group) each consisting of seven animals, using simple randomization performed by a technician blinded to the experimental procedure. The experimental groups were the LLLT group, the LIPUS group, and the combination (LLLT plus LIPUS) group.

Body Weights Measurements

The body weights of all animals were measured using a precision scale at the beginning and end of the study (days 0 and 11).

General Anesthesia

Placement of the RME appliances and administration of LLLT and LIPUS treatments were performed under general anesthesia. Xylazine (10 mg/kg; Xylazinbio 2%, Bioveta A.S., South Moravian, Czech Republic) and ketamine (90 mg/kg; Ketasol 10%, Richter Pharma AG, Wels, Austria) were administered via intraperitoneal injection.

Premaxillary Suture Expansion Procedure

RME appliances were fabricated from 0.014-inch stainless-steel wire and incorporated three helical springs (Figure 1A). The springs were adjusted to deliver a force of 100 g. Retention grooves were prepared on the distal surfaces of the incisors at the gingival level with a stainless-steel disc. The expansion appliances were fixed to the maxillary incisors of all animals with 0.010-inch stainless-steel ligature wires and covered with a light-curing glass-ionomer composite resin (Figures 1B and 1C). The springs were not reactivated at any point during the experimental period. The distance between the mesial edges of the maxillary incisors was defined as the 0-mm baseline at

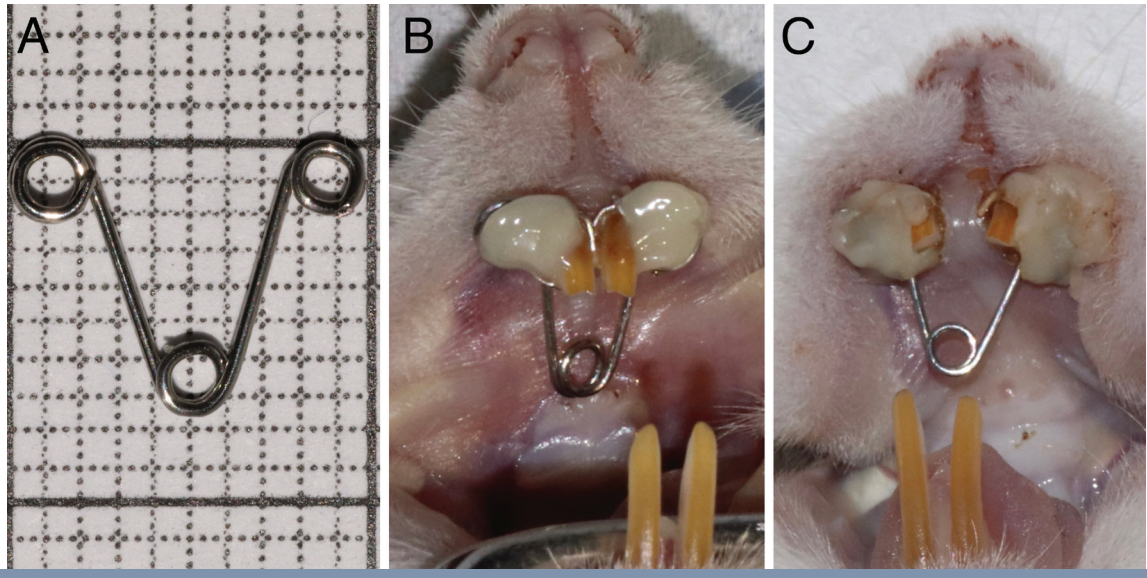

Figure 1. (A) The expansion spring on the grid; (B) The expansion appliance at the beginning; (C) The expansion appliance on 4th day.

the start of the study and remeasured at the end of the study. Occlusal radiographs were taken on days 4 and 11 to determine whether the premaxillary suture opened (Figure 2A). On day 11, an occlusal radiograph demonstrating and open premaxillary suture in a rat from the combination group is shown in Figure 2B. The RME procedure was applied to all experimental groups as well as to the control group, which did not receive any adjunctive biostimulatory treatment (e.g., LLLT or LIPUS).

LLLT Treatment

An aluminum gallium arsenide dental diode laser (Solase-976, Lazon Medical Laser Co. Ltd., Liaoning, China) was applied intraorally to the palatal mucosa immediately posterior to the maxillary incisors using a biostimulation probe (Figure 3A). Laser irradiation was performed on days 0, 4, and 8. The laser parameters used in the study are given in Table 1. Only the LLLT and combination groups received laser therapy. LLLT was applied to the combination group prior to LIPUS treatment.

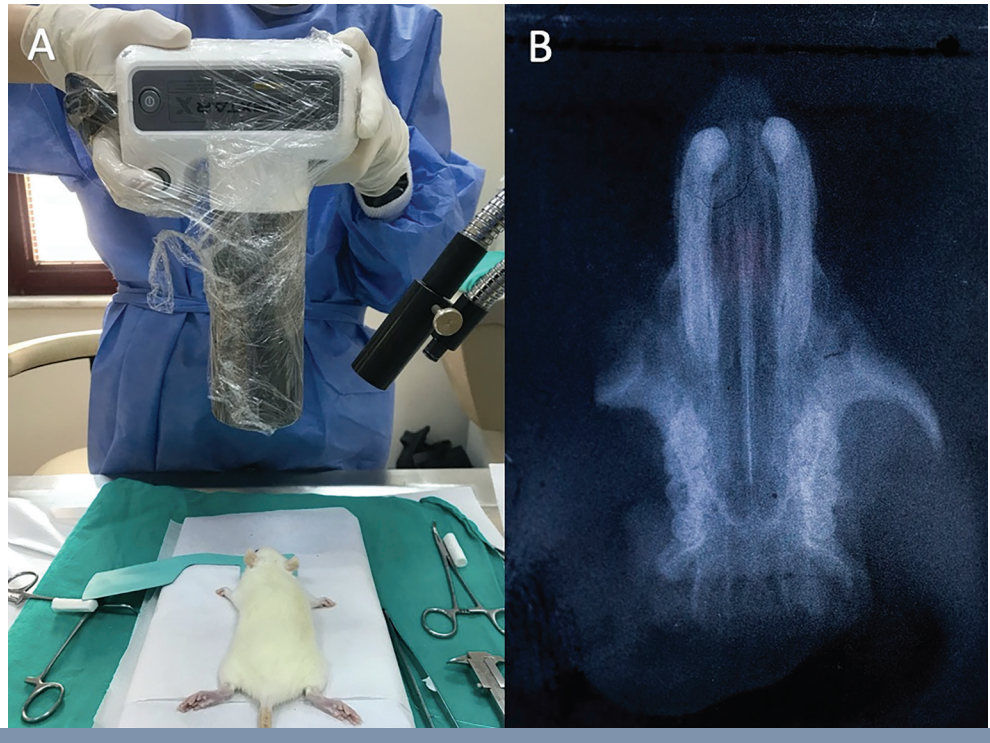

Figure 2. (A) Occlusal imaging technique with a portable X-ray device. (B) Radiographic image of an open premaxillary suture in a rat from the combination group.

LIPUS Treatment

LIPUS therapy was administered to all animals in the LIPUS and combination groups with a medical LIPUS device and a 1-cm-diameter ultrasound transducer (4710-Premium, BTL Industries Ltd., Hertfordshire, UK). After the rats' snouts were covered with coupling gel, the transducer was applied extraorally over each snout, perpendicular to the premaxillary suture (Figure 3B). Ultrasound irradiation was performed on days 0, 4, and 8. The ultrasound device parameters used in the study are given in Table 2. Only the LIPUS and combination groups received ultrasound therapy.

Specimen Preparation

On day 11, all animals were euthanized by intraperitoneal injection with an overdose of ketamine and xylazine. The premaxillae were surgically dissected, and the RME appliances were removed. After the premaxilla specimens were fixed in 10% neutral buffered formalin, they were decalcified with 10% formic acid for three weeks. Subsequently, the premaxillae were dissected perpendicular to the sagittal plane, using the incisors as primary guides. The first incision was made at the alveolar crest, and the second was made 4 mm apical to it. The tissue samples were dehydrated by passing through an ascending series of ethyl alcohol solutions, embedded in paraffin blocks and serially sectioned at 4-5 µm.

Histomorphometry

For histomorphometric evaluation, the sections were deparaffinized, rehydrated, and stained with hematoxylin and eosin. The numbers of osteoblasts, capillaries, and osteoclasts were counted in three randomly selected sections per animal. Suture width was measured between the frontal margins of the palatal bones at the most anterior region of the premaxillary suture. Newly formed bone areas were calculated by tracing the borders of the newly ossified areas of the suture using Cameram Gen III software (Argenit Ltd., İstanbul, Türkiye).

Immunohistochemistry

Sections obtained from paraffin tissue blocks were rehydrated by passing through a descending alcohol series. Following incubation in citrate buffer at high temperature, the sections were allowed to cool to room temperature. Endogenous peroxidase activity was inhibited with a 3% H_2O_2 solution. Sections were washed with phosphate-buffered saline (PBS) and then soaked in protein-blocking solution for 10 min. Anti-vascular endothelial growth factor (VEGF) (GTX22992, GeneTex

Table 1. The laser device parameters used in the study

Active medium	AlGaAs
Wavelength	976 nm
Irradiation mode	Continuous
Output power	500 mW
Irradiation time	60 sec
Energy (daily)	30 J
Dose (daily)	30 J/cm^2
Irradiation days	0th, 4th, 8th days

AlGaAs, aluminum gallium arsenide.

Table 2. The ultrasound device parameters used in the study

Intensity (I_{SATP})	200 mW/cm^2
Intensity (I_{SATA})	50 mW/cm^2
Duty cycle	25%
Irradiation time	10 min
Output power	0.1 W
Pulse repetition period	100 Hz
Frequency	3 MHz
Energy (daily)	30 J
Dose (daily)	30 J/cm^2
Irradiation days	0th, 4th, 8th days

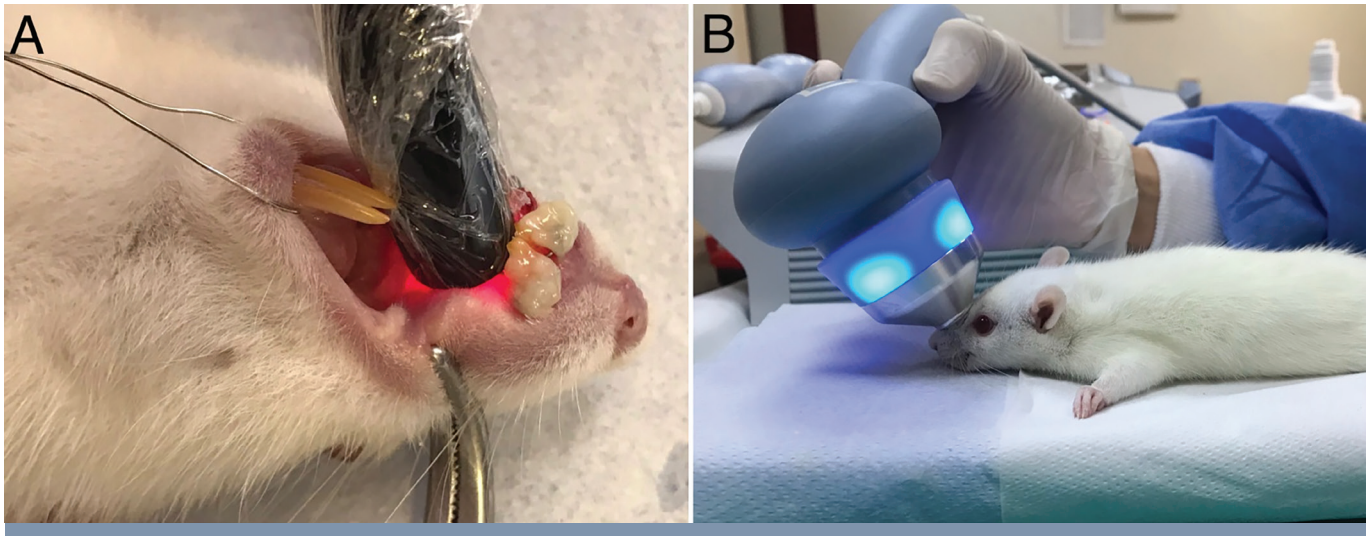

Figure 3. (A) LLLT and (B) LIPUS treatments.
LIPUS, low-intensity pulsed ultrasound; LLLT, low-level laser therap.

Inc., California, USA), anti- bone morphogenetic protein-2 (BMP-2) (GTX64355, GeneTex Inc., California, USA), or anti-osteopontin (OPN) (ab216402, Abcam plc, Cambridge, UK) primary antibodies were applied to the slides, and the sections were incubated for 24 hours at 4 °C.

After incubation, sections were washed with PBS and stained with a secondary antibody and 3,3′ diaminobenzidine. The tissue sections were counterstained with hematoxylin, passed through an ascending series of alcohols, cleared in xylene, and then mounted using Entellan mounting medium. Immunohistochemical evaluations were classified as general or cellular. For general evaluations, tissue preparations stained with anti-VEGF, anti-OPN, and anti-BMP-2 antibodies were graded as mild (+), moderate (++), or intense (+++) based on overall staining intensity. For cellular evaluations, three randomly selected areas from each section were examined, and the number of positively stained cells was graded as 1-10 (+, mild); 11-20 (++, moderate); or >20 (+++, high). All histomorphometry and immunohistochemistry assessments were performed by a single investigator who was blinded to the clinical procedures.

Statistical Analysis

Statistical analyses were performed using NCSS 2007 statistical software (NCSS LLC, Utah, USA). For data evaluation, in addition to descriptive statistics (e.g., means and standard deviations), variables were tested for normality using the Shapiro-Wilk test. One-Way ANOVA was used for comparisons of normally distributed variables; Tukey's multiple comparison test was used for pairwise comparisons among groups; the Kruskal-Wallis test was used for comparisons of variables that were not normally distributed; and the chi-squared test was used for comparisons of categorical variables. $p<0.05$ was considered statistically significant.

RESULTS

Bodyweight Change and Dental Expansion

Although the control group experienced significant weight loss, there was no significant difference between the groups in the magnitude of body weight change. Following RME, a midline diastema between the maxillary incisors occurred in all rats and measured 1.54±0.62 mm in the LLLT group, 1.83±0.32 mm in the LIPUS group, 1.69±0.34 mm in the combination group, and 2.03±0.58 mm in the control group. No statistically significant differences were detected among the groups with respect to dental expansion measurements.

Histological Observation Findings

Histological examination of hematoxylin and eosin-stained sections revealed that the width of the midpalatal suture was smaller in the LLLT group than in the other groups. Correspondingly, fewer osteoblasts were present adjacent to the new ossification areas, but they tended to be arranged in a regular pattern. In the LIPUS and combination groups, the midpalatal suture width increased compared with the LLLT group, and new ossification areas formed. The number of osteoblasts adjacent to these areas increased, and the osteoblasts were arranged in a regular pattern. In the control group, both the histological suture width and the areas of new ossification were smaller than those observed in the experimental groups. In addition, osteoblasts in the control group group had not yet achieved a regular arrangement.

Histomorphometric Findings

Histomorphometric values and intergroup comparisons are presented in Table 3.

Osteoblast, capillary, and osteoclast numbers

The combination group had a significantly higher number of osteoblasts than the control group ($p<0.05$); however, there were no significant differences among the other groups. Furthermore, no significant differences were detected among the groups regarding capillary and osteoclast numbers (Table 3).

Suture width and newly formed bone areas

Suture width was significantly greater in the LIPUS group than in the combination, LLLT, and control groups ($p<0.001$). The suture width in the control group was significantly lower than that in the combination ($p<0.01$) and LLLT ($p<0.05$) groups (Figure 4). The area of newly formed bone was significantly greater in the LIPUS group than in the LLLT group ($p<0.05$); no significant differences were observed among the other groups.

Immunohistochemical Findings

Immunohistochemical values and intergroup comparisons are presented in Table 4. Overall BMP-2 intensity in the combination group was significantly higher than in the LLLT ($p<0.05$), LIPUS ($p<0.01$), and control ($p=0.01$) groups. Also, cellular BMP-2 immunoreactivity in the combination group was higher than in the control group ($p<0.05$). There were no significant differences between the other groups in terms of BMP-2 staining ($p>0.05$).

The general intensity of VEGF staining in the LLLT group was significantly lower than that observed in the combination and LIPUS groups ($p<0.05$). Cellular VEGF immunoreactivity was significantly higher in the combination group than in the other three groups ($p<0.05$). The LIPUS group had higher scores for cellular VEGF immunoreactivity than the LLLT group ($p<0.05$).

When general OPN intensities were evaluated, no significant difference between the groups was observed ($p>0.05$). However, cellular OPN immunoreactivity in the LIPUS and combination groups was higher than in the control group ($p<0.05$) (Figure 5 and Table 4).

DISCUSSION

The aim of the study was to accelerate bone regeneration in the premaxillary suture area during RME in rats by applying

Table 3. Histomorphometric values and comparisons of experimental and control groups

Variables	LLLT	LIPUS	Combination	Control	p	Multiple comparisons**
Osteoblast*	18.06±2.23	21.08±2.44	22.33±5.83	16.21±3.24	**0.02**	LLLT-LIPUS-0.444 LLLT-Combination-0.168 LLLT-Control-0.787 LIPUS-Combination-0.922 LIPUS-Control-0.094 **Combination-Control-0.025**
Capillary*	0.841±0.734	0.667±0.476	0.988±0.533	0.234±0.274	0.071	-
Osteoclast‡	0.016±0.042	0.016±0.042	0.063±0.108	0.016±0.042	0.765	-
Suture width (µm)*	748.86±147.11	1262.71±175.31	785.71±110.27	500.14±157.5	**0.0001**	**LLLT-LIPUS-0.0001** LLLT-Combination-0.967 **LLLT-Control-0.023** **LIPUS-Combination-0.0001** **LIPUS-Control-0.0001** **Combination-Control-0.008**
Newly formed bone area (µm2)*	459152.14±197901.96	726396.57±69415.55	547663.71±103047.08	487069±276129.57	**0.046**	**LLLT-LIPUS-0.049** LLLT-Combination-0.797 LLLT-Control-0.991 LIPUS-Combination-0.276 LIPUS-Control-0.09 Combination-Control-0.922

The values marked in bold are: ($p<0.05$). *One-way ANOVA test, ‡Kruskal-Wallis test, **Tukey multiple comparison test.
LIPUS, low-intensity pulsed ultrasound; LLLT, low-level laser therapy.

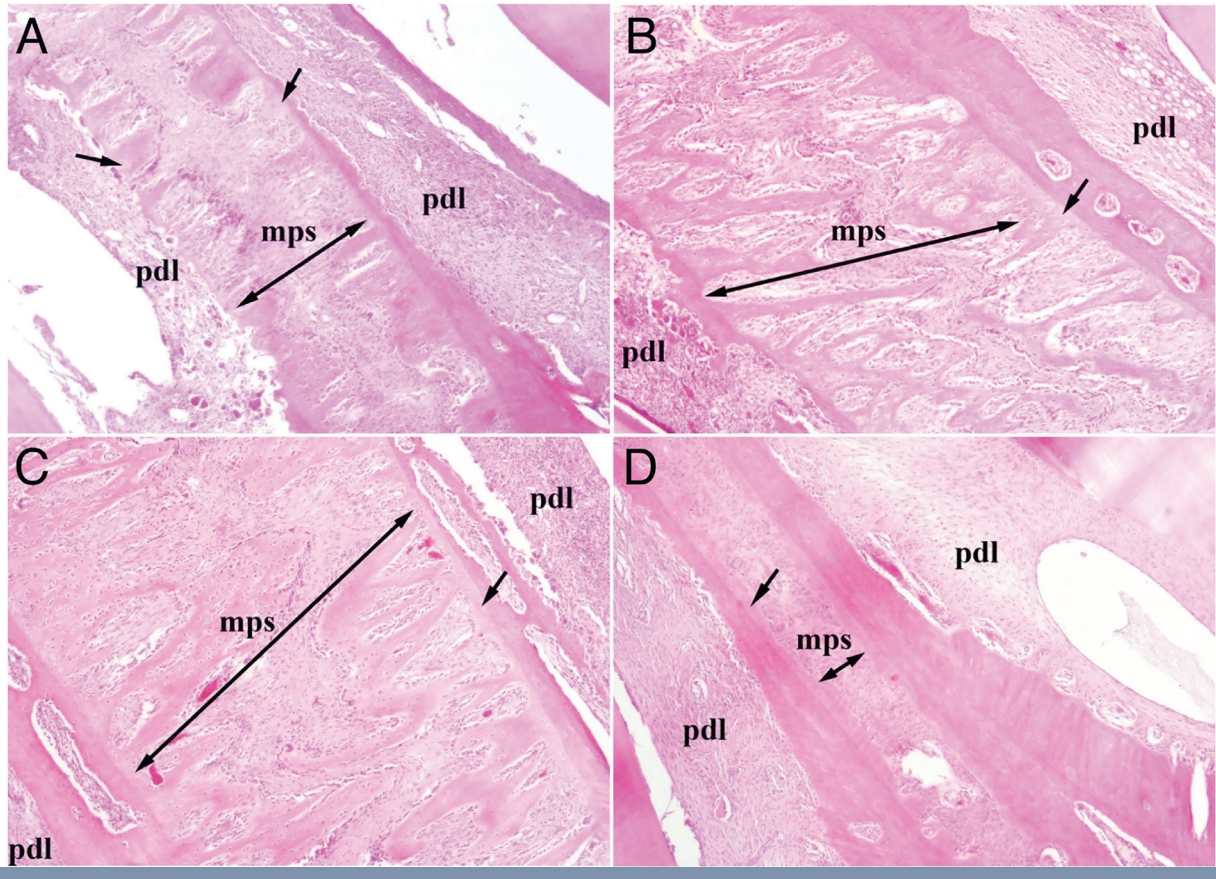

Figure 4. Morphology of midpalatal suture in the LLLT group (A), LIPUS group (B), combination group (C), control group (D) (400X magnification; mps: midpalatal suture, pdl: periodontal ligament).

LIPUS, low-intensity pulsed ultrasound; LLLT, low-level laser therapy.

Table 4. Immunohistochemical values and comparisons of experimental and control groups

Variables			LLLT	LIPUS	Combination	Control	p	Multiple comparisons**
BMP-2*	GI	(+)	57.14%	85.71%	0.00%	71.43%	**0.005**	LLLT-LIPUS-0.236 **LLLT-Combination-0.018** LLLT-Control-0.577 **LIPUS-Combination-0.004** LIPUS-Control-0.515 **Combination-Control-0.01**
		(++)	42.86%	14.29%	42.86%	28.57%		
		(+++)	0.00%	0.00%	57.14%	0.00%		
	CI	(+)	71.43%	85.71%	28.57%	100.00%	**0.03**	LLLT-LIPUS-0.515 LLLT-Combination-0.117 LLLT-Control-0.127 LIPUS-Combination-0.069 LIPUS-Control-0.299 **Combination-Control-0.021**
		(++)	28.57%	14.29%	28.57%	0.00%		
		(+++)	0.00%	0.00%	42.86%	0.00%		
VEGF*	GI	(+)	57.14%	0.00%	0.00%	42.86%	**0.041**	**LLLT-LIPUS-0.038** **LLLT-Combination-0.018** LLLT-Control-0.564 LIPUS-Combination-0.280 LIPUS-Control-0.147 Combination-Control-0.091
		(++)	42.86%	7.43%	42.86%	42.86%		
		(+++)	0.00%	28.57%	57.14%	14.29%		
	CI	(+)	71.43%	0.00%	28.57%	42.86%	**0.002**	**LLLT-LIPUS-0.018** **LLLT-Combination-0.016** LLLT-Control-0.427 **LIPUS-Combination-0.004** LIPUS-Control-0.135 **Combination-Control-0.043**
		(++)	28.57%	85.71%	0.00%	42.86%		
		(+++)	0.00%	14.29%	71.43%	14.29%		
OPN*	GI	(+)	28.57%	28.57%	0.00%	71.43%	0.061	-
		(++)	57.14%	71.43%	57.14%	14.29%		
		(+++)	14.29%	0.00%	42.86%	14.29%		
	CI	(+)	28.57%	14.29%	0.00%	71.43%	**0.006**	LLLT-LIPUS-0.515 LLLT-Combination-0.077 LLLT-Control-0.108 LIPUS-Combination-0.118 **LIPUS-Control-0.031** **Combination-Control-0.013**
		(++)	71.43%	85.71%	57.14%	28.57%		
		(+++)	0.00%	0.00%	42.86%	0.00%		

The values marked in bold are: ($p<0.05$). *Chi-square **Tukey multiple comparison test.
GI, general intensity; CI, cellular immunoreactivity; LIPUS, low-intensity pulsed ultrasound; LLLT, low-level laser therapy; VEGF, vascular endothelial growth factor; BMP-2, bone morphogenetic protein-2; OPN, osteopontin.

LIPUS and a combined LLLT-LIPUS protocol from the onset of maxillary expansion. To the best of our knowledge, this study is the first to compare the effects of LLLT, LIPUS, and their combined application (administered in equal doses during expansion) on the midpalatal suture.

In the literature, RME studies conducted in rats have applied heavy orthopedic forces to the maxillary incisors or molars. Forces ranging from 30-100 g have been applied to the maxillary incisors and are usually activated once.[2-4,7-10,18] Zahrowski and Turley[19] reported that the number of osteoprogenitor cells rose with increasing force levels up to 100 g during premaxillary expansion; however, at higher forces, cell numbers and bone formation decreased and eventually ceased. They noted that both low or high forces could result in insufficient sutural bone formation, and an expansion force of 100 g was suggested to ensure maximum sutural bone formation in the early period.[19] Therefore, although lower forces are commonly preferred in the literature, we applied 100 g of force between the maxillary incisors in our study. The expansion appliance used in our study was designed to contain three spiral springs, similar to the springs used by Aras et al.[9]

In the present study, the daily dose levels for therapeutic laser and ultrasound were determined based on Babuccu et al.,[14] who applied equal doses to compare the effects of LLLT, LIPUS, and their combination. Accordingly, LLLT and LIPUS were applied at equal daily doses of 30 J/cm^2. This approach ensured that any observed biological differences could be attributed to the biostimulation method itself, rather than to the amount of energy applied.

While no significant changes in body weight were observed in the experimental groups, the control group showed a significant decrease. LIPUS and LLLT are known to be effective in reducing orthodontic pain; therefore, the rats in the experimental groups may have experienced less pain following RME and been able to feed more comfortably, which may explain the absence of remarkable changes in these groups.[20,21]

In this study, the distance between the mesio-incisal edges of the maxillary incisors was initially set to 0 mm at baseline and measured using a caliper at the end of the study. The change in dental expansion did not differ significantly among the LLLT, LIPUS, combination, and control groups. This finding is consistent with the results of Toy et al.,[7] who reported that LIPUS did not influence the amount of dental expansion in rats during RME. However, this measurement approach assumes that the incisors of all rats were initially in full contact, which may not always be valid. Variations due to enamel wear, fractures, or positional changes resulting from applied forces might affect measurement accuracy, which is a limitation of our study. As a more reliable approach for future studies, we recommend measuring either between the mesial margins of incisors at the gingival level or between the disto-incisal edges of the incisors, both before and after activation.

Expansion of the intermaxillary suture was well tolerated by the experimental animals. No signs of inflammation or irritation were observed in the periodontal tissue, and no tooth fractures or pulpal damage occurred during appliance placement.

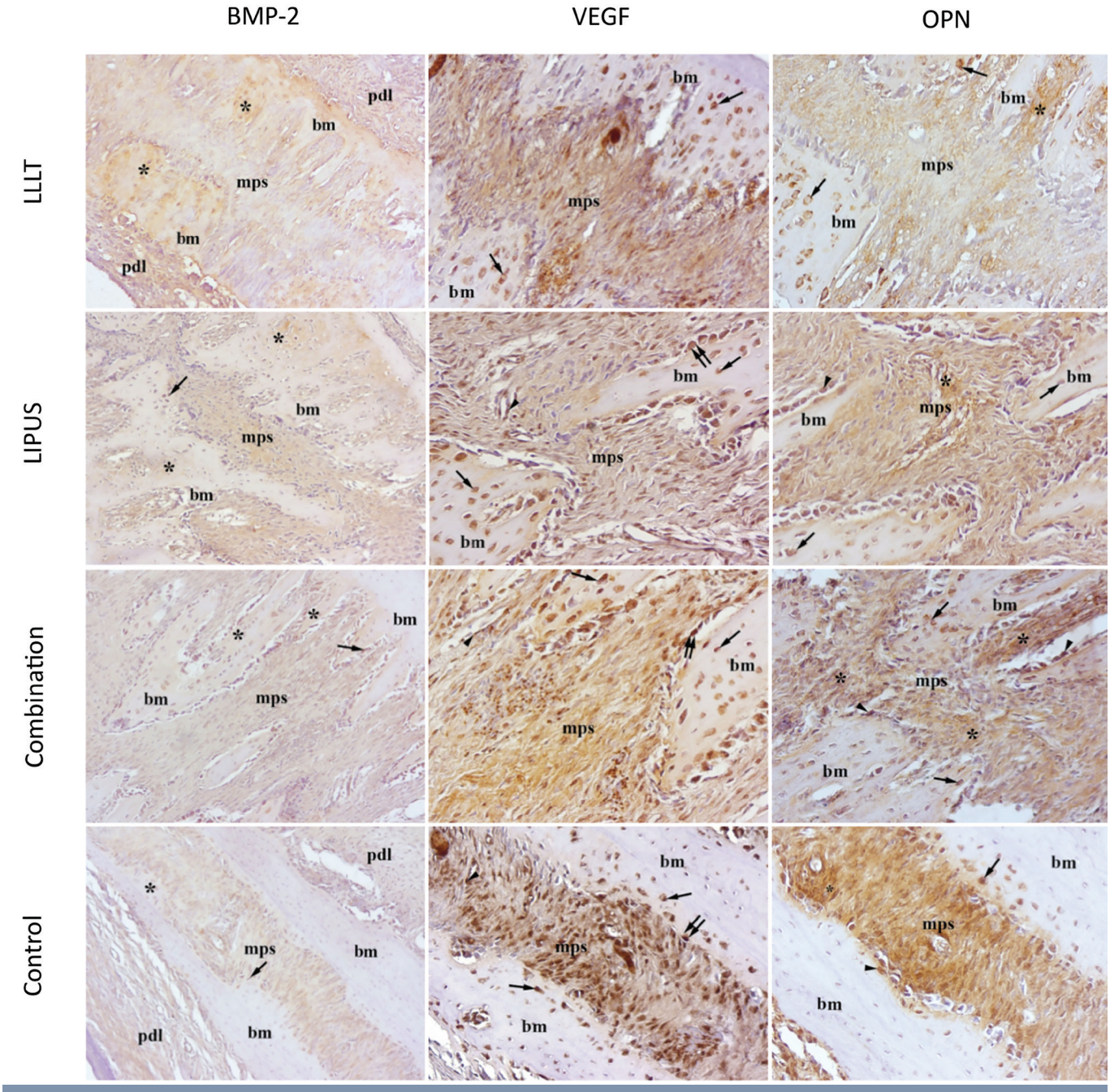

Figure 5. BMP-2, VEGF and OPN immunoreactivities of LLLT, LIPUS, combination and control groups (200X magnification; mps: midpalatal suture, pdl: periodontal ligament, bm: bone matrix).

LIPUS, low-intensity pulsed ultrasound; LLLT, low-level laser therapy; VEGF, vascular endothelial growth factor; BMP-2, bone morphogenetic protein-2; OPN, osteopontin.

However, some animals experienced appliance dislodgement and had their appliances replaced the same day.

Our results showed that the combined treatment notably increased the number of osteoblasts in the suture region compared with the control group. In contrast, LLLT and LIPUS treatments, individually, had no effect on the number of osteoblasts. Furthermore, LLLT, LIPUS, and the combination of treatments did not induce significant changes in the numbers of capillaries or osteoclasts in the premaxillary suture. Aras et al.[9] reported that LLLT did not cause any significant changes in the numbers of osteoblasts, capillaries, or osteoclasts in the premaxillary suture region on day,[17] corroborating our findings. Similarly, Toy et al.[7] reported that LIPUS treatment following RME did not significantly increase either the number of osteoblasts or the widths of capillaries, which is consistent with our findings.

Our findings indicated that LIPUS application significantly increased the sutural width and newly formed bone area compared with LLLT. Immunohistochemical analysis revealed that VEGF immunoreactivity was observed in osteocytes rather than in osteoblasts. Therefore, although the number of osteoblast, capillary, and osteoclast were similar between the two groups, the LIPUS group contained more osteocytes due to an increase in newly formed bone area; concomitantly, VEGF immunoreactivity may also have increased. No significant difference was observed between the two groups in BMP-2 and OPN expression.

Immunohistochemical evaluation demonstrated that the combination group showed the highest levels of BMP-2, VEGF, and OPN expression. In the combination group, the general BMP-2 intensity and cellular VEGF immunoreactivity were higher than those in all other groups; cellular BMP-2 and OPN immunoreactivity were higher than those in the control group; and the general VEGF intensity was significantly higher than that in the LLLT group. These results are consistent with previous studies that employed combined LLLT and LIPUS treatments.[14,22] No adverse effects were observed following combined treatment. In contrast, the combined treatment produced a synergistic effect and strengthened the outcomes of the monotherapies. This finding could be explained by different treatment methods having distinct effects at the cellular level.

BMP-2, VEGF, and OPN are key regulators of bone regeneration. Studies have shown that LLLT stimulates osteoblast differentiation and proliferation by increasing the expression of BMP-2, osteocalcin, and TGF-β1.[23] Suzuki et al.[24] demonstrated that BMP-2 expression increased when LIPUS was applied to rat osteoblasts. In the present study, BMP-2 was detected in the matrix and in some cells, especially in osteoblasts. Therefore, the increased BMP-2 expression observed in the combination group may reflect a greater number of osteoblasts.

Following RME, various tissue reactions begin in the palatal suture that are similar to those of the wound-healing process. The release of VEGF is one such tissue reaction, and angiogenesis plays a key role in healing midpalatal suture tissue and reparative bone formation under mechanical stress. LIPUS treatment during the retention period after RME has been reported to cause a significant increase in VEGF activity in mineralized and fibrous tissues.[7] However, the effects of LLLT on VEGF expression in the midpalatal suture have not been studied before. In the present study, LLLT had no effect on VEGF expression during the early stages of expansion, whereas LIPUS and combined therapy increased VEGF release by osteoblasts.

OPN plays an important role for bone remodeling under mechanical stresses. Perrien et al.[25] reported that OPN expression is biphasic, that primarily proliferating preosteoblasts express OPN, and that mature osteoblasts and osteocytes in newly ossified matrix show OPN immunoreactivity secondarily. In the present study, the LIPUS and combination groups showed a significant increase in both the number of OPN-positive cells and OPN activity, suggesting that the number of mature osteoblasts and osteocytes in the new bone matrix increased as a result of accelerated ossification and that secondary OPN expression had been initiated in the rats.

Clinical studies have shown that LLLT accelerates bone regeneration in the midpalatal suture.[26,27] However, to date, no clinical studies have evaluated the effects of LIPUS or their combined use during rapid RME. Clinical evidence supports the positive orthopedic effects of LIPUS treatment, including accelerated bone formation in fracture healing and distraction osteogenesis.[28] In addition, Maurya et al.[29] suggested that LIPUS may serve as an adjunctive therapy for treating class II malocclusion by enhancing bone remodeling of the condylar head and glenoid fossa when applied with a Forsus device. The present study can serve as a precursor to future clinical studies of LIPUS, including its combined use with LLLT during RME, particularly in young adults.

In this study, the suture width was measured only in the anterior region of the premaxilla in the transverse direction. Further histomorphological investigations and micro-computed tomography evaluations of the middle and posterior regions of the suture are required. Furthermore, the study was based on a small sample size; therefore, the findings should be validated by future in vivo studies with larger cohorts.

One advantage of LLLT is that dental laser devices are now widely used, and their costs have decreased over time. Additionally, the short application time of LLLT is advantageous for clinical use. Also, shortening treatment duration will reduce its overall cost. In contrast, LIPUS requires longer application times, and limited availability of dental-specific devices increases clinical application costs. In addition, the availability of dental laser devices equipped with small biostimulation probes suitable for application to the midpalatal suture enhances the clinical feasibility of LLLT. However, dental LIPUS devices are typically designed to accelerate orthodontic tooth movement and

have a parabolic arch (e.g., the Aevo system), making them unsuitable for use during RME. Therefore, clinical application of LIPUS during RME requires medical LIPUS devices; however, these devices often have large, bulky probes, making intraoral application in the palatal region challenging in a clinical study. Therefore, there is a need for the development of LIPUS devices specifically designed for palatal application during RME. Although these limitations currently restrict clinical applicability, increased adoption of medical and dental LIPUS technologies will lead to a wider variety of commercially available devices and reduced costs.

Study Limitations

This study has some limitations that should be considered. Firstly, in our study, the amount of dental expansion was measured between the mesioincisal edges of the maxillary incisors. The measurements obtained at the end of the study might have been affected by possible enamel wear, fractures of the incisal edges and, positional changes resulting from the expansion forces. Therefore, we recommend to measure the distance between the mesial surfaces at the gingival level for further studies to obtain more reliable results. Also, sutural width was measured only from anterior regions of the premaxilla on the transversal sections. Comprehensive histomorphological evaluations and micro-computed tomography analyses of the middle and posterior regions of the suture are necessary to provide a more complete understanding of sutural changes. Furthermore, this study was based on a small sample size; therefore, the findings should be validated by future in vivo studies with larger cohorts.

Additionally, long application time of LIPUS treatment and limited availability of dental LIPUS devices make the clinical application of the method challenging. Reducing of the device costs and devoloping of dental LIPUS devices which have smaller probes for the midpalatal suture area, are essential for the clinical application of this approach.

CONCLUSION

To accelerate sutural bone regeneration during RME, combined LLLT-LIPUS therapy was the most effective modality, followed by LIPUS therapy. The findings of this study suggest that LIPUS and combined therapy may promote more rapid cellular activation, accelerate bone regeneration, and shorten the retention period. However, further studies are needed to establish the validity of applying combined therapy in clinical practice.

Ethics

Ethics Committee Approval: All animal study procedures were approved by the University of Health Sciences Hamidiye Local Ethics Committee for Animal Experiments (approval no.: 2020-03/05, date: 25.06.2020).

Informed Consent: Not applicable.

Footnotes

Author Contributions: Surgical and Medical Practices - E.E., İ.Ö.P.; Concept - E.E., Ş.K.; Design - E.E., Ş.K., E.Ç.; Data Collection and/or Processing - E.E., İ.Ö.P.; Analysis and/or Interpretation - E.E., Ş.K., E.Ç.; Literature Search - E.E.; Writing - E.E.

Conflict of Interest: The authors have no conflicts of interest to declare.

Financial Disclosure: The authors declared that this study has received no financial support.

REFERENCES

1. Angell EH. Treatment of irregularity of the permanent of adult teeth. Dental Cosmos. 1860;1:540-544. [CrossRef]
2. Uysal T, Amasyali M, Olmez H, Karslioglu Y, Gunhan O. Stimulation of bone formation in the expanding inter-premaxillary suture by vitamin E, in rat. *Korean J Orthod.* 2009;39(5):337-347. [CrossRef]
3. Altan BA, Kara IM, Nalcaci R, Ozan F, Erdogan SM, Ozkut MM, Inan S. Systemic propolis stimulates new bone formation at the expanded suture: a histomorphometric study. *Angle Orthod.* 2013;83(2):286-291. [CrossRef]
4. Buyuk SK, Ramoglu SI, Sonmez MF. The effect of different concentrations of topical ozone administration on bone formation in orthopedically expanded suture in rats. *Eur J Orthod.* 2016;38(3):281-285. [CrossRef]
5. Zhao SY, Wang XX, Zhang WJ, Yang XY, Zhang J. Effect of osthole on bone regeneration in the mid-palatal suture of rats during rapid maxillary expansion. *Int J Clin Exp Med.* 2016;9(4):7548-7556. [CrossRef]
6. Zhao S, Yu S, Zhu D, Dai L, Yang P, Xing X. Stimulatory effects of simvastatin on bone regeneration of the expanded suture in rats. *Am J Transl Res.* 2020;12(5):1767-1778. [CrossRef]
7. Toy E, Oztürk F, Altindiş S, Kozacioğlu S, Toy H. Effects of low-intensity pulsed ultrasound on bone formation after the expansion of the inter-premaxillary suture in rats: a histologic and immunohistochemical study. *Aust Orthod J.* 2014;30(2):176-183. [CrossRef]
8. Ekizer A, Uysal T, Güray E, Yüksel Y. Light-emitting diode photobiomodulation: effect on bone formation in orthopedically expanded suture in rats--early bone changes. *Lasers Med Sci.* 2013;28(5):1263-1270. [CrossRef]
9. Aras MH, Erkilic S, Demir T, Demirkol M, Kaplan DS, Yolcu U. Effects of low-level laser therapy on osteoblastic bone formation and relapse in an experimental rapid maxillary expansion model. *Niger J Clin Pract.* 2015;18(5):607-611. [CrossRef]
10. Tas Deynek G, Ramoglu SI. Effects of different settings for 940 nm diode laser on expanded suture in rats. *Angle Orthod.* 2019;89(3):446-454. [CrossRef]
11. Lane N. Cell biology: power games. *Nature.* 2006;443(7114):901-903. [CrossRef]
12. Sasso Stuani MB, Sasso Stuani A, Leite Pedroso G, et al. The effect of low-level laser therapy after rapid maxillary expansion: micro-CT analysis. *Lasers Med Sci.* 2025;40(1):245. [CrossRef]
13. Johns LD. Nonthermal effects of therapeutic ultrasound: the frequency resonance hypothesis. *J Athl Train.* 2002;37(3):293-299. [CrossRef]
14. Babuccu C, Keklikoğlu N, Baydoğan M, Kaynar A. Cumulative effect of low-level laser therapy and low-intensity pulsed ultrasound on bone repair in rats. *Int J Oral Maxillofac Surg.* 2014;43(6):769-776. [CrossRef]

15. Lirani-Galvão AP, Jorgetti V, da Silva OL. Comparative study of how low-level laser therapy and low-intensity pulsed ultrasound affect bone repair in rats. *Photomed Laser Surg.* 2006;24(6):735-740. [CrossRef]
16. Fávaro-Pípi E, Feitosa SM, Ribeiro DA, et al. Comparative study of the effects of low-intensity pulsed ultrasound and low-level laser therapy on bone defects in tibias of rats. *Lasers Med Sci.* 2010;25(5):727-732. [CrossRef]
17. Mahmoud ES, El-Baky AMA, Gouda OM, Hussein HG. Low intensity pulsed ultrasound versus low-level laser therapy on peri-implant marginal bone preservation and soft tissue healing following dental implant surgery: a randomized controlled trial. *Head Face Med.* 2025;21(1):29. [CrossRef]
18. Uysal T, Gorgulu S, Yagci A, Karslioglu Y, Gunhan O, Sagdic D. Effect of resveratrol on bone formation in the expanded inter-premaxillary suture: early bone changes. *Orthod Craniofac Res.* 2011;14(2):80-87. [CrossRef]
19. Zahrowski JJ, Turley PK. Force magnitude effects upon osteoprogenitor cells during premaxillary expansion in rats. *Angle Orthod.* 1992;62(3):197-202. [CrossRef]
20. Farias RD, Closs LQ, Miguens SA Jr. Evaluation of the use of low-level laser therapy in pain control in orthodontic patients: a randomized split-mouth clinical trial. *Angle Orthod.* 2016;86(2):193-198. [CrossRef]
21. Badiee M, Tehranchi A, Behnia P, Khatibzadeh K. Efficacy of low-intensity pulsed ultrasound for orthodontic pain control: a randomized clinical trial. *Front Dent.* 2021;18:38. [CrossRef]
22. Alazzawi MMJ, Husein A, Alam MK, et al. Effect of low level laser and low intensity pulsed ultrasound therapy on bone remodeling during orthodontic tooth movement in rats. *Prog Orthod.* 2018;19(1):10. [CrossRef]
23. Pyo SJ, Song WW, Kim IR, et al. Low-level laser therapy induces the expressions of BMP-2, osteocalcin, and TGF-β1 in hypoxic-cultured human osteoblasts. *Lasers Med Sci.* 2013;28(2):543-550. [CrossRef]
24. Suzuki A, Takayama T, Suzuki N, Sato M, Fukuda T, Ito K. Daily low-intensity pulsed ultrasound-mediated osteogenic differentiation in rat osteoblasts. *Acta Biochim Biophys Sin (Shanghai).* 2009;41(2):108-115. [CrossRef]
25. Perrien DS, Brown EC, Aronson J, et al. Immunohistochemical study of osteopontin expression during distraction osteogenesis in the rat. *J Histochem Cytochem.* 2002;50(4):567-574. [CrossRef]
26. Dindaroglu F, Oncag G, Olmez S, Dogan S, Gumrukcu Erturk O. Düşük Enerji Seviyeli Lazer Uygulamasının Hızlı Üst Çene Genişletmesi Sonrası Midpalatal Suturada Kemik Rejenerasyonu Üzerine Etkisi. *Turkish J Orthod.* 2011;24:83-96. [CrossRef]
27. Angeletti P, Pereira MD, Gomes HC, Hino CT, Ferreira LM. Effect of low-level laser therapy (GaAlAs) on bone regeneration in midpalatal anterior suture after surgically assisted rapid maxillary expansion. *Oral Surg Oral Med Oral Pathol Oral Radiol Endod.* 2010;109(3):e38-e46. [CrossRef]
28. Palanisamy P, Alam M, Li S, Chow SKH, Zheng YP. Low-intensity pulsed ultrasound stimulation for bone fractures healing: a review. *J Ultrasound Med.* 2022;41(3):547-563. [CrossRef]
29. Maurya RK, Jayan B, Singh H, Nakra O, Sharma P. Effects of low-intensity pulsed ultrasound therapy on the temporomandibular joint complex in conjunction with a fixed functional appliance: a prospective 3-dimensional cone beam computed tomographic study. *J Ultrasound Med.* 2019;38(7):1661-1676. [CrossRef]

2025 Referee Index

Ahmet Yağcı
Ahmet Murat Artuç
Ali Borzabadi-Farahani
Aslı Baysal
Ayse Tuba Altuğ
Azize Atakan
Banu Kılıç
Berza Yılmaz
Betül Karaca
Beyza Hancıoğlu Kırçelli
Beyza Karadede
Beyza Tağrikulu
Buket Erdem
Burçin Akan
Bülent Baydaş
Can Arslan
Çağla Şar
Delal Dara Kılınç
Derya Dursun
Derya Germeç Çakan
Ebru Yurdakurban
Ece Başal
Ege Doğan
Elif Dilara Arslan
Elvan Önem Özbilen
Esra Genç
Eyüp Burak Küçük
Ezgı Atık
Ezgi Sunal Aktürk
Fatma Aslı Konca Taşova
Fırat Oğuz
Fulya Özdemir
Fundagül Bilgiç Zortuk
Gamze Yıldırım
Geetanjali Gandhi
Genta Aganı Sabah
Gizem Yazdan Özen
Göksu Trakyalı
Gonca Yıldırım
Gökhan SerhatDuran
Gönül Dinç
Guiseppe Minervini
Gülden Karabiber
Gulşilay Sayar
Gülcan Çoskun Akar
Hakan Amasya
Hande Pamukçu
Hande Uzunçıbuk
Hanife Nuray Yılmaz
Hatice Kök
Hüsamettin Oktay
Hüseyin Kurtulmuş
İpek Savkan
Javed Sodawala
Kübra Sucu
Kübra Gülnur Topsakal
Letizia Perillo
Liana Fattori
Mehmet Akın
Mehmet Ali Yavan
Mehmet Birol Özel
Melih Motro
Merve Nur Eglenen
Mete Özer
Mohammad Y Hajeer
Muhammed Hilmi Büyükçavuş
Musa Bulut
Mustafa Özcan
Mustafa Asım Aydın
Nazan Küçükkeleş
Nazlı Ece Güngör
Nehir Canıgür Bavbek
Neslihan Şenısık
Nilüfer Darendeliler
Nilüfer İrem Tunçer
Nurver Karslı
Ömür Özsoy
Orhan Çiçek
Ömer Faruk Sarı
Pelin Acar Ulutaş
Prasad Chitra
Puneet Batra
Rajiv Ahluwalia
Richard W. Ballard
Rumeysa Bilici Geçer
Sabahat Yazıcıoğlu
Saeed Reza Motamedian
Samet Özden
Sanaz Sadry
Sanjay Prasad Gupta
Seher Gündüz Arslan
Selvaraj Madhanraj
Sertaç Aksakallı
Siddik Malkoç
Silvio Augusto Bellini-Pereira
Sinem İnce Bingöl
Sumıtra Reddy
Taner Öztürk
Tarek Elshazly
Tord Hamran
Tuğba Haliloğlu Özkan
Turkan Sezen Erhamza
Türkan Nadire Yeşil
Ufuk Ok
Umi Mardhiyyah Mat Ali
Vasilios Zymperdikas
Vincy Antony
Wilana Moura
Yagmur Lena Sezici
Yasemin Acar
Yazgi Ay Ünüvar
Yevhenii Vyzhenko